

Anisotropic Model Colloids

ISBN: 987-90-393-4894-9



9 879039 348949 >

Anisotropic Model Colloids

Anisotrope Model Colloïden

(met een samenvatting in het Nederlands)

Proefschrift

ter verkrijging van de graad van doctor aan de Universiteit Utrecht op
gezag van de rector magnificus, prof.dr. J.C. Stoof, ingevolge het
besluit van het college voor promoties in het openbaar te verdedigen op

maandag 13 oktober 2008 des middags te 2.30 uur

door

CARLOS MARIA van KATS

geboren op 21 maart 1969
te Jaguariuna, Brazilië

PROMOTOR:

Prof. Dr. A. van Blaaderen

CO-PROMOTOR:

Dr. A. Imhof

...voor Bram

CONTENTS

Chapter 1

Introduction: Anisotropic Model Colloids

1.1. Model systems: Isotropic and Anisotropic model colloids	2
1.1.1. Isotropic model colloids	2
1.1.2. Anisotropic model colloids	2
1.2. Synthesis methods for anisotropic particles	2
1.2.1. Precipitation of anisotropic crystallites	3
1.2.2. Anisotropic virus particles	3
1.2.3. Template assisted synthesis	3
1.2.4. Directed growth particle formation	4
1.2.5. Stretching	4
1.2.6. Core-shell synthesis	4
1.2.7. External field induced directional growth	4
1.3. Outline of this thesis	5
1.4. References	6

Chapter 2

The Synthesis of Monodisperse High Aspect Ratio Colloidal Silicon and Silica Rods

2.1. Introduction	10
2.1.1. The electrochemical etching of silicon in HF solutions	11
2.2. Materials and Method	13
2.2.1. Materials	13
2.2.2. Instrumentation	13
2.2.3. The etching set-up	13
2.2.4. From macroporous silicon wafers to silicon/silica rods in suspension	14
2.3. Results and Discussion	16
2.3.1. Electrochemical etching of p-type silicon wafers	16
2.3.2. Fine tuning silicon structures	17
2.3.3. Growth of fluorescent silica on the rods	19
2.3.4. Phase behaviour of rods	20
2.4. Conclusions and Outlook	21
2.5. References	22

Chapter 3

The Synthesis of Silica Coated Gold Rods

3.1. Introduction	26
3.1.1. Optical properties of gold nanorods	26
3.2. Experimental	27
3.2.1. Gold rods synthesis	27
Chemicals	
Synthesis	
Seeded gold rod growth	
3.2.2. Silica growth on gold rods	28
3.2.3. Seeded silica growth	29
3.2.4. Mesoporous silica growth	29
3.3. Results and Discussion	30
3.3.1. Gold rods	30
3.3.2. Silica growth on gold rods	31
3.3.3. Mesoporous silica growth	33
3.4. Conclusions	33
3.5. References	35

Chapter 4

Deformation of Individual Gold Rods

4.1. Introduction	38
4.2. Experimental	39
4.2.1. Laser induced shape deformation of gold rods	39
4.2.2. Heat induced shape deformation of gold rods	42
4.3. Results and Discussion	42
4.3.1. Laser induced shape deformation of AuNR@SiO ₂	42
4.3.2. Laser induced shape deformation of AuNR, AuNR@SiO ₂ and AuNR@MPSiO ₂	44
4.3.3. Heat induced shape deformation of gold rods	48
4.4. Conclusions	51
4.5. References	53

Chapter 5

The Synthesis of Colloidal Silica Dumbbells

5.1. Introduction	56
5.2. Experimental	57
5.2.1. Chemicals	57
5.2.2. Dumbbell synthesis	57
5.2.3. Lowering the size ratio	59
5.2.4. Purification of Dumbbells	61
5.2.5. Small angle X-ray scattering	61
5.2.6. Confocal microscopy	61
5.2.7. Electric field	62
5.3. Results and Discussion	62
5.3.1. Synthesis results	62
5.3.2. Purification of dumbbells	63
5.3.3. Confocal microscopy results	68
5.4. Conclusions	70

Chapter 6

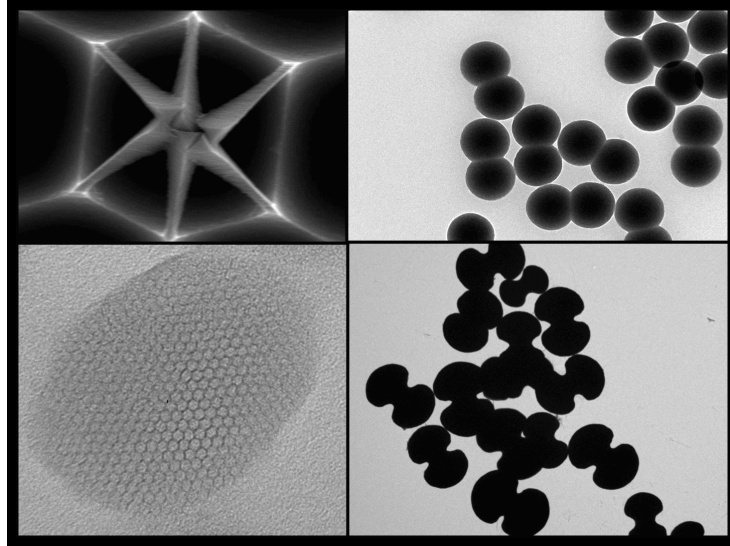
The Synthesis of Anisotropic PMMA Particles

6.1. Introduction	76
6.2. Theory	77
6.3. Experimental	78
6.3.1. Synthesis of PMMA spheres	78
6.3.2. Seeded growth of PMMA spheres	79
6.3.3. Swelling and polymerization	79
6.3.4. Density Gradient Centrifugation	79
6.4. Results and Discussion	80
6.4.1. Seeds of PMMA	80
6.4.2. Seeded growth of PMMA	80
6.4.3. Swelling and polymerization	82
6.4.4. Density gradient centrifugation	83
6.5. Conclusions	84
6.6. References	85

Chapter 7	
<i>Controlling the porosity of colloidal silica from macroporous to ultramicroporous</i>	
7.1. Introduction	88
7.2. From macroporous to ultramicroporous colloidal silica	88
7.2.1. Micrometer control, macroporous structures	88
7.2.2. Nanometer control, mesoporous colloidal silica	89
7.2.3. Ångström precision, microporous colloidal silica	90
7.3. Controlling the pore size of colloidal silica	91
7.3.1. Hollow colloidal particles	91
7.3.2. Closing the pores of colloidal silica: Ultramicroporous silica	93
Appendix: Synthesis methods	95
7.4. References	97
Summary	101
Samenvatting voor een breder publiek	103
Dankwoord	107
Curriculum Vitae	111
List of Publications	112

Chapter 1

Introduction: Anisotropic model colloids



Introduction: Colloids

A colloid can be defined as a particle with at least one dimension roughly between a nanometer and a micrometer¹. Colloids are abundant in many different materials, shapes and forms. Every day we are in touch with colloids, even without noticing. The earliest evidence of the usage of colloids goes back to the earliest records of civilization. In Stone Age paintings stabilized colloidal pigments were already found². Examples of colloids in present day life are: fat globules in milk, red blood cells in blood serum³, pigments in paint or inks, solid particles in smoke. These are all examples of naturally abundant colloids. In colloid science, besides naturally abundant colloids also model colloids are studied. Model colloids have the advantage that well defined uniformity with preferential sizes can be obtained. The study of model colloids enables us to tune (and get more insight into) the colloidal interactions. It is the fundamental understanding of these colloidal interactions and the role they play in the self-organization of colloidal particles that is the driving force for finding new and improved applications. Examples are fabrication of higher strength composite materials, porous materials, controlled, targeted drug delivery, improved medical diagnostic systems, (bio)sensors⁴, new (opto-) electronic devices and many other options.



1.1. Model systems: Isotropic and Anisotropic model colloids

1.1.1. Isotropic model colloids

Spherical (isotropic) particles dominate in colloidal research. The number of papers on spherical colloidal particles by far outnumbers those of anisotropic colloids. This is best illustrated by the number of citations of 2 papers of Werner Stöber, the key author of an important general synthesis method for monodisperse silica particles. His famous 1968 paper on “*Controlled growth of monodisperse silica spheres in the micron size range*”⁵ will soon be cited more than 2400 times, while his paper, published only a year later, on the “*Aerodynamic diameter of aggregates of uniform spheres*”⁶ only has 45 citations. (See <http://apps.isiknowledge.com> ISI Web of KnowledgeSM).

Colloidal particles usually tend to nucleate and grow as spheres because the interfacial free energy is minimal for such a shape. Model systems of spherical particles of many kinds have been studied. Since the beginning of the last century the number of materials from which monodisperse particles can be made, with a polydispersity smaller than 10 %, is still increasing^{7, 8}. A widespread variation of applications is found for such particles.

Although quite a few approaches have been developed for the creation of this class of particles, wet chemistry still is the preferred choice, because of its relative simplicity and use of inexpensive materials and equipment.

Wet chemical synthesis of isotropic colloids enables us to tune well defined sizes, shape and composition of particles. Doing so, the interaction between particles can be tuned at the same time, which makes them a perfect system serving as a model to study the behaviour of atoms and molecules; basic fundamental problems of condensed matter physics, such as the kinetics of melting and crystallization can be studied with these model systems⁹.

Nevertheless, not in all cases is the spherical shape sufficient to reach the desired research goals. For instance, it is believed by some that a full photonic band gap in a photonic crystal, a challenge for many researchers in colloid chemistry and physics, may be easier constructed from anisotropic colloids¹⁰. A photonic crystal is a crystal that consists of a material with periodically alternating refractive index. In a photonic crystal with a full photonic band gap an electromagnetic wave cannot propagate in any direction.

1.1.2. Anisotropic model colloids

The ability to control size and moreover shape will give an enormous boost to the search for more complex structures⁷. Anisotropic colloids used as a building block for complex structures are expected not only to lead to more control over the properties of photonic bandgap materials¹¹, they will also serve as new, more realistic, model systems for their molecular analogues. Therefore, the term “molecular colloids”¹² is sometimes used to qualify these anisotropic colloidal particles.

1.2. Synthesis methods for anisotropic particles

To move beyond conventional spherical growth, non-spherical particles synthesis techniques should break symmetry somehow and induce a path for the system to deviate from the usually energetically more favourable spherical shape. To date, not all specific mechanisms governing morphology and geometry control over particle growth are well understood⁸. This is expected to stimulate considerable research over

the next decade. In this respect this thesis can be seen as a contribution toward achieving a better insight in complications of uniform anisotropic particles synthesis. In this section a few frequently applied techniques to obtain anisotropic particles will be discussed. This overview is far from complete, but it spans a wide variety of known syntheses.

1.2.1. Precipitation of anisotropic crystallites

The clearest anisotropic shapes deviating from a sphere are rods and plates. The synthesis of Boehmite rods¹³ and Gibbsite plates¹⁴ are nice examples resulting in model colloids of which the phase behaviour can be studied. Beautiful examples of the formation of nematic, smectic and columnar phases have been demonstrated with these systems¹⁵⁻¹⁷. These particles can be made from precipitation of aluminumalkoxide solutions. Depending on the pH, temperature and starting aluminumalkoxide concentration via hydrothermal treatment for a few days Gibbsite platelets will precipitate at mild temperature while Boehmite rods will be formed at elevated temperatures.

1.2.2. Anisotropic virus particles

Nature also produces beautiful particles that can be used in colloidal research. The Tobacco Mosaic Virus (TMV) and the bacteriophage FD (FD-virus), are beautiful examples of colloidal rod-like particles that can serve as a hard rod model. A disadvantage of these materials is that it is laborious to obtain high quantities, large enough for experimental research. The advantage is that the particles are monodisperse. Therefore, they already have been used in phase behaviour studies. Fraden and coworkers¹⁸⁻²⁰ have observed beautiful isotropic-nematic phase transitions obtained with suspensions of these viruses.

1.2.3. Template assisted synthesis

In template assisted colloidal growth use is made of a pre-existing structure in which the growth is physically limited in specified directions, therefore an anisotropic growth is dictated. For instance if an inorganic aluminium oxide membrane is used with cylindrical shaped pores, these pores can be filled with materials that precipitate in it. In this case use is made of rigid solid templates. This "template-method" has already been used to prepare gold rods²¹ as well as polymers²² and metal and semiconductor rod-like particles²³. Furthermore, surfactants can be used to form soft templates²⁴, while it is known that surfactants can show a variety of phases in which cylindrical and lamellar phases can serve as templates^{2, 25}.

Lithographically defined particles:

Photolithography can be used to define and design a two dimensional pattern in a layer of photoresist. Brown, Smith and Rennie²⁶ showed that any desired structure can be written and can be filled with a large variety of materials. After polymerization of the filling materials, the mask can easily be removed by selective dissolution, while the particles are not dissolved, leaving monodisperse colloids of pre-defined shapes and sizes.

Xia and co-workers²⁷ used a prepatterned structure made via photolithography, where silica particles self assembled into single, dimer and multimer particles depending on the sizes of the colloids and the dimensions of the prepatterned structures that were used. Spherical particles settled and formed anisotropic aggregates whose structures were determined by the geometric confinement provided by the templates. A drawback of this synthesis method is that photolithography is only

applicable to a 2D surface and therefore the yield is very low. In chapter 2 of this thesis we will describe how a template assisted synthesis can be extended into the third dimension.

1.2.4. Directed growth particle formation

Anisotropic growth can be induced by the growth of monocrystalline particles, where specific facets of the crystal are shielded through absorption of an added agent. This agent can be a surfactant or ions of added salts. Growth directing agents are well known in the growth of iron oxides^{28, 29}. In case of iron oxide, sulphate ions are known to have a dramatic impact on the final (anisotropic) morphology of the precipitating particles originating from iron(III)chloride. Hematite spindles can be made by the hydrolysis of iron(III)chloride, while the concentration of phosphate ions determines the ellipsoidal shape and size of the final particles. A wide variety of shapes of calcium carbonates particles has also been found if particles are grown with different kinds of surface active polymers³⁰. For instance depending on the ratio of polyvinylpyrrolidone and sodiumdodecylbenzenesulfate, the final shape of calcium carbonates can change from spheres to rhombohedrons. Unfortunately, in most cases these syntheses lead to relatively polydisperse particles.

The addition of a catalyst can also induce directional growth as can be seen in the synthesis of carbon nanotubes, a widely investigated material with great potential in materials science^{31, 32}.

1.2.5. Stretching

An alternative route to obtain monodisperse anisotropic particles is to start from monodisperse isotropic particles and stretch them to an anisotropic (elongated) shape. This requires particles with a deformable structure, usually a polymer (soft condensed matter in its literal form). A very early example is a method where prolate ellipsoidals are obtained via shear of a dispersion of human erythrocytes³. Another example is a method where a polyvinyl alcohol (PVA) film containing PMMA particles that are arrested in it was stretched by Ottewill and co-workers³³. Mohraz and Solomon later extended this method for dyed PMMA particles. These ellipsoidal particles were studied with confocal microscopy³⁴.

1.2.6. Core-shell synthesis

A specific class of anisotropic particles are particles made of different materials in the inner part than at the outer part. These core-shell particles frequently are isotropic in shape, but anisotropic in composition. These particles are normally grown via layer by layer (LBL) growth. Commonly the core has physical properties that either makes them traceable, such as dyed core-shell particles³⁵, for confocal microscopy studies, or the shell has desirable chemical or surface properties. Other examples are core-shell particles where the core has specified optical or magnetic properties. Another reason to create core-shell particles is that the core by itself is not stable, while the growth of a shell provides stability.

1.2.7. External field induced directional growth

If an external field is applied during particles growth, (such as growth in a magnetic or electric field) anisotropic growth of a particle might be preferred instead of spherical growth. The most common way to make carbon nanotubes, a widely investigated material with great potential in materials science, is via chemical vapour deposition in an electric field³¹. Furthermore, particles can be aligned in an external

field to form (flexible) chains³⁶. Biswall and Gast³⁷ already showed that paramagnetic colloidal particles could aggregate into linear chains under an applied external magnetic field. These particles were chemically linked to create chains that could be magnetically actuated to manipulate microscopic fluid flow. A drawback of these methods is that it is difficult to control the final length polydispersity of such systems.

1.3. Outline of this thesis

In this thesis a few novel techniques to make anisotropic model colloids, as described above, will be discussed. In chapter 2 we show that via electrochemical etching of a patterned silicon wafer we are able to produce monodisperse silicon rods that can be turned into silica rods containing a dye to make them suitable for confocal study. Other rod-like particles with a gold core and again a silica surface will be treated in chapters 3 and 4. Chapter 3 mainly deals with the synthesis of the gold core silica shell colloidal particles, while in the next chapter the optical effects of deformation via heat treatment or ultra-short laser pulse irradiation is discussed. From rod-like particles we move to the synthesis method of making dimer³⁸ particles, or dumbbells (as we call them³⁹). In chapter 5 we start with the synthesis of monodisperse fluorescent spherical silica particles. The growth of clusters of these particles obtained via controlled aggregation will produce anisotropic particles, which can be separated by a nice sedimentation technique that will be described as well.

Actually the chapter uses controlled aggregation of uniform Stöber silica and thus is very much related to the early Stöber paper⁶, which deserves to be cited more frequently. The goal of chapter 6 is to obtain particles with a similar shape as in chapter 5, but with a different material. In chapter 5 silica dumbbells are made. Silica is a widely used material that has many options to do (chemical) surface modifications with and therefore is an interesting material to study particle interactions. In chapter 6 the resulting dumbbells are made from PolyMethylMethacrylate (PMMA). Like silica it can also be incorporated with dye to enable confocal study, but an extra advantage of PMMA is that it can easily be optically and density matched in a suspension which opens an even broader field of studying particles' interactions. An elegant technique to separate a dispersion with a variety of size and shapes into separate parts with equal size and shape will be discussed in both chapters as well.

Finally in chapter 7 synthesis techniques are discussed where not necessarily anisotropy of particle shape is the determining issue to fit in this thesis on anisotropic particles. It is more their anisotropy in composition of the materials they are made of that will be discussed. To be more specific in chapter 7 examples are shown of synthesized particles (made from silica) with a decreasing internal porosity. This variation in porosity and thus variation in density within a particle is what makes them anisotropic. Some examples of applications of this class of particles will also be discussed.

1.4. References

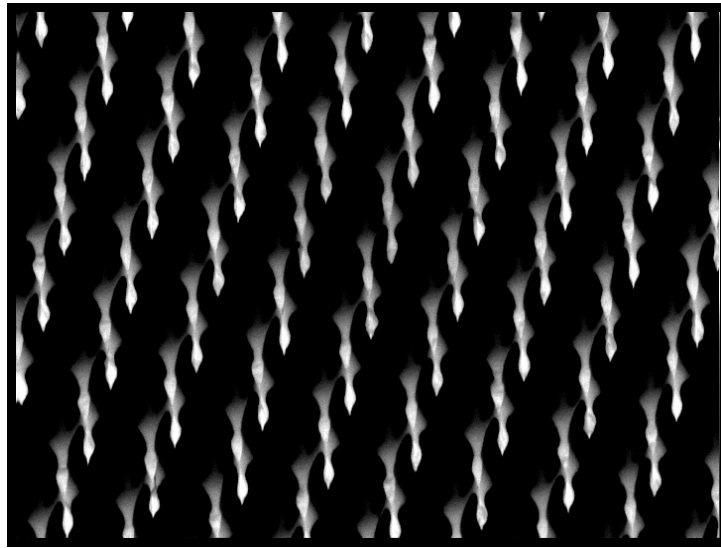
1. Everett, D. H., *Manual of Symbols and Terminology for Physicochemical Quantities and Units, Appendix II: Definitions, Terminology and Symbols in Colloid and Surface Chemistry*. Pure and Applied Chemistry **1972**, 31, (4), 577-638.
2. Evans, F. D.; Wennerström, H., *The Colloidal Domain, where physics, chemistry, biology and technology meet*. Wiley VCH: **1999**.
3. Sutura, S. P.; Boylan, C. W., *A nearly monodisperse population of prolate ellipsoidal particles potentially useful for colloidal research*. Journal of Colloid and Interface Science **1980**, 73, (1), 295-297.
4. Haes, A.; Stuart, D.; Nie, S.; Van Duyne, R., *Using Solution-Phase Nanoparticles, Surface-Confined Nanoparticle Arrays and Single Nanoparticles as Biological Sensing Platforms*. Journal of Fluorescence **2004**, 14, (4), 355-367.
5. Stöber, W.; Fink, A.; Bohn, E., *Controlled growth of monodisperse silica spheres in the micron size range*. Journal of Colloid and Interface Science **1968**, 26, (1), 62-69.
6. Stöber, W.; Berner, A.; Blaschke, R., *The aerodynamic diameter of aggregates of uniform spheres*. Journal of Colloid and Interface Science **1969**, 29, (4), 710-719.
7. Glotzer, S. C.; Solomon, M. J., *Anisotropy of building blocks and their assembly into complex structures*. Nature Materials **2007**, 6, (7), 557-562.
8. Pérez-Juste, J.; Pastoriza-Santos, I.; Liz-Marzán, L. M.; Mulvaney, P., *Gold nanorods: Synthesis, characterization and applications*. Coordination Chemistry Reviews **2005**, 249, (17-18), 1870-1901.
9. Poon, W., *Colloids as Big Atoms*. Science **2004**, 304, (5672), 830-831.
10. Yin, Y.; Xia, Y., *Self-Assembly of Monodispersed Spherical Colloids into Complex Aggregates with Well-Defined Sizes, Shapes, and Structures*. Advanced Materials **2001**, 13, (4), 267-271.
11. Penninkhof, J. J.; van Dillen, T.; Roorda, S.; Graf, C.; van Blaaderen, A.; Vredenberg, A. M.; Polman, A., *Anisotropic deformation of metallo-dielectric core-shell colloids under MeV ion irradiation*. Nuclear Instruments and Methods in Physics Research Section B: Beam Interactions with Materials and Atoms **2006**, 242, (1-2), 523-529.
12. Yang, S.-M.; Kim, S.-H.; Lim, J.-M.; Yi, G.-R., *Synthesis and assembly of structured colloidal particles*. Journal of Materials Chemistry **2008**, 18, (19), 2177-2190.
13. Buining, P. A.; Pathmamanoharan, C.; Jansen, J. B. H.; Lekkerkerker, H. N. W., *Preparation of Colloidal Boehmite Needles by Hydrothermal Treatment of Aluminum Alkoxide Precursors*. Journal of the American Ceramic Society **1991**, 74, (6), 1303-1307.
14. Wierenga, A. M.; Lenstra, T. A. J.; Philipse, A. P., *Aqueous dispersions of colloidal gibbsite platelets: synthesis, characterisation and intrinsic viscosity measurements*. Colloids and Surfaces A: Physicochemical and Engineering Aspects **1998**, 134, (3), 359-371.
15. van der Kooij, F. M.; Kassapidou, K.; Lekkerkerker, H. N. W., *Liquid crystal phase transitions in suspensions of polydisperse plate-like particles*. Nature **2000**, 406, (6798), 868-871.

16. van der Kooij, F. M.; Lekkerkerker, H. N. W., *Liquid-Crystalline Phase Behavior of a Colloidal Rod-Plate Mixture*. *Physical Review Letters* **2000**, 84, (4), 781.
17. van Bruggen, M. P. B.; Dhont, J. K. G.; Lekkerkerker, H. N. W., *Morphology and Kinetics of the Isotropic-Nematic Phase Transition in Dispersions of Hard Rods*. *Macromolecules* **1999**, 32, (7), 2256-2264.
18. Dogic, Z.; Fraden, S., *Cholesteric Phase in Virus Suspensions*. *Langmuir* **2000**, 16, (20), 7820-7824.
19. Fraden, S.; Maret, G.; Caspar, D. L. D.; Meyer, R. B., *Isotropic-nematic phase transition and angular correlations in isotropic suspensions of tobacco mosaic virus*. *Physical Review Letters* **1989**, 63, (19), 2068.
20. Dogic, Z.; Purdy, K. R.; Grelet, E.; Adams, M.; Fraden, S., *Isotropic-nematic phase transition in suspensions of filamentous virus and the neutral polymer Dextran*. *Physical Review E* **2004**, 69, (5), 051702.
21. van der Zande, B. M. I.; Bohmer, M. R.; Fokink, L. G. J.; Schonenberger, C., *Colloidal Dispersions of Gold Rods: Synthesis and Optical Properties*. *Langmuir* **2000**, 16, (2), 451-458.
22. Steinhart, M.; Wendorff, J. H.; Greiner, A.; Wehrspohn, R. B.; Nielsch, K.; Schilling, J.; Choi, J.; Gosele, U., *Polymer Nanotubes by Wetting of Ordered Porous Templates*. *Science* **2002**, 296, (5575), 1997-.
23. Martin, C. R., *Nanomaterials: A Membrane-Based Synthetic Approach*. *Science* **1994**, 266, (5193), 1961-1966.
24. Adair, J. H.; Li, T.; Kido, T.; Havey, K.; Moon, J.; Mecholsky, J.; Morrone, A.; Talham, D. R.; Ludwig, M. H.; Wang, L., *Recent developments in the preparation and properties of nanometer-size spherical and platelet-shaped particles and composite particles*. *Materials Science and Engineering: R: Reports* **1998**, 23, (4-5), 139-242.
25. Burda, C.; Chen, X.; Narayanan, R.; El-Sayed, M. A., *Chemistry and Properties of Nanocrystals of Different Shapes*. *Chemical Reviews* **2005**, 105, (4), 1025-1102.
26. Brown, A. B. D.; Smith, C. G.; Rennie, A. R., *Fabricating colloidal particles with photolithography and their interactions at an air-water interface*. *Physical Review E* **2000**, 62, (1), 951.
27. Yin, Y.; Lu, Y.; Gates, B.; Xia, Y., *Template-Assisted Self-Assembly: A Practical Route to Complex Aggregates of Monodispersed Colloids with Well-Defined Sizes, Shapes, and Structures*. *Journal of the American Chemical Society* **2001**, 123, (36), 8718-8729.
28. Ocaña, M.; Morales, M. P.; Serna, C. J., *The Growth Mechanism of [alpha]-Fe₂O₃ Ellipsoidal Particles in Solution*. *Journal of Colloid and Interface Science* **1995**, 171, (1), 85-91.
29. Ohmori, M.; Matijevic, E., *Preparation and Properties of Uniform Coated Inorganic Colloidal Particles: 8. Silica on Iron*. *Journal of Colloid and Interface Science* **1993**, 160, (2), 288-292.
30. Shen, Q.; Wei, H.; Zhao, Y.; Wang, D.-J.; Zheng, L.-Q.; Xu, D.-F., *Morphological control of calcium carbonate crystals by polyvinylpyrrolidone and sodium dodecyl benzene sulfonate*. *Colloids and Surfaces A: Physicochemical and Engineering Aspects* **2004**, 251, (1-3), 87-91.
31. Eftekhari, A.; Jafarkhani, P.; Moztarzadeh, F., *High-yield synthesis of carbon nanotubes using a water-soluble catalyst support in catalytic chemical vapor deposition*. *Carbon* **2006**, 44, (7), 1343-1345.

32. Ren, Z. F.; Huang, Z. P.; Xu, J. W.; Wang, J. H.; Bush, P.; Siegal, M. P.; Provencio, P. N., *Synthesis of Large Arrays of Well-Aligned Carbon Nanotubes on Glass*. *Science* **1998**, 282, (5391), 1105-1107.
33. Ho, C. C.; Keller, A.; Odell, J. A.; Ottewill, R. H., *Preparation of monodisperse ellipsoidal polystyrene particles*. *Colloid and Polymer Science* **1993**, 271, (5), 469-479.
34. Mohraz, A.; Solomon, M. J., *Direct Visualization of Colloidal Rod Assembly by Confocal Microscopy*. *Langmuir* **2005**, 21, (12), 5298-5306.
35. van Blaaderen, A.; Vrij, A., *Synthesis and characterization of colloidal dispersions of fluorescent, monodisperse silica spheres*. *Langmuir* **1992**, 8, (12), 2921-2931.
36. Vutukuri, H. R., Unpublished results.
37. Biswal, S. L.; Gast, A. P., *Micromixing with Linked Chains of Paramagnetic Particles*. *Analytical Chemistry* **2004**, 76, (21), 6448-6455.
38. Ibisate, M.; Zou, Z.; Xia, Y., *Arresting, Fixing, and Separating Dimers Composed of Uniform Silica Colloidal Spheres*. *Advanced Functional Materials* **2006**, 16, 1627-1632.
39. Johnson, P. M.; van Kats, C. M.; van Blaaderen, A., *Synthesis of Colloidal Silica Dumbbells*. *Langmuir* **2005**, 21, (24), 11510-11517.

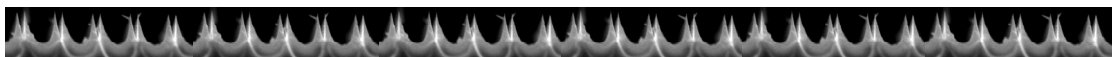
Chapter 2

The synthesis of monodisperse high aspect ratio colloidal silicon and silica rods



Abstract

We describe the synthesis and the physical properties of suspensions of colloidal silicon and silica rod-like particles. In addition to pure silicon and pure silica rods, we have also synthesized silicon rods with a silica shell, and silica rods with a fluorescent silica layer. Pre-patterned p-type (100) silicon wafers were electrochemically etched in electrolyte solutions containing hydrogen fluoride. By varying the current density while etching, macropores were etched with controllable modulated pore diameters. These silicon structures were transformed into rods with indentations $5.5\ \mu\text{m}$ apart and with lengths up to $100\ \mu\text{m}$, using iterative oxidation in air and dissolution of the silica by HF. Complete oxidation of these rods was also achieved. Sonication of the modulated rods resulted in monodisperse particles of $5.5\ \mu\text{m}$ length and $300\ \text{nm}$ width. A high yield of 10^{12} particles, or more, is possible with this method. At high concentrations, these particles show nematic ordering in charge-stabilized suspensions. The oxidized silica outer layer of the silicon rods makes the further growth of silica in solution or on a wafer possible. This allows for control of the particles' interaction potential. Labeling with a fluorescent dye and index matching of the complete silica rods enable the study of concentrated dispersions quantitatively, on a single particle level with confocal microscopy. Because of their high refractive index in the near IR, the nematic phases of rods with a silica core are also interesting for photonic applications.



2.1. Introduction

Colloidal rods are interesting as condensed matter model systems and for applications¹, because of anisotropy in the particle properties, and their ability, at high aspect ratios, to form liquid crystalline phases.²

Recent fundamental studies have shown that a combination of index matching and fluorescent labeling make it possible to quantitatively study both the structure and dynamics of concentrated colloidal dispersions of spheres, with confocal microscopy, on a single particle level³⁻⁷. The extensive knowledge that is available on the modification of the surface of silica makes it possible to tune interactions from long-range repulsive⁸ to hard-sphere like^{3,4} to even dipolar⁹. Since such fundamental real-space studies have only been carried out using colloidal spheres, it is our motivation to extend these studies to rod-like colloidal model systems with tunable aspect ratios.

On the applied side, semiconductor colloidal rods in particular are increasingly important as functional components for new types of electro-optical, electromechanical, and sensing devices in microelectronics¹⁰. We would like to explore the photonic properties of (liquid) crystalline phases of rod-like particles with a silicon core. Silicon does not absorb in the near IR and has a very high refractive index ($n=3.5$ at $\lambda = 1.5 \mu\text{m}$).¹¹ Photonic (liquid) crystals made from anisotropic particles have until now scarcely been explored.¹²⁻¹⁴

The theory of the liquid crystalline behaviour of rod-like colloidal particles has consistently preceded the experimental study of these systems. As early as 1949 Onsager showed that a system of long hard rods interacting with purely repulsive forces exhibits orientational (nematic) order at critical densities far from the closest packing¹⁵. The Onsager theory was extended to polydisperse solutions and soft interactions by several groups.^{2,16} Computer simulations have further shown that not only nematic phases, but also smectic and crystalline phases can occur.¹⁷⁻¹⁹ Experimental studies on rod-like colloidal model systems are far less numerous than that on spheres. Nevertheless, examples of isotropic-nematic phase behaviour have been observed with several different (more or less stiff) organic rods (FD-, TMV-viruses, poly-glutamates, DNA),^{16,20,21} and inorganic materials (vanadium pentoxide (V_2O_5), β -ferric oxyhydroxide ($\beta\text{-FeOOH}$), Boehmite (AlOOH))²²⁻²⁵. The first real-space observation of self-ordering of liquid crystals from rod-like colloidal particles on a single particle level has recently been reported by Maeda²⁶. However, these observations are not yet quantitative. The high refractive index of β -ferric oxyhydroxide will make it hard to carry out real space analysis on this system.

In this chapter we describe the synthesis of stable dispersions of silicon rods, their conversion to pure silica and their labeling with a fluorescent dye. Our synthetic method yields large enough quantities of particles to allow the study of the dynamic behaviour of concentrated dispersions of rods.

Silicon rods of sizes from a few nanometers to micrometers have recently been produced by several different methods. Various groups have reported making silicon nanowires via laser ablation²⁷ where single crystalline rods grow from an oversaturated nanocolloid of catalyst material (e.g. gold). Chemical Vapor Deposition (CVD) of SiH_2Cl_2 ²⁸ on TiSi_2 islands has also been performed, allowing smaller silicon wires to be grown with nanometer precision. Silicon rods have also been made via a template-directed synthesis²⁹ where particles nucleate and grow in supporting channels in anodic alumina membranes.

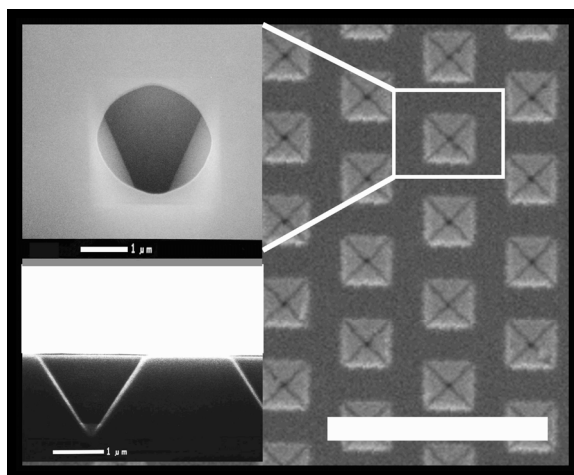


Fig. 2.1. The pit pattern of a silicon wafer before electrochemical etching (Top view; right, diagonal side-view; top left, and side-view of a cleaved wafer bottom left). Etch pits are 3.5 micrometers apart. Each pit has an inverse pyramidal shape (due to anisotropic etching with KOH) with a width of 1.5 μm and a depth of 1 μm . A 6-inch silicon wafer contains ~ 4 billion pits. The scale bar on the right represents 10 μm , while the scale bars on the left represent 1 μm

For a survey of other methods see the papers of Xia and co-workers^{1, 30}.

While these methods may be useful in a number of applications, they are not suitable for producing colloidal model systems because the polydispersity of the rod lengths is very high and/or the yield is too low. In our synthesis method we begin by creating pores by etching into silicon. When widened, the pores start to overlap resulting in long rods. In addition, we modulate the width of the pores creating rods with regularly spaced indentations. The advantage of our method is that we have a high control over the particle dimensions. Moreover, we can obtain a relatively high yield of particles (10^{12}), because the method is essentially 3D. We can estimate the maximum possible rod yield as follows: the wafers contain ~ 4 billion pits. The maximum possible depth of etched pores is ~ 0.5 mm. The minimum rod length is several microns. This suggests a maximum yield of $\sim 10^{12}$ particles

Lehmann and co-workers demonstrated for relatively small n-type wafers that modulating the light intensity during electrochemical etching resulted in modulated macropore formation³¹. In our experiments we show that modulations of pore formation can also be achieved with p-type silicon by modulating the applied current. We have achieved structures with uniform lengths and diameters, up to 100 micrometers deep. This ability to etch modulated rods deep into the wafer allows us to use an entire 6-inch wafer to obtain a relatively high yield of particles. As far as we know, this is the first example of modulated pore etching in p-type silicon³².

2.1.1. The electrochemical etching of silicon in HF solutions

Macroporous etching of silicon, first reported by Lehmann and co-workers,^{33, 34} has been used to make photonic crystals,¹⁴ micropumps and membranes,³⁵ and solid-state capacitors from 6-inch wafers³⁶. In this article we use similar techniques to make silicon nanowires from silicon wafers.

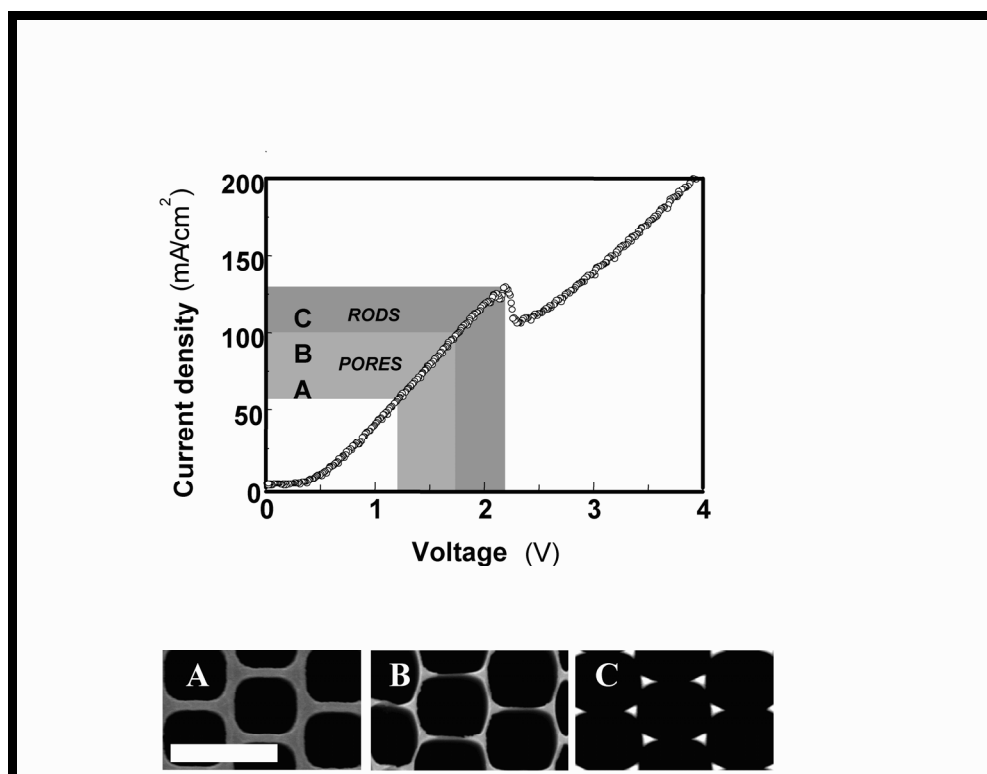


Fig. 2.2. Typical current to voltage plot. The ranges of expected rod formation (upper part (dark gray) at higher current densities) and pore formation (lower part, light gray) are marked. **Fig. 2.2.a,b,c:** Top view of different stages of pore etching (Scale bar represents 2 μm). Etched structures with: (a) macropores and thick walls, (b) broad macropores and thin walls, and (c) overlapping macropores which form rods. The SEM pictures correspond to the ranges a, b and c in the upper graph. At higher current densities electro-polishing of the wafer occurs.

Under anodic polarization in HF solution silicon is oxidized and dissolves. Positive charge carriers (holes) are required to drive the electrochemical reaction. In p-type silicon, holes are available in the valence band at room temperature. In n-type silicon electron-hole pairs can be created by illuminating the semiconductor³⁷.

Electrochemical etching at strongly positive potentials can be used to create macropores. To control the pore spacing and pore dimensions, pre-patterned silicon wafers can be used. Regularly spaced anisotropically etched macropores can be formed with patterned structures containing pre-etched indentations³⁸ (Figure 2.1).

Once electrochemical etching begins, the holes are driven towards the front of the patterned wafer by the applied potential. The pores will begin etching at the tip of the inverted pyramid in the direction parallel to the applied electric field. In this way unidirectional etching is realized and a highly regular array of macropores can be formed. In p-type silicon the diameter of the formed macropores can be controlled by the applied current. Increasing the total applied current increases the pore size. At a high applied current, the pores start to overlap and silicon rods are formed. Under the right conditions, highly anisotropic pores of up to microns in diameter can be etched in p-type silicon up to 400 μm in depth³⁹. If a high enough current is applied, the pores completely overlap and the whole surface of the wafer becomes etched. This results in electropolishing of the silicon surface. These different stages in etching are illustrated in Figure 2.2.

Modulating the current density can modulate the diameter of these pores during the etching process. This was shown previously for n-type silicon wafers by modulating the light intensity.^{31, 35} The process of etching uniform macropores is well explained for n-type silicon, for which the concentration of charge carriers, and thus the diameter of the pores, can be regulated by light-induced electron-hole pair formation at constant applied potential.^{31, 40} For p-type silicon, the physical and chemical processes that regulate the etching process are not yet well understood.

2.2. Materials and Method

2.2.1. Materials: All chemicals and solvents were used as received without further purification. Ethanol (Technical grade, containing 5% methanol), hydrogen fluoride (HF) 50%, (Merck), a 25 % w/w cetyltrimethylammoniumchloride (CTAC) solution in water, potassium sulfate (K_2SO_4)(Aldrich) and demineralized water were used in the etching set-up. Tetraethoxysilane (TES), 3-aminopropyltriethoxysilane (APS), fluorescein isothiocyanate (FITC) (Fluka), ammonia 25% w/w and ethanol p.a. (Merck) were used for the silica growth on the rods. Dimethylsulfoxide (DMSO) (Fluka) was used to index match the silica rods under the confocal microscope. Biorad AG501-X8 mixed ion exchange resin was used to deionize the water.

2.2.2. Instrumentation: The current was controlled via a LabView computer program, with a Philips power source (PM2811). Scanning Electron Microscopy (SEM) images were taken on a Philips XL30FEG microscope. High Resolution Transmission EM (HRTEM) was performed on a TECNAI20. Silicon wafers were oxidized in air by heating in a Carbolite ESF oven. Confocal microscopy images were taken on a Leica DM IRB confocal microscope. Samples were supercritically dried on a Bal-tec critical point dryer (CPD030). Samples were centrifuged with a Hettich Rotina 46S table centrifuge and were sonicated with a Bransonic 8510 sonicator, operating at a power of 250 W with a frequency of 44 kHz.

2.2.3. The etching set-up

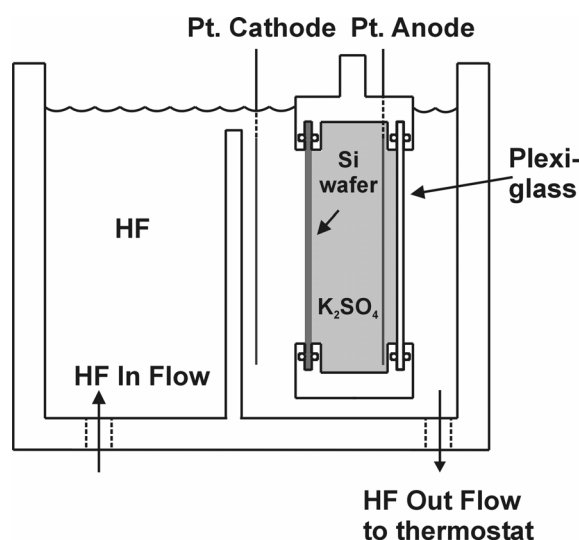


Fig. 2.3. The experimental set-up: a container with 8 liter HF solution in an ethanol water mixture that is pumped via a thermostat to control the temperature. The closed plexiglass container with potassium sulfate electrolytic solution keeps the electric field uniform over the whole silicon wafer.

In our experiment we used 6-inch p-type (boron doped) (100) silicon wafers with a resistivity of 10 – 20 Ωcm with pre-etched indentations on one side (see Figure 2.1). A pattern with a hexagonal array of ~4 billion holes in the etch mask was obtained as described in earlier publications³⁸ by standard lithographic techniques. This patterning was realized by exposing a wafer to an 8.8 M KOH solution at 70 °C for 8 min. using a Si_3N_4 mask. These pre-etched pyramidal holes had widths of 1.5 μm and a pitch of 3.5 μm (see Figure 2.1.). Before the pore etching started, the mask was removed in concentrated H_3PO_4 at 140 °C.

For large (6-inch) silicon wafers, a number of steps were taken to ensure a uniform electric field, temperature, and HF flow rate over the entire wafer surface. An electrolyte solution of HF, CTAC, ethanol and water was thermostatted at a temperature of 30 °C (unless otherwise stated) in a polycarbonate container by pumping the solution via a Teflon-coated pump through a temperature controlled water bath (see Figure 2.3.).

The 6-inch silicon wafer was held in a polypropylene container filled with a 0.16 M K_2SO_4 electrolyte solution, which acted as an electrolytic back contact of the wafer. In this way a uniform electric field over the silicon wafer was obtained. The chamber contained a 137 cm^2 Pt grid as anode. The cathode counter electrode was a Pt sheet of 196 cm^2 positioned parallel to the Si wafer at a distance of about 3 cm ³⁶. The electrolytic HF solution was pumped via a thermostatted bath over the cathode sheet along the silicon wafer. This pumping regulates the temperature of the solution, homogenizes the HF concentration and facilitates the flow of hydrogen gas created at the wafer surface during etching. Macropores were etched by generating an electric potential across the electrodes.

The optimum etching conditions were determined from a current to voltage diagram (IV-curve (see Figure 2.2)). The current was measured while the potential across the wafer was decreased at a scan rate of 10 mV/s. The resulting IV-curve peaks at the point when electro-polishing begins. Pores or rods were obtained by choosing an appropriate applied current relative to this peak.

We performed etching experiments with an electrolyte solution of 7.9 liters containing 1300 ml HF, (4.7 M), 2600 ml ethanol (5.7 M), 100 ml of the 25% CTAC solution and 3900 ml demineralized water. The polypropylene container holding the platinum anode and the silicon wafer was filled with a 0.16 M K_2SO_4 electrolyte solution. Typical current densities used for a 6-inch wafer (with ~133 cm^2 available surface area for etching) were 100 mA/cm^2 for making rods and 67 mA/cm^2 for making macropores.

We etched 6-inch silicon wafers to give varying rod thicknesses by alternating the current density between 13.5 A and 9 A, five to twenty times for 1 minute each period.

A few tests were performed at 25 °C with the same solutions to explore the influence of temperature on the etch conditions.

2.2.4. From macroporous silicon wafers to silicon/silica rods in suspension

The structure obtained after modulation of current density on large 6-inch wafers can be repeatedly oxidized thermally and etched in HF to create modulated rods with desired dimensions. This is illustrated in Figure 2.4.

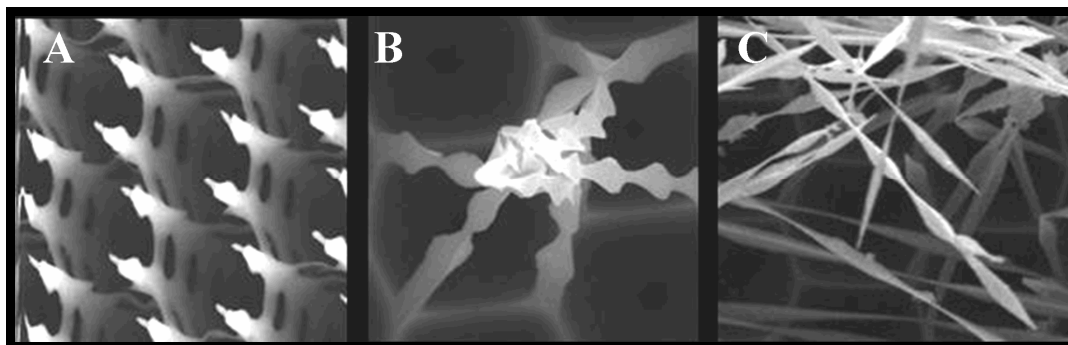


Fig. 2.4. Examples of etched silicon wafers: (a) the result after etching in the set-up. (b) the result after 2 oxidation/etch cycles (c) the result after 4 oxidation/etch cycles. The SEM pictures are taken at different viewing angles. Thin particles tend to bend on the wafer; therefore, particles can be seen in different directions. After 4 oxidation cycles the particles are thin enough to be rinsed off, without sonication.

The sample etched with alternated current densities during etching was put in a Carbolite ESF oven at 950 °C for 15 minutes. The silica layer formed was subsequently removed by etching for 15 min. in 3.75 M HF.

After fine tuning the average thickness, the rods were washed off the wafer by rinsing with water or (more vigorously) by ultrasonication in distilled water.

We grew silica on the rods using well-known methods. The silicon rods that were rinsed off and sonicated were transferred to ethanol and a thin silica layer was grown on the particles. In a typical fluorescent silica growth experiment⁴¹, the sonicated rods ($\sim 2 \times 10^9$) were dispersed in 0.5 ml ethanol containing 50 μ l 25% ammonia. A fresh mixture of 44 μ l TES and the FITC-APS dye (30.6 μ g FITC reacted with 0.18 μ l APS in 250 μ l ethanol overnight) were added at once and stirred for 16 hrs. A fluorescent layer of ~ 50 nm was grown on the rods. Secondary-nucleated particles were removed by repeated centrifugation (15 min, 750 rpm).

To create all-silica particles, we thermally oxidized silicon rods completely on the wafer. However, if the wafer was dried in air, drying forces would lead to bending and bunching of the rods and, ultimately, sintering during thermal oxidation. For this reason, we dried the wafer supercritically. Due to the small size of our supercritical dryer, a 1 cm² piece of wafer was used. This supercritically dried wafer was then thermally oxidized for 16 hours at 950 °C.

After this oxidation step a fluorescent layer of silica was grown on the rods on this piece of a wafer with a method described by Vossen et al⁴². The piece of wafer was put in a 1.1 vol % solution of silica spheres with a diameter of 1030 nm, containing 1.0 ml 25% ammonia in 15.0 ml ethanol. To grow a layer of 50 nm fluorescent silica on the rods, 395 μ l TES was added to this dispersion, together with the FITC-APS dye (1.3 mg FITC coupled to 8.4 μ l APS in 250 μ l ethanol stirred overnight).

Stable suspensions of rods in water were sedimented (in normal gravity) at different concentrations. To achieve low ion concentrations, water was deionized with an ion exchange resin.

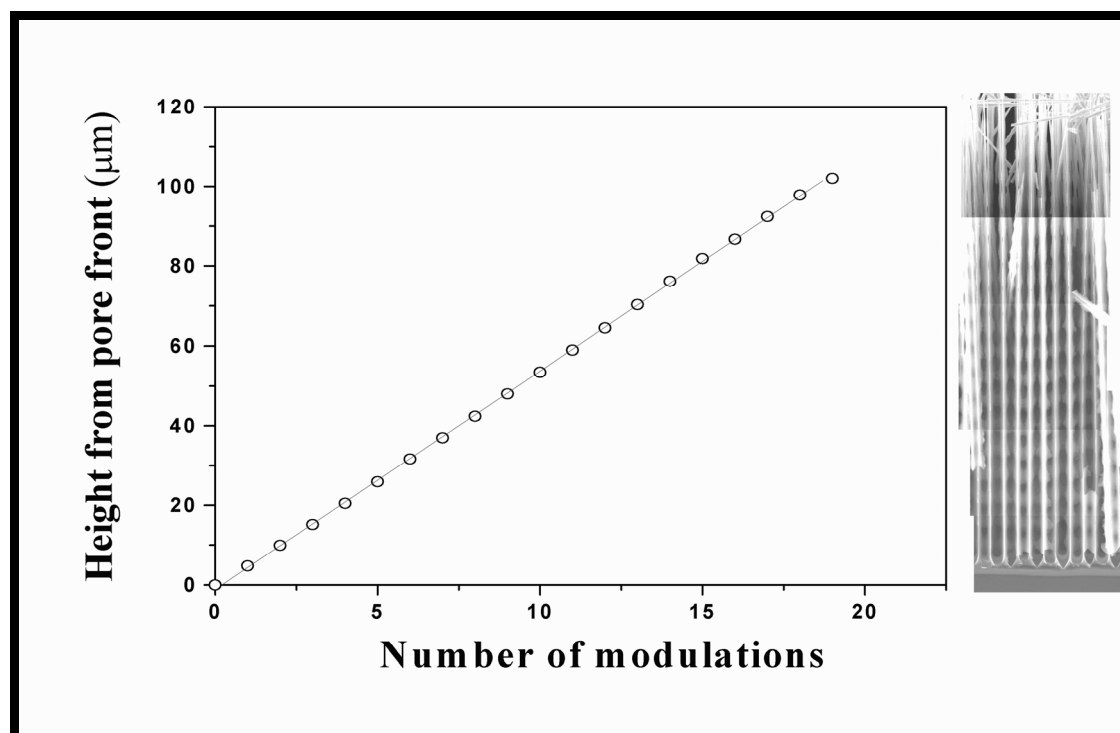


Fig. 2.5. Silicon etched to a depth of $\sim 100 \mu\text{m}$. 20 modulations are visible. A plot of the height of the rods at the pore front versus the number of modulations shows a constant etching rate, with a modulation length of $5.5 \mu\text{m}$. The top of the etched structure is damaged due to cleaving the sample for SEM observation.

2.3. Results and Discussion

2.3.1. Electrochemical etching of *p*-type silicon wafers

The different regimes we obtained during the electrochemical etching are shown in Figure 2.2: macropores are formed (case A), macropores are broadened (case B), and macropores start to overlap in such a way that rods are formed (case C). When currents higher than 150 mA/cm^2 were applied, the wafer was electropolished. By the proper choice of current density, we could form either pores or rods.

Alternating the current density during etching modulated the pore width; therefore in our samples we find regions where pores overlap (rods) and regions where pores do not overlap. We etched with a square wave current alternating between 100 mA/cm^2 and 67 mA/cm^2 for 1 minute each. While the pore diameter is modulated with the same frequency as the current, sharp steps in the diameter were not observed. Instead, a gradual transition from wide to thin pores (and vice versa) was observed. We analyzed SEM images of the electrochemically etched wafers to measure the polydispersity in modulation lengths and pore diameters. Under ideal etch conditions, each modulation length was extremely reproducible and independent of depth or location on the wafer. This can be seen from the constant slope of etching depth versus the number of complete modulation cycles in Figure 2.5.

We also found the local variations in pore diameter to be immeasurably small, i.e. pores within a few mm of each other were the same size to within tens of nm. Also, these pores did not narrow or widen with depth. Over larger distances across the wafer, slight variations in diameter on the order of 100 nm could be seen. Regions of uniform pore diameter formed alternating rings with widths of $\sim 0.5 \text{ cm}$. This ring pattern suggests that the diameter polydispersity was caused by variations in the

silicon induced during the wafer growth, e.g. variations in boron doping concentration. A locally higher or lower dopant level can cause local differences in etching kinetics. For instance, a locally higher dopant level could cause a higher flux of holes to the pore tips, which gives wider pores or smaller rods since locally more silicon will be etched.

Lehmann showed that for electrochemical etching of pores in at n-type wafers the etch rate slowly decreased in depth³¹. This was attributed to a decrease in the HF concentration at the pore tips, because of diffusion. In our experiments, in which we used etch rates up to 6.5 times higher, no decrease was observed as can be seen from the straight line in etch depth as a function of the number of modulation cycles in Figure 2.5. Even at an etch depth of 100 μm , the HF diffuses fast enough to the pore tips. However, we also performed similar experiments tests at lower temperature (25 $^{\circ}\text{C}$) and surprisingly we always found widening of pores even at etch depths of 10-20 μm . Under these conditions it was not possible to modulate the pores in a regular fashion, therefore, we could not determine whether the etch rate changed with the widening of the pores.

2.3.2. Fine tuning silicon structures

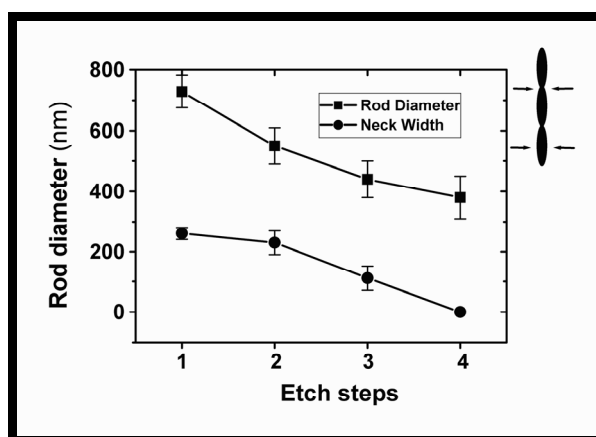


Fig. 2.6. Thickness of the rods as a function of the number of etch steps. One etch step consists of oxidation at 950 $^{\circ}\text{C}$ and etching with 3.75 M HF. The error bars are given by the polydispersity in thickness, caused mainly by the non-constant doping level. The arrows in the inset indicate the locations at which the rod diameter and neck width were measured.

To increase the pore size further and produce isolated modulated rods we oxidized the structures in air and dissolved the silica in 3.75 M HF. In the example shown in Figure 2.4 the oxidation/HF-dissolution cycle was repeated 4 times until the desired rod thickness was obtained. In each cycle the average diameter of the silicon rods was reduced by ~ 125 nm. Figure 2.6 shows a plot of the rod diameter after each oxidation/HF-etch cycle. This method allows us to control the diameter to within tens of nanometers. Figure 2.4 shows that thin rods (maximum rod diameters of 400 ± 50 nm) were etched from initially thick silicon structures (maximum rod diameters of 725 ± 50 nm). While Figure 2.4 shows results for rods produced with five modulation cycles, identical results were obtained with rods after twenty modulation cycles (Figure 2.5). After the desired rod thickness was achieved, the particles could be removed by agitating the wafer in water or ethanol. The intensity of the agitation determined the amount of rods that were removed from the wafer.

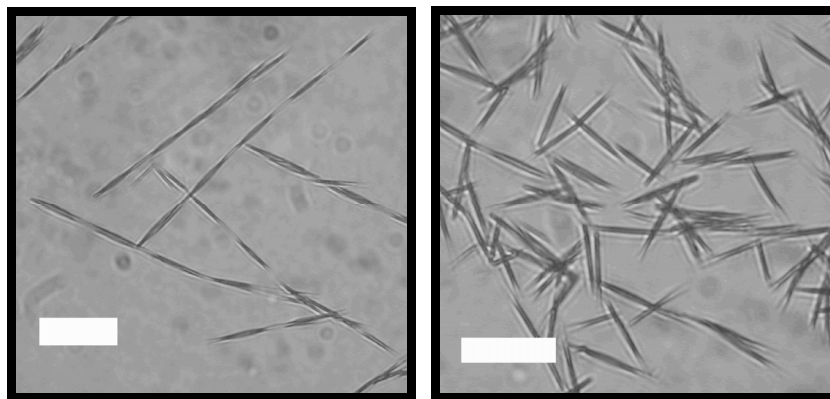


Fig 2.7. Breaking up rods at the indentations: The rods are removed from the silicon wafer by flushing with water. The scale bar represents 5 μm .

(left) Optical microscope picture taken after only flushing the silicon wafer with water, no sonication.

(right) Optical microscope picture taken after 60 min sonication, result: single particles.

For example, ultrasonication of the wafer in water caused all of the rods to break off from the wafer within seconds. By contrast, applying a mild water jet to the surface of the wafer caused only the thinnest rods to fall off. This result proved to be useful for reducing the polydispersity in rod diameter. Using a mild water jet to rinse off the rods allowed rings of the thinnest rods to be removed from the wafer, while rings of thicker rods remained attached.

Following a rinse, the thicker rods that remained on the wafer could be further etched. In this way all of the rods removed from the wafer had a minimum diameter of (100 ± 25) nm and an average diameter of (250 ± 50) nm. This rinsing method reduced but did not eliminate the diameter polydispersity. In the future, a more homogeneous boron doping process could further improve the pore diameter monodispersity.

Once removed from the wafer, the modulated rods were transformed into individual rods by sonication. Sonication causes the rods to break at the thinnest points. After a short period (less than 10 minutes) of sonication in an ultrasonic bath, the suspension still contains many rods that have more than one modulation (Figure 2.7.). A longer sonication period (60 minutes) resulted in a more monodisperse rod dispersion where more than 95% of the particles have only one modulation length (Figure 2.7). The dimensions of this final rod dispersion are: 5.5 μm length and 250 nm width, with a size polydispersity of $\sim 25\%$. Polydispersity in length is mainly caused by those particles that do not break exactly at the thinnest points.

The variation in length of the final rods might be improved by shortening the high current density period during etching. With shorter periods of high current, the thinnest regions of the modulated rod will become shorter. In this way the thin necks where segmented rods will break during sonication could be determined more precisely, resulting in a higher monodispersity. Since we already saw that the etching of rods does not immediately follow the block current that is imposed, there are limitations to the minimal length of the periods of the alternations of the current. Too drastic change in current density may also result in a sudden death of formed macropores during etching. This effect has been observed in the etching of n-type silicon³¹. We have not seen this effect at p-type silicon under comparable conditions.

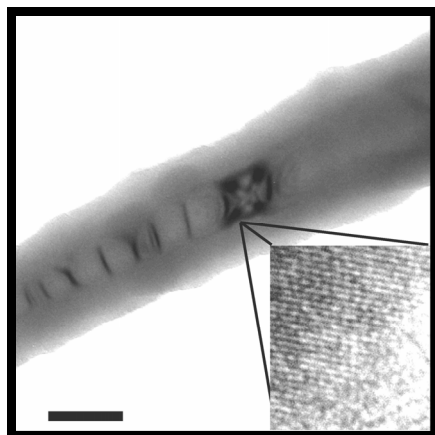


Fig. 2.8. HRTEM of a silicon rod on which silica was grown (scale bar represents 200 nm). The inset is a further magnification of the boundary between the crystalline silicon and the amorphous silica layer. The crystalline part shows different dark regions in the HRTEM picture, probably caused by stress exerted by thermal silica, during thermal oxidation. Stress in the crystal plane and an unknown viewing angle hinders the exact determination of the lattice spacing.

2.3.3. Growth of fluorescent silica on the rods

Stöber growth was used to coat silicon rods in two different experiments; the rods were coated either while dispersed as colloidal particles or they were coated before dispersing when they were still attached to the wafer.

In the first experiment fluorescent silica growth on silicon particles according to the method of van Blaaderen ⁴¹ resulted in coated particles, with a layer of 50-100 nm fluorescently labeled silica. During growth of silica on the rods silica particles formed as new nuclei, since the rod concentration was low ($\sim 2 \cdot 10^9$ particles). These secondary nucleated particles could easily be removed from the rods in repeated centrifugation with a table centrifuge (15 min 750 rpm), by allowing the rods to sediment and refreshing the supernatant containing small particles. Figure 2.8. shows a HRTEM picture of a silica-coated silicon rod. The silica layer can be clearly distinguished from the silicon core. For example, the silicon core shows dark regions, likely stress induced during thermal oxidation. Also, the transition from the silicon core to the silica shell can be clearly identified by the change in atomic structure from ordered (crystalline silicon) to disordered (amorphous silica).

In the second experiment, a sample (1 cm^2) that was supercritically dried after the last etch step was then oxidized with the rods still attached to the wafer, by placing it in the oven at 950 °C overnight. This resulted in freestanding silica rods with very few sintered connections. After that, the completely oxidized silica rods still on the wafer were coated with a fluorescent silica layer, according to a method of Vossen and co-workers.⁴² This method allows an accurate control of silica growth on the surface of small silicon structures by carrying out the growth in a dispersion of silica spheres. The amount of TES that was added was based on the combined surface area of the rods and the added 1030 nm spheres. Figure 2.9. shows a confocal microscope image of fluorescently labeled, silica-coated rods in a refractive index matching solution of 88% DMSO in water. The index-matched silica rods become translucent and the fluorescence intensity increases at the overlapping regions. This suggests that most, if not all, of the silicon has been thermally oxidized. These index matched fluorescent rods will allow a 3D analysis of concentrated suspensions.

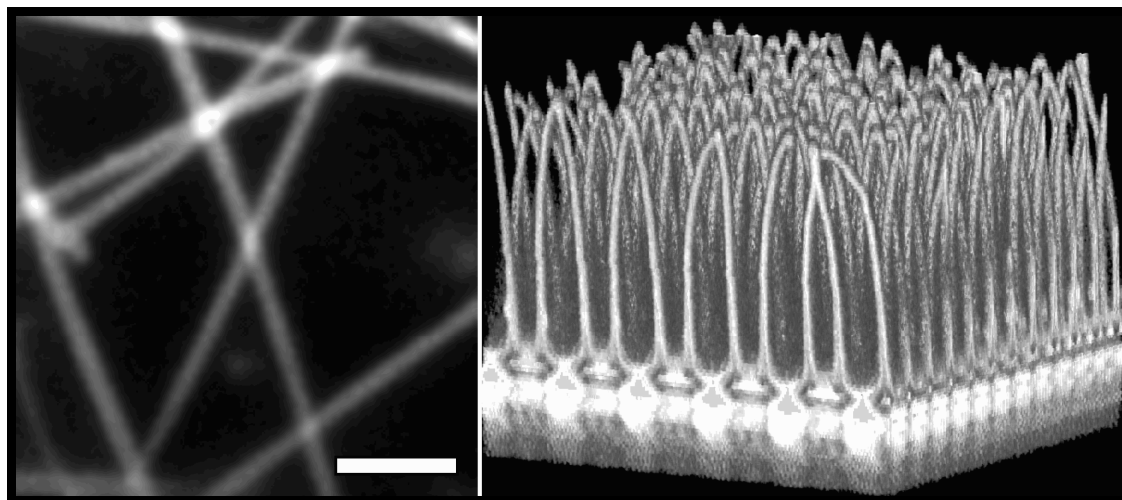


Fig. 2.9. Fluorescence confocal microscopy images (488 nm excitation) of FITC labeled silica rods in solution (**left**), FITC labeled silica rods on a wafer (**right**). (The scalebar represents 2.5 micrometer)

An example of a reconstructed 3D image of fluorescent rods on the wafer is shown in Figure 2.9. A stack of scans in the focal plane parallel to the wafer (x-y) at different heights (z) was combined to obtain the 3D-picture.

2.3.4. Phase behaviour of rods

Suspensions of all-silicon rods in demineralized water were stable; no aggregated clusters of rods were found. This stability is very likely enhanced by monolayers of silica on the silicon surface ('native oxide'). After growth of a thin layer of fluorescent silica the particles were charged and the interaction potential could be tuned by the salt concentration of the suspension; such suspensions were stable for at least several weeks. We looked at both thin and thick sediments of rods in water, which produced low and relatively high concentrations of rods, respectively. We also looked at sediments of diluted rod suspensions in highly deionized water (see Figure 2.10). The water was deionized by mixing it for at least 12 hours with ion exchange resin. It can be seen that with increasing rod concentration in the suspension, the ordering in the sediment increases.

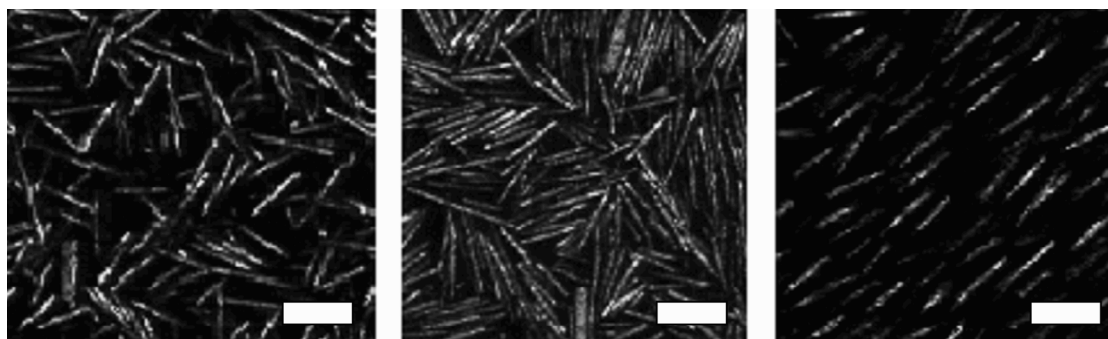


Fig. 2.10. Confocal reflection images of sedimented silicon rods in water with: Low rod concentrations (**left**), high rod concentrations (**middle**) and low rod concentrations at low ionic strength after deionization (**right**). (The scalebar represents 5 micrometer).

At lower ion concentrations particles will repel each other at larger distances, since their charges are less screened. In this case particles align at much lower concentrations and the ordered domains are larger than in water with higher ion concentration.

These experiments show qualitatively the expected dependence of ordering effects on particle concentration and charge. They show that we can control the particle interaction potential via the ion concentration

In future, full 3D analysis of ordered concentrated dispersions with FITC-silica coated rods should be possible.

2.4. Conclusions and Outlook

We have shown that under the appropriate conditions it is possible to etch silicon rods from p-type silicon wafers and fine-tune their thickness by iterative oxidation and HF-etching steps. We succeeded in etching regular deep pores with alternating thickness in silicon wafers. The dimensions of these multisegmented structures can be well tuned and turned into single silicon rods that display liquid crystalline phase behavior, with interesting properties for photonic applications. Coating of pure silica rods with a fluorescent layer opens a promising route concentrated dispersions of these rods quantitatively in real space on a single particle level.

Acknowledgements.

John Kelly is thanked for useful discussions, Anton Kemmeren is thanked for his assistance in the etching experiments at Philips Research and Maurits Weeda and Maxime Mellier are thanked for the explorative work on p-type silicon etching at Philips Research. Hans Meeldijk is thanked for the HRTEM measurements.

The work presented here was done together with Patrick Johnson. This work was financially supported by the Foundation for the Fundamental Research of Matter (FOM), which is part of The Netherlands Organization for Scientific Research (NWO).

2.5. References

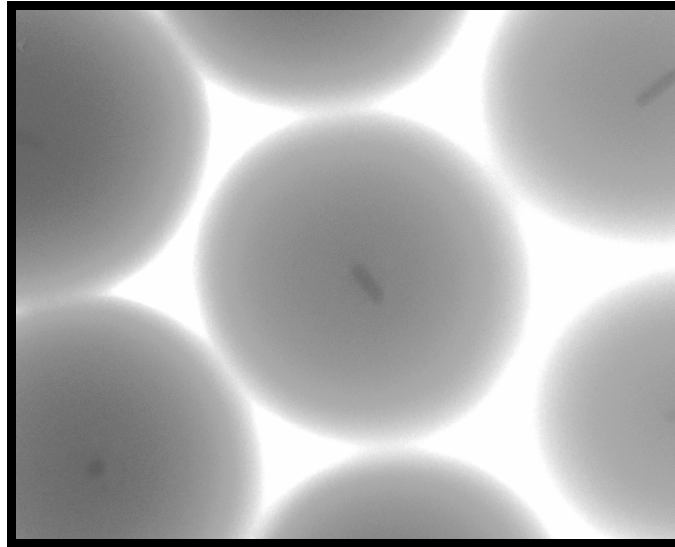
1. Xia, Y.; Yang, P.; Sun, Y.; Wu, Y.; Mayers, B.; Gates, B.; Yin, Y.; Kim, F.; Yan, H., *One-Dimensional Nanostructures: Synthesis, Characterization, and Applications*. *Advanced Materials* **2003**, 15, (5), 353-389.
2. Vroege, G. J.; Lekkerkerker, H. N. W., *Phase transitions in lyotropic colloidal and polymer liquid crystals*. *Reports on Progress in Physics* **1992**, 55, (8), 1241-1309.
3. van Blaaderen, A.; Wiltzius, P., *Real-Space Structure of Colloidal Hard-Sphere Glasses*. *Science* **1995**, 270, (5239), 1177-1179.
4. van Blaaderen, A.; Ruel, R.; Wiltzius, P., *Template-directed colloidal crystallization*. *Nature* **1997**, 385, (6614), 321-324.
5. Kegel, W. K.; van Blaaderen, A., *Direct Observation of Dynamical Heterogeneities in Colloidal Hard-Sphere Suspensions*. *Science* **2000**, 287, (5451), 290-293.
6. Gasser, U.; Weeks, E. R.; Schofield, A.; Pusey, P. N.; Weitz, D. A., *Real-Space Imaging of Nucleation and Growth in Colloidal Crystallization*. *Science* **2001**, 292, (5515), 258-262.
7. Yethiraj, A.; van Blaaderen, A., *A colloidal model system with an interaction tunable from hard sphere to soft and dipolar*. *Nature* **2003**, 421, (6922), 513-517.
8. van Blaaderen, A., *From the de broglie to visible wavelengths: Manipulating electrons and photons with colloids*. *MRS Bulletin* **1998**, 23, (10), 39-43.
9. Dassanayake, U.; Fraden, S.; Blaaderen, A. v., *Structure of electrorheological fluids*. *Journal of Chemical Physics* **2000**, 112, (8), 3851-3858.
10. Yi, C.; Lieber, C. M., *Functional Nanoscale Electronic Devices Assembled Using Silicon Nanowire Building Blocks*. *Science* **2001**, 291, (5505), 851.
11. Dargys, A.; Kudrotas, J., *Handbook on Physical Properties of Ge, Si, GaAs and InP*. Academic Press: New York, : 1975.
12. Yin, Y.; Xia, Y., *Self-Assembly of Monodispersed Spherical Colloids into Complex Aggregates with Well-Defined Sizes, Shapes, and Structures*. *Advanced Materials* **2001**, 13, (4), 267-271.
13. Velikov, K. P.; van Dillen, T.; Polman, A.; van Blaaderen, A., *Photonic crystals of shape-anisotropic colloidal particles*. *Applied Physics Letters* **2002**, 81, (5), 838-840.
14. Birner, A.; Wehrspohn, R. B.; Gösele, U. M.; Busch, K., *Silicon-Based Photonic Crystals*. *Advanced Materials* **2001**, 13, (6), 377-388.
15. Onsager, L., *The Effects of Shape on the Interaction of Colloidal Particles* *Annals of the New York Academy of Sciences* **1949**, 51, (4), 627-659.
16. Stroobants, A.; Lekkerkerker, H. N. W.; Odijk, T., *Effect of electrostatic interaction on the liquid crystal phase transition in solutions of rodlike polyelectrolytes*. *Macromolecules* **1986**, 19, (8), 2232-2238.
17. Frenkel, D.; Mulder, B. M., *The hard ellipsoid-of-revolution fluid*. *Molecular Physics* **1985**, 55, (5), 1171 - 1192.
18. Frenkel, D.; Lekkerkerker, H. N. W.; Stroobants, A., *Thermodynamic stability of a smectic phase in a system of hard rods*. *Nature* **1988**, 332, (6167), 822-823.

19. Bolhuis, P. G.; Stroobants, A.; Frenkel, D.; Lekkerkerker, H. N. W., *Numerical study of the phase behavior of rodlike colloids with attractive interactions*. Journal of Chemical Physics **1997**, 107, (5), 1551-1564.
20. Fraden, S.; Maret, G.; Caspar, D. L. D.; Meyer, R. B., *Isotropic-nematic phase transition and angular correlations in isotropic suspensions of tobacco mosaic virus*. Physical Review Letters **1989**, 63, (19), 2068.
21. Tracy, M. A.; Pecora, R., *Synthesis, characterization, and dynamics of a rod/sphere composite liquid*. Macromolecules **1992**, 25, (1), 337-349.
22. Pelletier, O.; Davidson, P.; Bourgaux, C.; Livage, J., *The effect of attractive interactions on the nematic order of V2O5 gels*. Europhysics Letters **1999**, 48, (1), 53-59.
23. Maeda, H.; Maeda, Y., *Atomic Force Microscopy Studies for Investigating the Smectic Structures of Colloidal Crystals of β -FeOOH*. Langmuir **1996**, 12, (6), 1446-1452.
24. Buining, P. A.; Philipse, A. P.; Lekkerkerker, H. N. W., *Phase Behavior of Aqueous Dispersions of Colloidal Boehmite Rods*. Langmuir **1994**, 10, (7), 2106-2114.
25. van Bruggen, M. P. B.; Dhont, J. K. G.; Lekkerkerker, H. N. W., *Morphology and Kinetics of the Isotropic-Nematic Phase Transition in Dispersions of Hard Rods*. Macromolecules **1999**, 32, (7), 2256-2264.
26. Maeda, H.; Maeda, Y., *Liquid Crystal Formation in Suspensions of Hard Rodlike Colloidal Particles: Direct Observation of Particle Arrangement and Self-Ordering Behavior*. Physical Review Letters **2003**, 90, (1), 018303.
27. Morales, A. M.; Lieber, C. M., *A laser ablation method for the synthesis of crystalline semiconductor nanowires*. Science **1998**, 279, (5348), 208.
28. Kamins, T. I.; Williams, R. S.; Chen, Y.; Chang, Y. L.; Chang, Y. A., *Chemical vapor deposition of Si nanowires nucleated by $TiSi_2$ islands on Si*. Applied Physics Letters **2000**, 76, (5), 562.
29. Lew, K.-K.; Reuther, C.; Carim, A. H.; Redwing, J. M.; Martin, B. R., *Template-directed vapor-liquid-solid growth of silicon nanowires*. Journal of Vacuum Science & Technology B: Microelectronics and Nanometer Structures **2002**, 20, (1), 389-392.
30. Yin, Y.; Gates, B.; Xia, Y., *A Soft Lithography Approach to the Fabrication of Nanostructures of Single Crystalline Silicon with Well-Defined Dimensions and Shapes*. Advanced Materials **2000**, 12, (19), 1426-1430.
31. Lehmann, V., *The Physics of Macropore Formation in Low Doped n-Type Silicon*. Journal of The Electrochemical Society **1993**, 140, (10), 2836-2843.
32. van den Meerakker, J. E. A. M.; van Kats, C. M.; van Blaaderen, A. *Dispersion of nanowires of semiconducting material*
Patent: EP 02079837.7 (filed November 18, 2002).
33. Lehmann, V., *Electrochemistry of Silicon*. Wiley VCH: Weinheim,; 2002.
34. Lehmann, V.; Ronnebeck, S., *The Physics of Macropore Formation in Low-Doped p-Type Silicon*. Journal of The Electrochemical Society **1999**, 146, (8), 2968-2975.
35. Müller, F.; Birner, A.; Schilling, J.; Gösele, U.; Kettner, C.; Hänggi, P., *Membranes for Micropumps from Macroporous Silicon*. Physica Status Solidi A **2000**, 182, (1), 585-590.
36. van den Meerakker, J. E. A. M.; Elfrink, R. J. G.; Roozeboom, F.; Verhoeven, J. F. C. M., *Etching of Deep Macropores in 6 in. Si Wafers*. Journal of The Electrochemical Society **2000**, 147, (7), 2757-2761.

37. Zhang, X. G., *Electrochemistry of Silicon and its oxide*. Kluwer Academic/Plenum Publishers: New York.: 2001.
38. van den Meerakker, J. E. A. M.; Elfrink, R. J. G.; Weeda, W. M.; Roozeboom, F., *Anodic silicon etching; the formation of uniform arrays of macropores or nanowires*. *Physica Status Solidi A* **2003**, 197, (1), 57-60.
39. Chao, K. J.; Kao, S. C.; Yang, C. M.; Hseu, M. S.; Tsai, T. G., *Formation of High Aspect Ratio Macropore Array on p-Type Silicon*. *Electrochemical and Solid-State Letters* **2000**, 3, (10), 489-492.
40. van den Meerakker, J. E. A. M.; Mellier, M. R. L., *Kinetic and Diffusional Aspects of the Dissolution of Si in HF Solutions*. *Journal of The Electrochemical Society* **2001**, 148, (3), G166-G171.
41. van Blaaderen, A.; Vrij, A., *Synthesis and characterization of colloidal dispersions of fluorescent, monodisperse silica spheres*. *Langmuir* **1992**, 8, (12), 2921-2931.
42. Vossen, D. L. J.; Dood, M. J. A. d.; Dillen, T. v.; Zijlstra, T.; Drift, E. v. d.; Polman, A.; Blaaderen, A. v., *Novel Method for Solution Growth of Thin Silica Films from Tetraethoxysilane*. *Advanced Materials* **2000**, 12, (19), 1434-1437.

Chapter 3

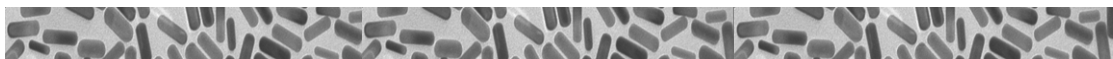
The synthesis of silica coated gold rods



Abstract

In this chapter we show that by solution based chemistry gold rods with an aspect ratio around 4 can be grown in bulk that are monodisperse and stable enough that they self organize after drying in 2D (smectic like) and thin 3D locally ordered structures. We succeeded in growing silica onto the gold rods, ultimately allowing us to turn the rods to an almost spherical shape through a continuous silica growth of a 310 nm silica shell. These particles also show local ordering on a TEM grid and are monodisperse enough to form 3D colloidal crystals.

Applying a PVP coating as precursor for silica growth and transfer of a dispersion of gold rods from water to an isopropanol/ammonia/water mixture was found to cause partial aggregation of the suspension with as a result multiple gold rods ending up in a single silica particle. In contrast mesoporous silica growth onto gold rods resulted in a suspension with almost exclusively single anisotropic gold cores in a silica particle. Therefore the growth of a mesoporous silica layer on gold rods seems a more promising route to obtain monodisperse spherical silica particles with an anisotropic gold core that can be used to grow colloidal crystals from.



3.1 Introduction

The interest in gold nanoparticles has a long history. Already in the 5th century B.C. gold particles have been used as a colorant to stain glasses and ceramics¹. Nevertheless it took many centuries before Michael Faraday became the first to recognize that the color is due to metallic gold² in colloidal form; Michael Faraday's famous gold sol can still be visited in the royal institution of Great Britain. Ever since, the gold nanoparticle synthesis has been studied. Since 1990 the number of publications on metal nanoparticles has grown exponentially³. Many reports of different methods to make gold nanoparticles have appeared amongst others photo-, electro-, sonochemical synthesis, template assisted synthesis, and seeded growth. For a nice review see Daniel and Astruc⁴. In the last decade also the synthesis of gold nanorods has received increasing attention⁵. A nice and well developed method to produce fairly monodisperse and size tuneable gold rods is the seeded growth method of El Sayed⁶, which is described in this chapter and is based on an improvement of Jana et al⁷. The broad attention the synthesis of gold nanorods (AuNR) has received recently can be understood if we take into account their numerous potential in biological⁸, optical, electronic and photonic applications⁵.

3.1.1. Optical properties of gold nanorods

Optical properties of gold rods can be measured by studying their absorption of light. In a dilute colloidal suspension with N particles per unit volume, the measured attenuation of light of intensity I_0 over an optical path length of x cm in spectrophotometer is given in differential form as:

$$\frac{dI(x)}{dx} = -NC_{ext}I(x) \quad (4.1)$$

Integration of eq. 4.1 results in an expression of the absorbance A of the suspension.

$$A = \log_{10} \frac{I_0}{I(x)} = \frac{NC_{ext}x}{2.303} \quad (4.2)$$

Here, C_{ext} is the extinction cross-section of a single particle. The optical properties of gold nanorods are unique in the sense that they have two intense surface plasmon resonance peaks, a longitudinal surface plasmon peak and a transverse surface plasmon peak corresponding to the oscillation of the free electrons along and perpendicular to the long axis of the rods⁹⁻¹¹. With control of the aspect ratio of the gold nanorods their optical properties can be tuned independently.

Already in 1912 Gans¹² predicted that for small ellipsoids the surface plasmon mode in the absorption spectrum would split into two distinct modes, a transverse mode and a longitudinal mode. To explain the optical properties of sphero-capped cylinders it is common to treat them as ellipsoids, so that the classical Gans theory can be applied. The polarizability ($\alpha_{x,y,z}$) of an ellipsoid is given by :

$$\alpha_{x,y,z} = \frac{4\pi abc(\epsilon_{Au} - \epsilon_m)}{3\epsilon_m + 3L_{x,y,z}(\epsilon_{Au} - \epsilon_m)} \quad (4.3)$$

Here a, b , and c refer to the length of the ellipsoid along the x, y and z axis ($a > b = c$), ϵ_{Au} the dielectric function of gold, ϵ_m the dielectric function of the medium at optical frequencies and $L_{x,y,z}$ is the depolarization factor for the respective axis, which is given by:

$$L_x = \frac{1-e^2}{2} \left(-1 + \frac{1}{2e} \ln \frac{1-e^2}{1+e^2} \right)$$

$$L_{y,z} = \frac{1-L_x}{2} \quad (4.4)$$

In this expression e^2 is the rod ellipticity given by eq (4.5)

$$e^2 = 1 - (b/a)^2 \quad (4.5)$$

Since the polarizability is related directly to the extinction of light by

$$C_{ext} = k \text{Im}(\alpha) \quad (4.6)$$

Eq. 4.6 can now be inserted in Eq. (4.2) which then gives an expression for the absorbance of a dilute suspension of rods.

3.2 Experimental

3.2.1. Gold rods synthesis

Chemicals. Hydrogen tetrachloroaurate(III) trihydrate ($\geq 99.9\%$), L(+)-ascorbic acid (99%) were obtained from Sigma-Aldrich . A number of polyvinylpyrrolidone ((PVP) batches were used varying in brand and/or average molar masses. PVP with average molecular weight (MW) of 3.5 kg/mol and 58 kg/mol were obtained from Acros Organics (art. # 27614, 22754), PVP with MW of 10 kg/mol (PVP10, lot106K0130 and 105K0120), 40 kg/mol (PVP40), 360 kg/mol (PVP360) were obtained from Sigma-Aldrich and PVP with MW of 24 kg/mol was obtained from Fluka (81400).

Cetyltrimethylammonium bromide ((CTAB) Sigma (H9151), Fluka (52370) or Aldrich (85,582-0). Sodium borohydride, poly(sodium-*p*-styrenesulfonate) ((PSS), MW 70 kg/mol) and poly(allylamine hydrochloride) ((PAH) MW, 15 kg/mol) were obtained from Aldrich. Silver nitrate was obtained from Riedel-de Haën. Sodium chloride (p.a.) was obtained from Acros. Isopropanol and ammonia (29.1 wt.% in water) were obtained from Merck. Tetraethoxysilane (TES) and methanol (p.a.) were obtained from Fluka. Deionized water was used in all experiments.

Characterization

All synthesized gold rods were imaged by Transmission Electron Microscopy (TEM) on a Philips Tecnai10 or Philips Tecnai12. TEM images were prepared by drying drops of suspensions and let them evaporate on copper TEM grids with a polymer carrier film (Pilioform coating). Absorption spectra were taken on a HP 8452A Diode Array Spectrophotometer or on a Bruker Vertex 70 FTIR.

Synthesis

Gold rods were made by the seeded growth method of El-Sayed et al. ⁶. In this synthesis small gold seeds are added to a gold salt growth solution. Gold seeds were made by reducing a hydrogen tetrachloroaurate solution with sodium borohydride. In a typical experiment the seeds were made by addition of 0.60 ml ice-cold freshly

prepared 10 mM sodiumborohydroxide solution to a vigorously stirred 10 ml 0.1 M CTAB, 2.5 mM hydrogentetrachloroaurate solution.

The growth solution was made by addition of 50 ml 5 mM hydrogen tetrachloroaurate solution to 50 ml 0.2 M CTAB and 2.5 ml 4 mM silver nitrate. 0.70 ml 78.8 mM ascorbic acid was added to mildly reduce the gold salt. The temperature was kept constant at 30°C. Finally, 0.12 ml of the freshly prepared gold seeds was added to the growth solution. The reaction mixture was gently stirred overnight.

Seeded gold rod growth

In order to get gold rods with a higher aspect ratio we tried 2 known methods. In the first method we used a synthesis procedure according to El-Sayed⁶ which requires a surfactant mixture of CTAB and BDAC. The procedure followed for making the longer gold rods is as described above, but instead of using 0.2 M CTAB in the growth solution we used a mixture of 0.15M BDAC and 0.055M CTAB. In a different experiment we tried to further reduce the gold salt solution by extra feeds of ascorbic acid, according to a method by Park¹⁰. In this experiment gold rods were made in the procedure described in section 3.2.1. and an extra amount of ascorbic acid (AA) was added to the gold rod reaction mixture: To 10 ml of the gold rod solution an additional feed of 7 µl 78.8 mM AA was added twice at a time interval of 30 minutes.

3.2.2. Silica growth on gold rods

After the synthesis of the gold rods silica was grown following the method described by Pastoriza-Santos¹³. To remove excess of CTAB, the dispersion was centrifuged 2 times and redispersed in deionized water. To this end the dispersion was put in polypropylene centrifuge tubes and centrifuged 45 min 8000 rpm (7940 g) on a Sorvall (Du Pont) ultracentrifuge. This centrifugation was performed 1 day after the synthesis of the gold rods. Polyelectrolyte solutions (PAH and PSS) were made by adding 2 g/L polyelectrolyte to a 6 mM sodium chloride solution. First the sediment of the CTAB coated gold rods (AuNR@CTAB)ⁱ was redispersed in 50 ml PSS solution in water (final concentration 6 mM sodium chloride and 2 g/L PSS). This dispersion was centrifuged twice, 45 min 5000 rpm (3100 g), the sediment was redispersed in 50 ml deionized water, then it was mixed with 50 ml PAH solution in water (final concentration 6 mM sodium chloride and 2 g/L PAH). Again it was centrifuged twice, 45 min 5000 rpm and redispersed in water. In the last coating step it was mixed with a 50 ml PVP (4 g/L) solution and stirred overnight. The coating with PVP was performed with different batches of PVP varying in MW or supplier (for a list of all PVP batches we tried, see chemicals section).

To coat the AuNR@CTAB@PSS@PAH@PVP with a layer of silica, the dispersion needs to be transferred to an alcoholic suspension, therefore the excess of PVP was removed by centrifuging the dispersion twice at 2500 rpm (780 g) for 2 hrs. Low centrifugation speeds were applied to prevent aggregation. The resulting sediment was redispersed in a volume of 2.0 ml water, 3.0 ml isopropanol was added under agitation and sonication of the dispersion. Then 4.3 ml of an ammonia solution in isopropanol (4.0 vol% (29.1 wt% NH₃ in water) in isopropanol) was added dropwise again under simultaneous agitation and sonication. The last step was addition of 0.40 ml of a 1% v/v TES/ethanol solution. The reaction mixture was

ⁱ The use of the symbol @ is frequently used in literature as a short notation for core shell particles. AuNR@CTAB is used to describe gold nanorods coated with a layer of CTAB. To our knowledge this convention was introduced by Liz Marzan and Mulvaney (*New J. Chem.*, 1998, 22, 1285 – 1288)

stirred overnight. After that the particles were stable to continue with growing a thicker silica layer onto the gold rods.

3.2.3. Seeded silica growth

A thick silica layer on the silica coated gold rods was obtained by additional seeded growth on the AuNR@SiO₂. The silica coating described in the previous paragraph could have been repeated a few times, but this would have resulted in small silica layers (10-20 nm each step) and the risk of a secondary nucleation is present in each step. Therefore, we decided to apply a continuous seeded growth method as described by Giesche¹⁴ for the silica coated gold rods. 5 ml AuNR@SiO₂ with a silica layer of 50 nm after 2 batchwise additions of TES were dispersed in the isopropanol/ammonia mixture. The number of particles at the start of the synthesis was $\sim 1.7 \cdot 10^{12}$ particles. Two separate 10 ml feeds were added both with a syringe pump at an addition speed of 10 $\mu\text{l}/\text{min}$. The TES feed contained 1 vol% TES in ethanol, the ammonia feed contained 0.8 ml ammonia, 2.2 ml water, and 7 ml ethanol.

The final concentration of ammonia in the dispersion was 0.7 M and 7.5 M water, comparable to the Giesche conditions¹⁴ for seeded silica growth. A part of the as grown particles was centrifuged to remove 2nd nucleated particles and a thicker silica layer was grown using the same concentrations of chemicals for the feed and seed reaction mixture.

3.2.4. Mesoporous silica growth

For coating of a mesoporous layer on AuNR@CTAB the method described by Matsuura¹⁵ was followed. After the gold rod growth the AuNR@CTAB suspension was centrifuged only once and redispersed in deionized water to 2/3rd of its starting concentration. Then the pH was adjusted to 10-11 by adding 670 μl 0.1 M NaOH. Subsequently, at 30 min intervals 200 μl of 20 % v/v TES in methanol was added. The reaction was stirred overnight and centrifuged to remove possible 2nd nucleated silica and unreacted TES.

A part (10 ml, 1/10th of the total) of these mesoporous silica coated gold rods was transferred by centrifugation to a 10 M water and 0.8 M ammonia in methanol solution to grow a denser layer of silica according to the method of Matsuura¹⁵. Hereto 5 μl TES was added and the mixture was reacted overnight.

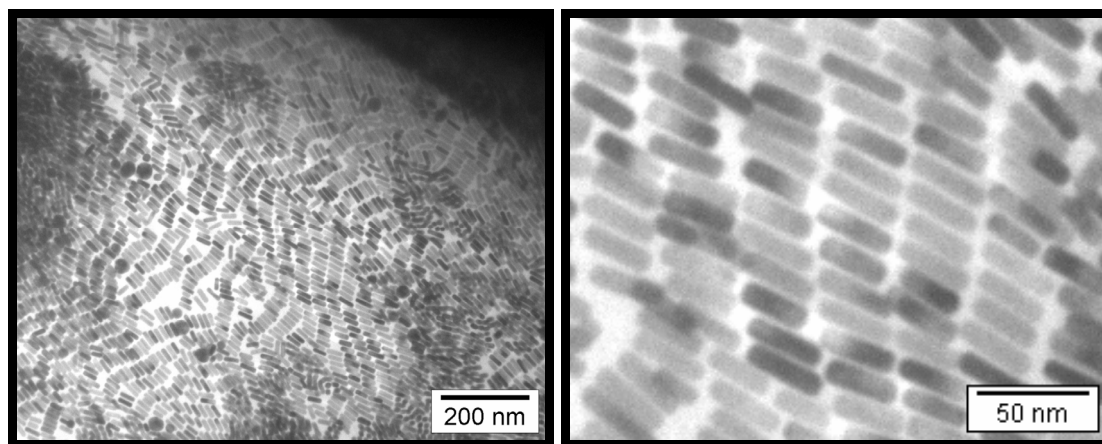


Fig 3.1. Self assembled 2D and thin 3D patterns of gold rods 11nm by 40nm (aspect ratio 3.6) on a TEM grid.(left) overview, (right) zoomed in, showing a 2D smectic arrangement.

3.3 Results and Discussion

3.3.1. Gold rods

Gold rods synthesized by the method of El-Sayed described in section 3.2.1. typically have dimensions of 11 nm in thickness and 35 – 50 nm in length. Therefore, they have an aspect ratio between 3.2 and 4.5. Furthermore, the rods look like spherocapped cylinders. This corresponds to a longitudinal plasmon peak in the absorption spectrum at a wavelength roughly between 700 nm and 850 nm^{9-11, 16}. The synthesis procedure for gold rods of El-Sayed⁶ is well known and well accepted as a standard procedure. Different mechanisms for rod formations have been proposed in literature. It is now believed that the rod formation is not due to a template directed growth assisted by the surfactant, but is merely caused by a preferential directional growth of specific crystal facets of the crystalline gold rods¹⁷⁻²⁰.

We found that when a drop of a dispersion of CTAB coated gold rods that were centrifuged once was spread on the piliiform polymer layer, which covered the copper TEM grid, was allowed to slowly evaporate, the particles self assembled in nice regular structures (see Figure 3.1.) resembling 2D smectic order and thin 3D order. This phenomenon has been seen by others as well and is related to a balance in the concentration of the particles, the evaporation rate of the solvent and the interactions that need to keep the particles stable when they are pressed together by surface tension effects^{10, 21-23}.

The influence of many parameters on the synthesis outcome, such as surfactant concentration (CTAB/BDAC ratio)⁶, temperature, AA concentration²⁴ and aging in time have been well studied^{5, 10, 25}. Nevertheless we find some deviations in these observations, which is unfortunately not that unusual for the synthesis of metal colloids²⁶ and described in the following.

It is known that the influence of (unknown) trace materials can have a significant influence on the final result. For instance, according to Smith and Korgel²⁷, a choice of a different supplier of the CTAB surfactant with comparable purities can already make the difference of a successful gold rod growth or no nucleation at all (!). Nevertheless, we succeeded to make gold rods from 3 different batches from Sigma, Fluka and even Aldrich (855820). Unfortunately, our attempts to find out what actually causes these differences have remained unsuccessful. However, recently it was found that trace amounts of iodide ions, serving as a key shape directing element, are of great influence on the gold rod formation. Our attempts to reproduce the work of El-Sayed⁶ to grow larger gold rods using a mixture of BDAC/CTAB all failed, making one wonder if (a lack of) minor trace impurities in the BDAC batch supplied by Fluka (13400) might have changed the result of our synthesis.

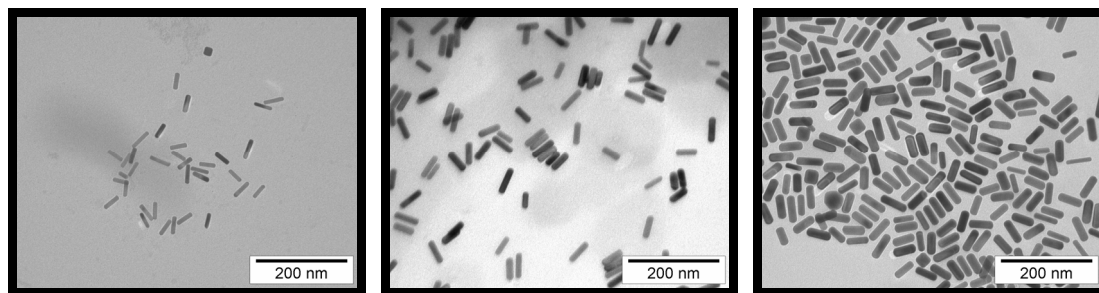


Fig.3.2. Seeded growth on gold rods by extra additions of ascorbic acid leading to larger and thicker gold rods with decreased aspect ratio (Aspect ratios of respectively 3.9, 3.3 and 2.9). (Note that the scale bar is the same for each picture).

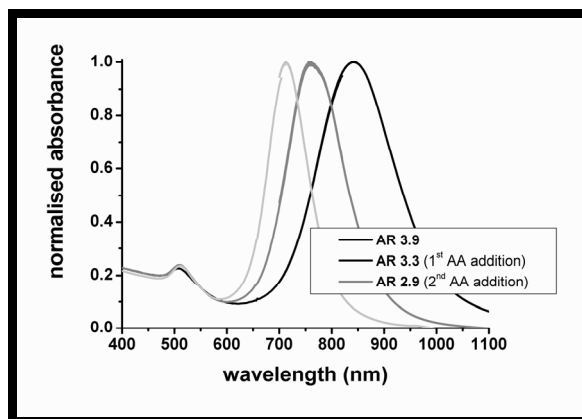


Fig. 3.3. Absorption spectra of gold rods with decreasing aspect ratio (3.9, 3.3 and 2.9) after reduction of the gold salt solution with ascorbic acid.

In our attempt to try to grow larger gold rods according to a method of Park¹⁰ we also found a remarkable difference. The CTAB assisted gold rod growth with extra AA resulted not only in longer gold rods, the particles also grew thicker and thus they resulted in smaller aspect ratio gold rods in contrast to what was expected from the reported results¹⁰. Figure 3.2 shows TEM pictures of the synthesized gold rods and the grown gold rods after one and two extra additions of AA. The gold rods prepared by the El-Sayed method⁶ measured 10.0 nm in width and 38.6 nm in length (aspect ratio 3.9). The dimensions after an extra AA reduction were $w = 14.4$ nm and $l = 48.1$ (AR= 3.3) and $w = 17.8$ nm, $l = 52.4$ nm (AR 2.9) respectively. The absorption spectra are shown in Figure 3.3. These results confirm that still not all gold salt has reacted and slowly continues to grow on nucleated rods^{5, 25}. Another deviation from what is reported in literature is the stability of the seeds. Although Murphy²⁴ reports that the seeds are stable for weeks and can be used more than once, we could only synthesize reproducible gold rod batches with freshly prepared seeds, that were added in a fixed interval (5 min) after addition of all reaction chemicals.

3.3.2. Silica growth on gold rods

For a stable silica layer growth on the gold rods the method of Pastoriza et al.¹³ was followed. Similarly as the varying results reported with the different brands of CTAB for the gold rod synthesis²⁷, we found that variation in the brand of PVP had a dramatic influence on the stability of the AuNR@CTAB@PSS@PAH@PVP particles. Severe stability problems in the AuNR@CTAB@PSS@PAH@PVP solutions were found after attempts to redisperse the synthesized rods after the PVP coating in water. A broadening or shoulder in the absorption spectrum was observed, indicating the coupling of longitudinal plasmon absorption peaks. This indicates that the gold rods in solution are forming small clusters, which could not be redispersed by sonication. When PVP was used with the same MW (10 kg/mol) the result varied with the supplier we chose. Even PVP with different lotnumbers of the same supplier (PVP10, Sigma Aldrich) we had different result, while all other parameters were kept constant.

In some cases sonication caused more aggregation. The stability of the PVP coated gold rods was improved when PVP with higher MW was used. Finally when high MW PVP was used (MW = 360 kg/mol) the rod suspension stayed stable, as was confirmed by absorption spectroscopy. The risk of bridging flocculation for higher

MW PVP, as suggested by Pastoriza¹³ was not confirmed in our experiments. Our results seem to indicate that the use of higher MW PVP stabilizes the particles better than smaller MW PVP since the gold rods are better protected against van der Waals like aggregation. Previously, this conclusion was also reached in a paper on coating (spherical gold) particles with silica²⁸.

Another risk in aggregation of the particles is a change of the reaction medium, from water to an isopropanol, water, ammonia mixture. A too sudden change of the medium can cause (partial) aggregation, for instance if the local ionic strength becomes too high, which is clearly unwanted. Therefore, the redispersed sediment in water was carefully added to a sonicated mixture of isopropanol ammonia mixture. The stability of the suspension was observed by eye, but a spectrum was also taken. If the absorption spectrum did not show a broadened longitudinal absorption peak the stability was confirmed. Nevertheless, Figure 3.4. shows seen that still $\sim 10\%$ of the single particles have more than a single gold rod covered with silica. We still succeeded in growing a silica layer of 310 nm on these gold rods. Note that the concentration of particles in the synthesis was downscaled 10-20 times compared to Giesche and that the initial growth on the PVP coated particle is rather irregular. Figure 3.4 indicates that silica coated gold rod particles will almost become spherical after growth of a thick silica shell. This relatively thick silica shell makes it possible to tune the aspect ratio of individual particles by femtosecond laser pulses as will be shown in the next chapter.

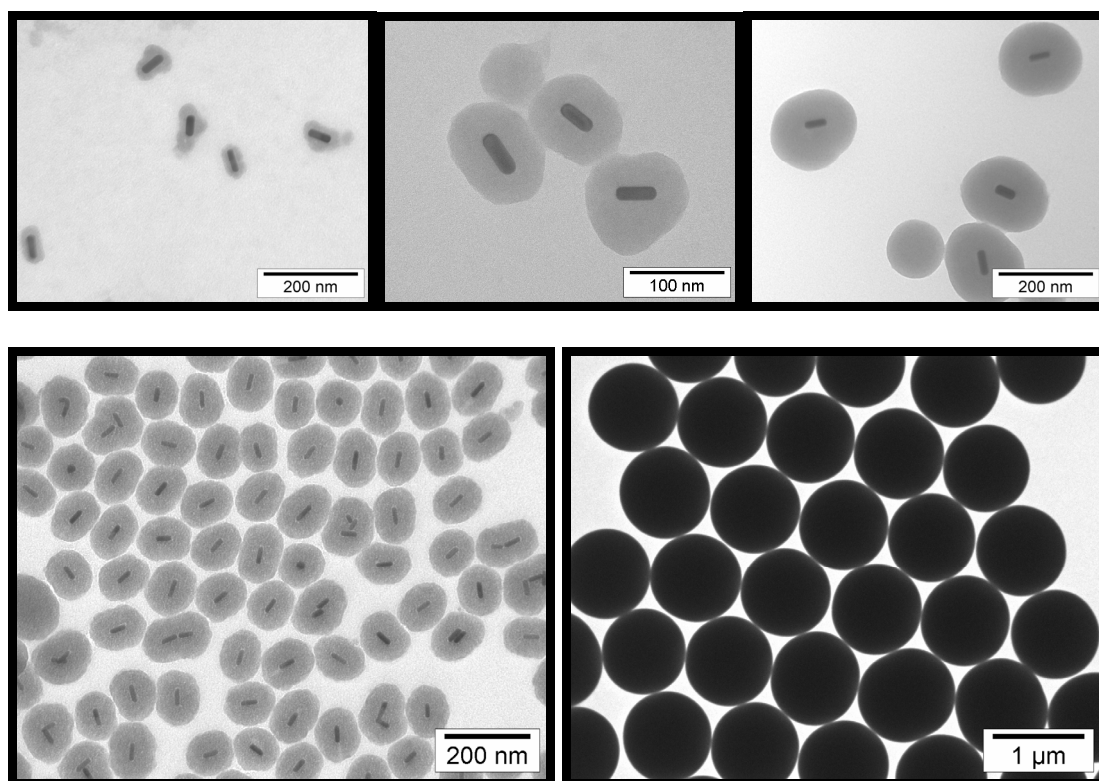


Fig 3.4. Various stages of seeded silica growth on the same gold rods. Note the irregular thickness of the silica shell at the start becoming smooth and round. With a thick silica layer there is not enough contrast at the TEM to be able to observe the gold rods inside.

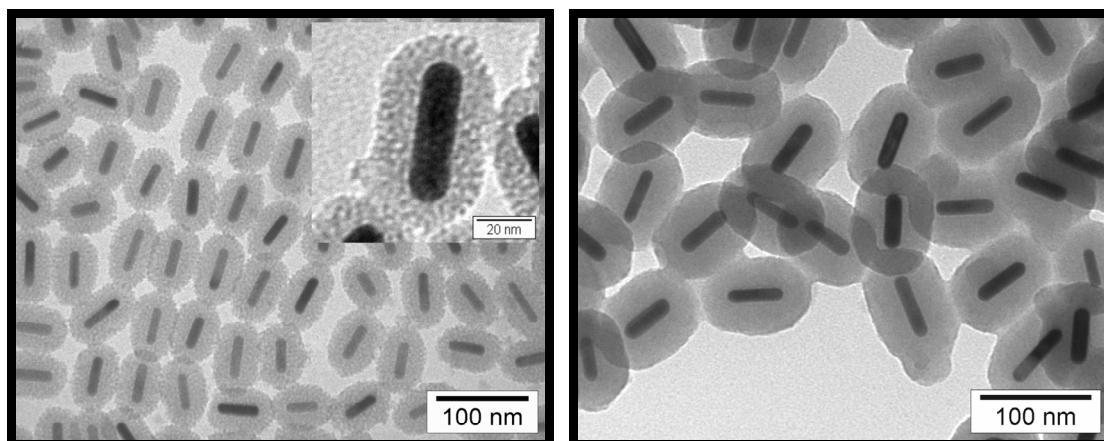


Fig. 3.5. Silica seeded growth on gold rods. (a, left) 1st mesoporous silica layer, the inset clearly shows the mesoporosity. (b, right) further seeded growth resulting in a denser silica layer, therefore the mesoporosity of the inner part becomes less visible with TEM.

3.3.3. Mesoporous silica growth

Figure 3.5.a shows gold rods with dimensions of 43.0 nm by 10.6 nm, with a mesoporous silica shell of 18 nm in thickness. The CTAB still present after centrifugation once is enough to force the silica to grow a mesoporous shell^{13, 15}. Subsequent centrifugation and further growth of silica results in a layer thickness of 28 nm thick. The extra silica layer is no longer mesoporous and thus more dense as can be seen in Figure 3.5.b. A drawback of this extra silica growth is that while the mesoporous silica growth results in a very smooth homogeneous mesoporous silica coating, where only single gold rods are coated, a more dense silica layer ~ 2-3 % of the particles forms clusters of 2-4 particles that grow together. Probably the particles stick together after the solvent transfer from water to methanol. Due to large van der Waals forces between the particles some stay connected, even after sonication. The distances measured between the gold cores within particles that had grown together (less than 40 nm) confirms early aggregation of the particles in the dense silica growth procedure. The low level of aggregation suggests it should be preventable in an optimized procedure.

3.4 Conclusions

The sometimes contrasting information about the syntheses found in^{7, 10, 24} and our own observations in the synthesis of gold nanorods confirm that it is not a straightforward synthesis and small changes can have a huge impact on the final result. However, from all reports on gold rod synthesis, we found only 2 papers that clearly reported on this sensitivity^{27, 29}.

Nevertheless, monodisperse gold rods were made and were coated with a smooth silica layer. The claim to make gold rods with an aspect ratio¹⁰ larger than 5 could not be reproduced. In contrast, our experiments resulted in *lower* aspect ratio of gold rods if ascorbic acid was added to the reaction mixture. Another known method to grow higher aspect ratio gold rods (without the use of silver ions)²⁰ failed as well. During the further growth of silica coated gold rods the stability of the dispersions is crucial for making gold rods with a thick silica layer. In the coating procedure the adsorption of PVP and subsequent cleaning is a step where stability is a problem. Also the transfer of the dispersion medium was found to give stability problems. In the

initial mesoporous silica coating this problem shows up during the subsequent silica growth on top of the mesoporous coating. Here particles were transferred from water to methanol. In case of the “Stöber-like” growth the transfer of the AuNR@CTAB@PSS@PAH@PVP from water to an isopropanol/water/ammonia mixture induced partial clustering of the rods. The fairly mild clustering suggests that conditions can be found where it can be avoided completely, which is important for use of particles in subsequent colloidal crystallization.

Acknowledgments

Menno Bergmeijer is thanked for his assistance in the gold particles synthesis. Dannis 't Hart is acknowledged for his assistance with TEM and for valuable discussions.

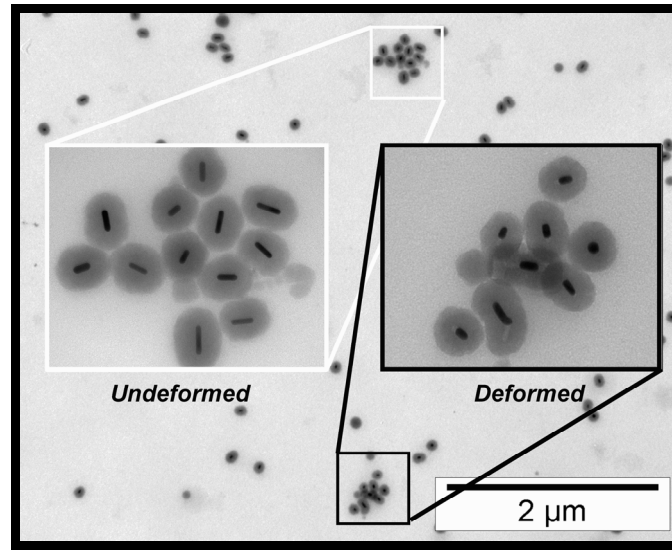
3.5 References

1. Pollard, A. P.; Heron, C., "Archaeological Chemistry" (Chapter 5). Royal Society of Chemistry: 1996.
2. Faraday, M., *The Bakerian Lecture: Experimental Relations of Gold (and Other Metals) to Light*. Philosophical Transactions of the Royal Society of London **1857**, 147, 145-181.
3. Eustis, S.; El-Sayed, M. A., *Why gold nanoparticles are more precious than pretty gold: Noble metal surface plasmon resonance and its enhancement of the radiative and nonradiative properties of nanocrystals of different shapes*. Chemical Society Reviews **2006**, 35, (3), 209-217.
4. Daniel, M-C.; Astruc, D.; *Gold Nanoparticles: Assembly, Supramolecular Chemistry, Quantum-Size-Related Properties, and Applications toward Biology, Catalysis, and Nanotechnology*. Chemical Reviews **2004**, 104, 293-346
5. Pérez-Juste, J.; Pastoriza-Santos, I.; Liz-Marzán, L. M.; Mulvaney, P., *Gold nanorods: Synthesis, characterization and applications*. Coordination Chemistry Reviews **2005**, 249, (17-18), 1870-1901.
6. Nikoobakht, B.; El-Sayed, M. A., *Preparation and Growth Mechanism of Gold Nanorods (NRs) Using Seed-Mediated Growth Method*. Chemistry Of Materials **2003**, 15, (10), 1957-1962.
7. Jana, N. R.; Gearheart, L.; Murphy, C. J., *Seed-Mediated Growth Approach for Shape-Controlled Synthesis of Spheroidal and Rod-like Gold Nanoparticles Using a Surfactant Template*. Advanced Materials **2001**, 13, (18), 1389-1393.
8. Bauer, L.-A.; Birenbaum, N. S.; Meyer, G. J., *Biological applications of high aspect ratio nanoparticles*. Journal of Materials Chemistry **2004**, 14 517 - 526.
9. Kelly, K. L.; Coronado, E.; Zhao, L. L.; Schatz, G. C., *The Optical Properties of Metal Nanoparticles: The Influence of Size, Shape, and Dielectric Environment*. Journal of Physical Chemistry B **2003**, 107, (3), 668-677.
10. Park, K. *Synthesis, characterization, and Self-assembly of size tunable gold nanorods*. Georgia, institute of technology, Georgia, 2006.
11. Prescott, S. W.; Mulvaney, P., *Gold nanorod extinction spectra*. Journal of Applied Physics **2006**, 99, (12), 123504-7.
12. Gans, R., *"Über die Form ultramikroskopischer Goldteilchen"*. Annalen der Physik **1912**, 37, 881-900.
13. Pastoriza-Santos, I.; Perez-Juste, J.; Liz-Marzán, L. M., *Silica-coating and hydrophobation of CTAB-stabilized gold nanorods*. Chemistry Of Materials **2006**, 18, (10), 2465-2467.
14. Giesche, H., *Synthesis of monodispersed silica powders II. Controlled growth reaction and continuous production process*. Journal of the European Ceramic Society **1994**, 14, (3), 205-214.
15. Gorelikov, I.; Matsuura, N., *Single-Step Coating of Mesoporous Silica on Cetyltrimethyl Ammonium Bromide-Capped Nanoparticles*. Nano Letters **2008**, 8, (1), 369-373.
16. Link, S.; Burda, C.; Nikoobakht, B.; El-Sayed, M. A., *How long does it take to melt a gold nanorod?: A femtosecond pump-probe absorption spectroscopic study*. Chemical Physics Letters **1999**, 315, (1-2), 12-18.

17. Jana, N. R.; Gearheart, L.; Murphy, C. J., *Wet Chemical Synthesis of High Aspect Ratio Cylindrical Gold Nanorods*. Journal of Physical Chemistry B **2001**, 105, (19), 4065-4067.
18. Liu, M.; Guyot-Sionnest, P., *Mechanism of Silver(I)-Assisted Growth of Gold Nanorods and Bipyramids*. Journal of Physical Chemistry B **2005**, 109, 22192-22200.
19. Orendorff, C. J.; Murphy, C. J., *Quantitation of Metal Content in the Silver-Assisted Growth of Gold Nanorods*. Journal of Physical Chemistry B **2006**, 110, (9), 3990-3994.
20. Busbee, B. D.; Obare, S. O.; Murphy, C. J., *An Improved Synthesis of High-Aspect-Ratio Gold Nanorods*. Advanced Materials **2003**, 15, (5), 414-416.
21. Nikoobakht, B.; Wang, Z. L.; El-Sayed, M. A., *Self-Assembly of Gold Nanorods*. Journal of Physical Chemistry B **2000**, 104, (36), 8635-8640.
22. Sreepasad, T. S.; Samal, A. K.; Pradeep, T., *One-, Two-, and Three-Dimensional Superstructures of Gold Nanorods Induced by Dimercaptosuccinic Acid*. Langmuir **2008**.
23. Jiang, P.; Bertone, J. F.; Hwang, K. S.; Colvin, V. L., *Single-Crystal Colloidal Multilayers of Controlled Thickness*. Chemistry Of Materials **1999**, 11, (8), 2132-2140.
24. Sau, T. K.; Murphy, C. J., *Seeded High Yield Synthesis of Short Au Nanorods in Aqueous Solution*. Langmuir **2004**, 20, (15), 6414-6420.
25. Zweifel, D. A.; Wei, A., *Sulfide-Arrested Growth of Gold Nanorods*. Chemistry Of Materials **2005**, 17, (16), 4256-4261.
26. Graf, C.; van Blaaderen, A., *Metallodielectric Colloidal Core-Shell Particles for Photonic Applications*. Langmuir **2002**, 18, (2), 524-534.
27. Smith, D. K.; Korgel, B. A., *The Importance of the CTAB Surfactant on the Colloidal Seed-Mediated Synthesis of Gold Nanorods*. Langmuir **2008**, 24, (3), 644-649.
28. Graf, C.; Vossen, D. L. J.; Imhof, A.; vanBlaaderen, A., *A General Method To Coat Colloidal Particles with Silica*. Langmuir **2003**, 19, (17), 6693-6700.
29. Jiang, X. C.; Brioude, A.; Pileni, M. P., *Gold nanorods: Limitations on their synthesis and optical properties*. Colloids and Surfaces A: Physicochemical and Engineering Aspects **2006**, 277, (1-3), 201-206.

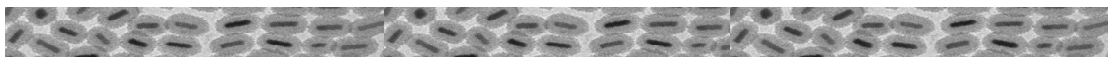
Chapter 4

Deformation of individual gold rods



Abstract

The shape transformation of individual gold rods observed by TEM before and after irradiation with fs laser pulses was investigated for 3 different batches of gold rods. Next to fs laser pulses, the shape change of bare gold rods, gold rods coated with Stöber silica and gold rods coated with mesoporous silica was investigated as well by heating particles in an oven. The deformation of the three different batches was compared after they were dried together on a TEM grid. At pulse intensities lower than 2 pJ (pulse duration 100-150 fs, repetition rate 82 MHz) with a wavelength close to the longitudinal plasmon frequency of the rods no deformation occurred, while at higher intensities deformation to almost spherical shape was reached for a pulse energy of 25 pJ. Surprisingly, irradiation at different wavelengths did not result in larger deformation at wavelengths where the absorption was at maximum. These results, as well as those obtained for different irradiation times and effects of the laser polarization, need to be checked with a scanning protocol that is less sensitive to a small mismatch in the focus plane. The effect of heat was also studied directly by heating particles as a function of time and temperature in an oven. As observed previously, particles were deformed at much lower temperature than the bulk gold melting temperature via mobile surface atoms. Finally, no confinement effects of the silica coating on the gold were found when the gold rods were deformed inside a silica shell.



4.1. Introduction

As was explained in the previous chapter the optical response of rod-like gold nanoparticles can be controlled quite effectively by changing the aspect ratio of the particles. Not that long ago¹⁻³ it was found that irradiation of a dispersion of gold nanorods with short laser pulses could result in a shape transformation from rods to a much more spherical shape.

This transformation was investigated in detail⁴ from which it was concluded that the transformation originates from internal crystal defects followed by a crystal and surface reconstruction. The minimum Wulff crystal structure⁵ is less anisotropic than the rod shaped particles thus the recrystallization transforms the particles into a more spherical crystal shape. Under certain conditions, mostly determined by how many photons are absorbed within a certain time frame, and if this is less than needed to completely melt the particle, the particles can recrystallize through a molten surface layer. This has been nicely demonstrated by El Sayed et al. by the analysis of the intermediate particles shapes found in their experiments performed on bulk dispersions⁴.

They showed that their gold rods were single crystals with {100}, {111} and {110} facets. By laser irradiation crystal defects were initiated causing locally twinned crystal lattices. The unstable {110} crystal plane, stabilized by the surfactant CTAB, recrystallizes at the same time as the twinned crystal grows toward the surface. Via a ϕ -shaped particle the particles turn into their thermodynamically favourable shape; a more spherical crystal.

Furthermore, they showed and explained why different results in particle deformation were obtained via femto- as compared to nanosecond laser irradiation. In a laser irradiation experiment with femtosecond laser pulses, four distinct processes are of importance: The absorption of the photons by the electrons is typically on a time scale of ~ 100 ps, the heat transfer of the hot electrons to the crystal lattice is very fast (< 10 ps), melting of the crystal lattice is accomplished within (30-35 ps). The cooling of the lattice, by heat loss to the surroundings is the slowest process and depends on details that determine the heat flux (> 100 ps). In a nanosecond laser pulse experiment the significant longer heating time results in a much larger chance of fragmentation of the nanoparticle⁴. With sufficiently small power, however, also in this case transformation to a spherical particle shape can be achieved.

Mulvaney and Liz-Marzan and co-workers showed that thermal heating of rods also induces a shape transformation even at much lower temperatures than that of bulk gold⁶. The difference in heat induced shape transition versus an ultra-short laser pulse induced shape transition is that the first is believed to take place solely via reconstruction by mobility of surface atoms, while the latter also takes place through reconstruction of the crystal lattice itself, and or complete melting depending on the energy deposited in the nanorod^{6, 7}. Strong evidence for the 'surface melting' mechanism in the case of thermal heating has recently been provided by results in which a 1.4 nm thick layer of carbon on gold and silver nanorods prevented the 'low' temperature deformation by frustrating the mobile surface atoms till a temperature close to the bulk melting temperature⁸.

Until now many studies in shape deformation of gold rods were performed with "bare" gold rods and most of them were performed in dilute dispersions. Recently, the optical behaviour of deformed gold rod particles in environments different than the solvent they were dispersed in, were studied. Marzan and coworkers⁹ looked at the

change in optical properties of gold rods in a (PVA) polymer matrix, while Min Gu and coworkers¹⁰ looked at the optical properties of irradiated gold rods in silica.

In this chapter we will show, as far as we know for the first time, that it is possible to image this shape change for an individual particle. We do this by literally focussing the ultra-fast laser pulse through the objective of a microscope to a diffraction limited spot in a 2-photon microscopy set up. Moreover, we will show that it is possible to specifically select individual particles and transform only these. Our ultimate goal here is to perform this optical programming of individual particles in a 3D metallo-dielectric photonic crystal. Not only would such control lead trivially to 3D data storage, it would more importantly also lead to significant control over the photonic properties of the 3D photonic crystal. For instance, Moroz has shown that if the symmetry of the lattice is optimized a full photonic band gap is possible with an amazingly low filling fraction of metal of just a few percent inside a dielectric lattice using band structure calculations¹¹. In addition, it has already been shown experimentally that nano gold rods as used in this paper can be aligned in strong electric fields¹².

Embedding the gold particles in silica facilitates not only the surface chemistry of the particles it also allows control over the spacing between particles that are touching, can be easily matched and can also be used to allow for easy self organization using external fields¹³.

In this chapter we will compare two different methods to deform gold rods that were made as was described in the previous chapter. A laser induced heat transformation where a precise control on the micro scale is possible with a focussed fs laserbeam and a heat induced shape deformation, where the influence of temperature on the reshaping of gold rods is investigated. We investigate 3 different batches at the same time; bare gold rods (AuNR), gold rods coated with Stöber silica (AuNR@SiO₂) and gold rods coated with a mesoporous silica layer (AuNR@MPSiO₂). The particles were embedded in a different matrix and have different aspect ratios and therefore a different longitudinal surface plasmon (LSP) absorption peak. The general concept of our irradiations is that overlap of the irradiated wavelengths with the LSP induces a stronger absorption and thus deformation of the gold rods, because the laser light is more efficiently absorbed. Furthermore, by comparing the results of the 3 different batches we will be able to investigate whether there is a ‘confinement effect’ in the shape deformation for instance by modification of the heat flux, hindering of surface diffusion or simply the physical presence of a boundary. The heat induced shape deformation of gold rods was performed as a supporting experiment to verify some of these confinement effects and in addition to probe possible differences in the mobility of the surface atoms caused by the different coatings.

4.2 Experimental

4.2.1. Laser induced shape deformation of gold rods

Gold rods were made as described in the previous chapter. Three different batches of gold rods were chosen to explore the shape deformation caused by femtosecond laser pulses. The first batch consisted of bare gold rods (AuNR) coated with CTAB and PSS, and measured 38.6 by 10.0 nm with an aspect ratio (AR) of 3.9

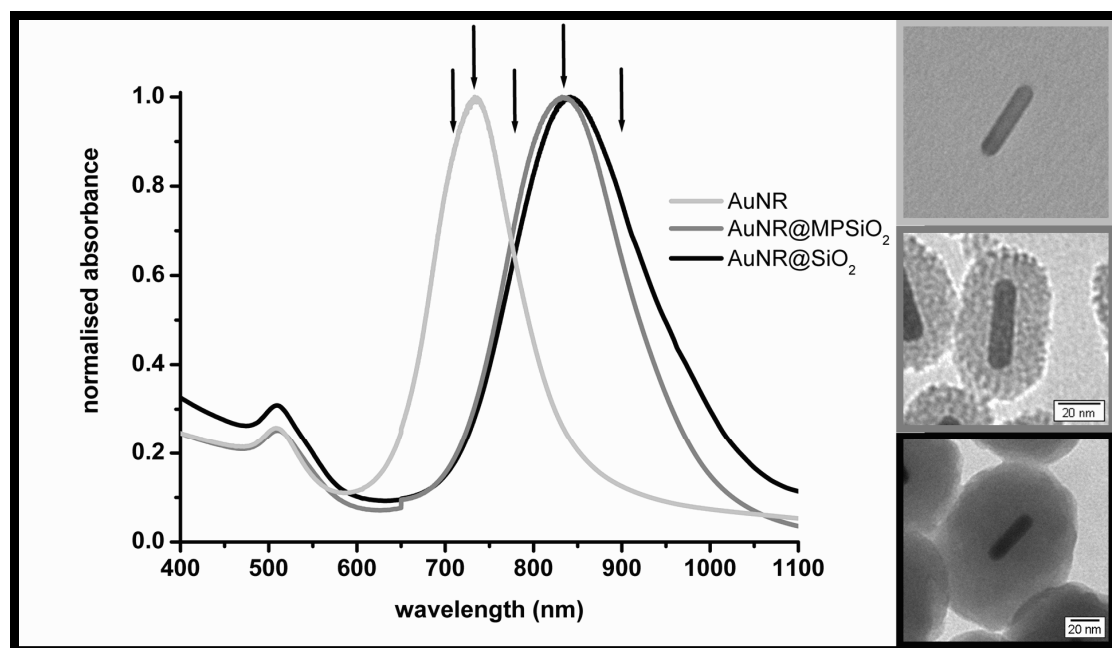


Fig. 4.1. The absorption spectra of the 3 different gold rod samples that were irradiated with 5 different wavelengths, $\lambda = 710, 735, 780, 838$ and 900 nm. The arrows indicate the corresponding irradiation wavelengths in the absorption spectra. During our experiments the position of the LSP peaks was red-shifted for ~ 20 nm in case of AuNR and AuNR@MPSiO₂, and 15 for AuNR@SiO₂, because our experiment was performed in a different medium than the recording of these absorption spectra.

The second batch were silica coated gold rods (AuNR@SiO₂) of 43.3 nm by 10.3 nm (AR = 4.2) coated with a 38 nm silica layer. The third batch we studied consisted of mesoporous silica coated gold rods (AuNR@MPSiO₂) of 43.0 by 10.6 nm (AR = 4.1) with a mesoporous silica layer of 18 nm. In Figure 4.1. TEM pictures of the particles and the corresponding absorption spectra are illustrated. In this figure the 5 wavelengths that we irradiated with are indicated with black arrows. The arguments for choosing these specific wavelengths are given in the next section.

Experimental laser irradiation set-up:

Femtosecond laserpulses were generated with 2 different lasers. A Tsunami (Spectra-Physics), where fs laserpulses were generated with a titanium-sapphire (Ti:Sa) laser pumped by a 5W neodymium-yttrium vanadate (Nd:YVO4) laser (Millennia, Spectra-Physics) and a Chameleon (Coherent), which is essentially a comparable laser, but, as the name suggests, more suitable for tuning the laser wavelength. Both lasers operated at a repetition rate of 82 MHz with a typical pulse width of 100- 150 fs. The Chameleon was used in experiments where we changed the wavelengths. The Tsunami was used in all other experiments described below. The attenuation of the laser intensity was controlled by a dual filter wheel (5254, New Focus, CA) with a set of neutral density filters with varying optical density (OD) ranging from 0.0 to 3.0 (attenuation factor 10^{-OD}). Beam scanning was accomplished by a galvanometer mirror scanner (040EF, LSK, Stallikon, Switzerland).

In addition to the beam-scanning mechanism, the microscope was also equipped with an XYZ translation stage to allow positioning of the scanned area. The laser light was focused with an objective lens (oil immersion lens (60 \times /1.4 NA)) on the sample,

and the reflected and emitted light was collected by the same objective lens. Using a dichroic mirror and a short wavelength pass emission filter, only the emitted light with wavelengths of 300 - 600 nm was detected with a GaAsP photodiode. In this multiphoton imaging set-up, we used the emitted light to establish the focal plane of illumination by locating the brightest signal.

With the Tsunami (Spectra-Physics) we first explored the intensities where the particles showed deformation. After these experiments we explored the wavelength dependency with the Chameleon (Coherent) for 3 different batches of particles at the same time.

In our first explorative experiments with the Tsunami operating at $\lambda = 780$ nm, we changed 3 parameters during the laser irradiation. We looked at the effect of the pulse energy by changing the optical density (OD). We varied the dwell time (DT) per pixel between 8 and 128 μs and we varied the number of repetitive scanning frames (NoF) from one to ten. A 2D scan normally consisted of a frame of $25 \times 25 \mu\text{m}^2$, 224×224 pixels.

With a power meter the intensity of the laser was measured at the sample stage. From this we could determine the intensity of the pulses. At the Tsunami for OD settings of 1.4, 1.7, 2.0, 2.3, 2.5 and 2.8 the laser intensity was 25.6, 13.6, 7.5, 3.1, 2.3 and 1.1 pJ/pulse respectively, in the experiments with the 3 batches of gold rods mixed on the TEM grid. To find the focal plane we illuminated our particles using an OD of 2.5 or 2.8. TEM analysis confirmed that at these settings no deformation was observed. Unfortunately in our very first experiments described in section 4.3.1. we did not measure the laser intensities, therefore the intensities can deviate from the experiments described in section 4.3.2.

With the Chameleon the wavelength was tuned to $\lambda = 710, 735, 780, 838$ and 900 nm. Using $\text{OD} = 1.24$, resulted in laser energies of respectively 21, 17, 10, 14 and 20 pJ per pulse. (The output intensity of the Chameleon is not the same if the wavelength is tuned, so for practical reasons we did not use exactly equal laser intensities, besides the output is different from the Tsunami, therefore at lower OD's still reasonably high intensities are obtained. In these experiments the pre-focusing occurred at $\text{OD} = 2.04$, again TEM confirmed that this setting caused no deformation)

In Figure 4.1 black arrows are drawn at the positions in the absorption spectra of the illuminated particles that correspond to the 5 laser wavelengths we irradiated with, using the Chameleon. The wavelengths were chosen such that there is a specific overlap with the longitudinal surface plasmon (LSP) peak of the gold rod particles that were illuminated. The shortest wavelength was chosen such that there was no overlap between the LSP absorption peak of the silica coated particles at the irradiated wavelength ($\lambda = 710$ nm). At the next wavelength ($\lambda = 735$ nm) the LSP absorption peak of the 'bare' gold rods (not silica coated) has its maximum, the third wavelength ($\lambda = 780$ nm) all particles had equal absorption, at the 4th wavelength ($\lambda = 838$ nm) the LSP absorption peak of the silica coated gold rods has its maximum and at the highest wavelength ($\lambda = 900$ nm) the LSP absorption peak of the uncoated gold rods particles has no overlap. In the choice of the wavelength we did not account for the small shift of the absorption of the LSP when the medium is changed. The absorption spectra of AuNR and AuNR@MPSiO₂ were recorded in water, while AuNR@SiO₂ was taken in isopropanol. During our experiments the particles were immersed in a 70 vol% glycerol/water mixture. There is a linear relation with the change of the position of the LSP peak with the refractive index of the dispersion medium¹⁴. Therefore, the LSP

absorption peaks of the AuNR@MPSiO₂ and the AuNR@SiO₂ particles are red shifted by ~ 20 and 15 nm respectively, in our irradiation experiments.

In a typical experiment, gold rod particles were dried on a (300 mesh) TEM grid. The TEM grid was coated with an extra layer of Polyallylhydrochloride (PAH) which is positively charged, to allow the (negatively charged) particles to stick to the grid. The regular raster of the 300 square mesh TEM grid was used to obtain positional coordinates for the laser irradiation such that at the irradiated spots could be found back in the TEM microscope. For each laser irradiation experiment we took a different box on the TEM grid, to ensure the particles were not irradiated twice when the irradiation parameters were changed. The particles adsorbed onto the TEM grids were immersed in a 70 vol% glycerol/water mixture during the laser experiments and dried in an oven at 100 °C overnight, before observation with TEM (Tecnai10 (100kV) and/or Tecnai12 (120kV), FEI). Absorption spectra were recorded on a Bruker Vertex 70 FTIR and a HP 8452A Diode Array spectrophotometer.

4.2.2. Heat induced shape deformation of gold rods

The effect of temperature alone (i.e. not induced by short laser pulses) on the deformation of (silica coated) gold rods was studied by putting a small drop of concentrated gold rod dispersion on glass substrates into a Carbolute EDF 12 oven and the temperature was kept constant for half an hour at temperatures between 200 °C and 400 °C. Then the absorption spectrum was measured and the particle shape was observed with TEM. Hereto, after the absorption spectra were recorded, the dried dispersion was redispersed in a small volume and dried on a TEM-grid.

In another experiment the temperature was kept at 300 °C and the deformation of the particles was followed in time, the sample was taken out of the oven to take an absorption spectrum and put back again. These experiments were done only with AuNR@SiO₂ and AuNR@MPSiO₂, while the absorption spectra of dried AuNR samples do not give a reliable result. Furthermore, in the same temperature range we looked at the stability of CTAB, PSS, PAH and PVP. We put the polymers into the Carbolute oven and observed at what temperature the polymers decomposed. Decomposition of the particles was judged by color. All observed polymers were white, decomposition made them darker and finally a black carbon powder was observed to remain.

4.3 Results and Discussion

4.3.1. Laser induced shape deformation of AuNR@SiO₂

To find the right parameter settings where our gold rods deformed, we first explored only the AuNR@SiO₂ on a PAH coated TEM grid. The PAH is positively charged and thus our negatively charged particles stuck to the polymer film of the TEM grid efficiently. Even after being immersed in a water glycerol mixture, they stayed at the same position after drying the grid. In Figure 4.2 it is shown that we were able to find the same particles back after they had been irradiated.

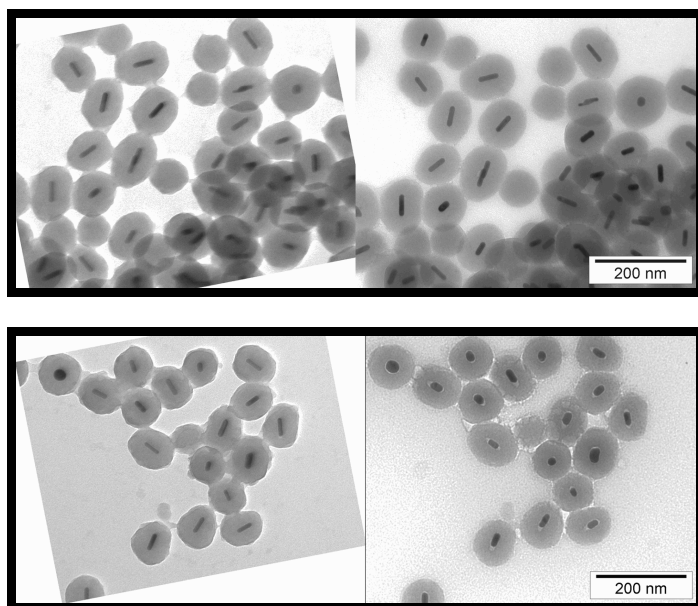


Fig. 4.2. AuNR@SiO₂ particles before (left pictures) and, exactly the same particles after irradiation (right pictures) were found back on the TEM grid.

To help pattern recognition the TEM picture before irradiation is tilted ~ 15°.

Irradiation parameters:

λ = 780nm (Tsunami)
 DT = 64 μ s,
 NoF = 10
 OD = 1.84 (top),
 1.60 (bottom).

The top picture shows a decrease in AR of 7 %, while the lower picture shows a decrease of 54 % in AR.

From this picture it can also be seen that by only changing the OD from 1.84 to 1.60 (and leaving all other irradiation parameters the same ($\lambda = 780$ nm, DT = 64 μ s, NoF = 10) the deformation of the particles increased drastically. At OD = 1.84 the decrease of AR was only 7% (from 3.62 to 3.39), while the decrease of the AR for AuNR@SiO₂ was 54 % at OD = 1.60 (from 3.27 to 1.72). Only the particles in the viewing area of Figure 4.2 were measured. Although the statistics is poor, the effect is obvious. Also note that the AR is smaller then the average AR of AuNR@SiO₂, because some particles have their axis positioned towards the electron beam of the TEM. Remarkably, even the position of the particles stays exactly intact after irradiation, once again indicating the strong attachment of the particles on the oppositely charged PAH surface of the grid.

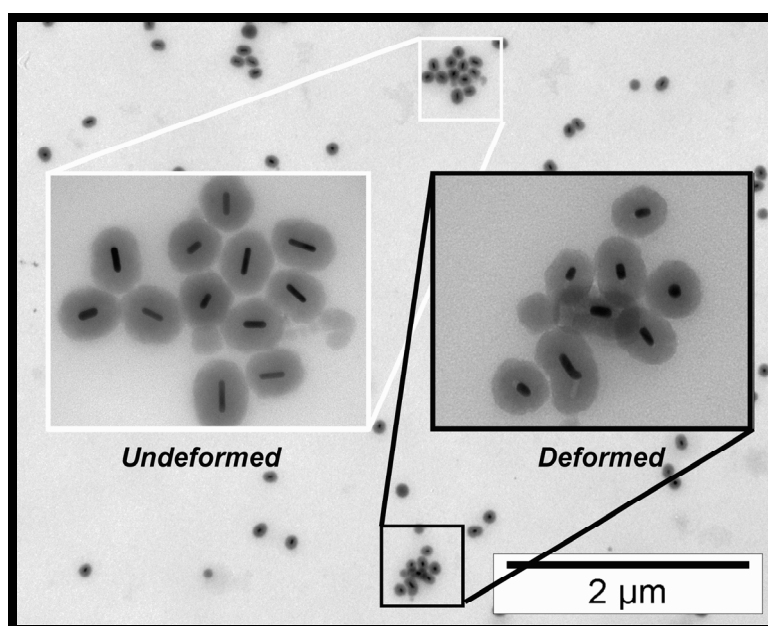


Fig. 4.3. The line between the irradiated area and not irradiated area is very sharp. On the top of the picture all particles are undeformed, while at the lower part on the TEM grid all particles inside the illuminated area were deformed by a 780 nm scanned laserbeam (DT= 64 μ s, OD=1.44, NoF = 10) .

This allows us to study deformation of a particle, or a group of particles, individually on a TEM grid. Making it in principle possible to look for correlations that are almost impossible to obtain from bulk measurements. For instance, a correlation with a change in aspect ratio as a function of the thickness of the rods, the orientation with respect to the polarization of the laser beam etc. Figure 4.3. shows a TEM picture, where it can be seen that the illuminated area (of $25 \mu\text{m}^2$) is very sharp. At the top of the TEM picture the AuNR@SiO₂ particles remained undeformed where they were not illuminated, while at the bottom they lie inside of the field of $25 \mu\text{m}^2$ that was illuminated and thus the particles were deformed.

4.3.2. Laser induced shape deformation of AuNR, AuNR@SiO₂ and AuNR@MPSiO₂

In our explorative experiments with AuNR@SiO₂ we already observed a larger deformation when a higher intensity was used to irradiate with. To be able to compare the results of coated gold rods (AuNR@SiO₂ and AuNR@MPSiO₂) with bare gold rods (AuNR) we made a mixture of these 3 batches and put them altogether on the same electron microscope grid. For each experiment we took a new box on the grid. We again checked the influence of the intensity by changing the OD's and, indeed, we observed a larger deformation at lower OD, as we already saw in the experiments described in the previous section. At OD = 2.3 (3.1 pJ/pulse) the observed deformation was small while at OD = 2.5 (2.3 pJ/pulse) and 2.8 (1.1 pJ/pulse) we did not observe any deformation. The threshold for deformation therefore lies between 1-3 pJ/pulse.

In Figure 4.4. we plotted the average aspect ratio of the gold rods as a function of the pulse intensity we irradiated with (generated by changing the OD). It should be noted that the average AR is calculated by only measuring 15-20 particles as we were limited by the number of TEM pictures we took, therefore the error in the datapoints is large. Nevertheless, the effect of higher deformation at higher pulse energy is obvious. When we used the OD = 1.4 (25.6 pJ/pulse) we caused damage to the polymer film of our TEM grid, which carries the particles. Consequently, we could not investigate the effect of higher pulse intensities.

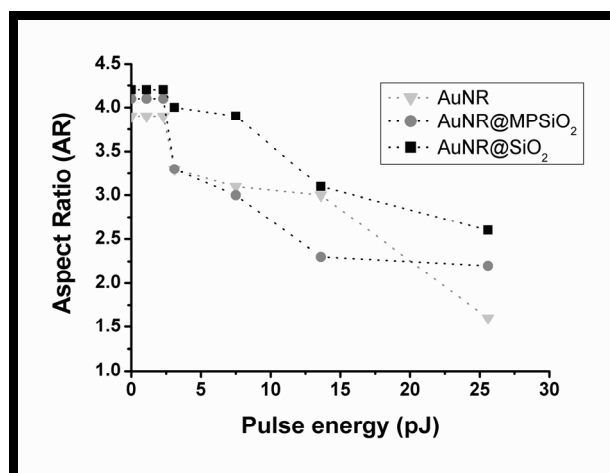


Fig. 4.4. Change of the aspect ratio of the gold rods with an increasing pulse intensity (modified by changing the OD setting). The average aspect ratio of the particles is derived from measuring 15-20 particles.

Furthermore we noticed that in specific alignments particles seemed less affected than others. Irradiating the sample after it was turned for 90° also showed particles that were less affected with an orientation shifted with 90° accordingly. We irradiated with polarized light. This suggests that the particles were aligned perpendicular to the polarization of the laser and therefore absorb the light much less efficient. In Figure 4.5a, 4.6a, and 4.7a particles that are aligned diagonally (towards north-east) seem to be less effected, although this effect is not very clear. We conclude that there might be a polarization dependent shape deformation, but this needs to be investigated into more detail.

The influence of changing the DT and NoF, as well as the wavelength dependency were less clear. Keeping the DT and OD fixed at $64 \mu\text{s}$ and 1.7 we changed the NoF from 1 to 10. We found that all particles were already affected by the first scan and increasing the NoF only affected the particles slightly more, as can be seen in Figure 4.5.

Changing the DT from 8 to 128, by doubling the DT in each experiment, keeping OD fixed at 1.7 and the NoF at 10, the changes were not very large either. It seemed as if the deformation was a bit larger at a DT of $64 \mu\text{s}$ compared to $8 \mu\text{s}$, as shown in Figure 4.6.

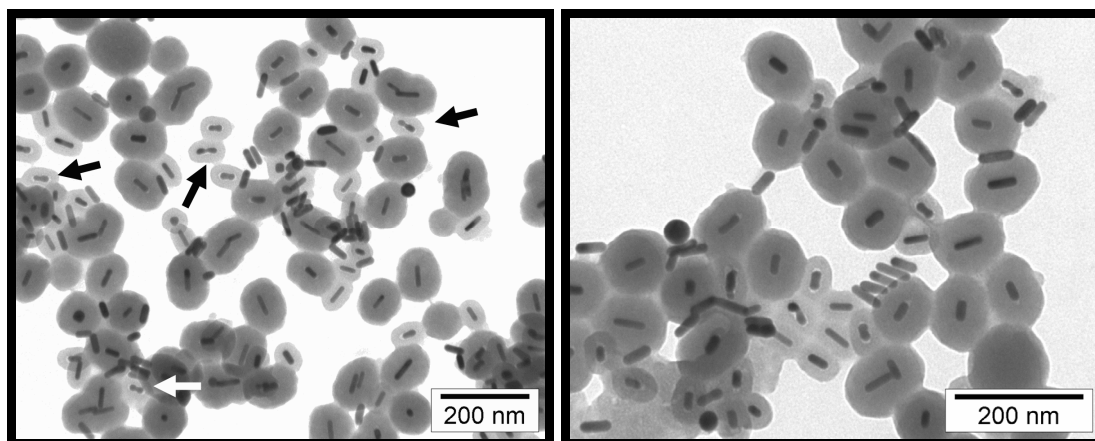


Fig. 4.5. Result of laser illumination $\lambda = 780 \text{ nm}$, $DT = 64 \mu\text{s}$, $OD = 1.24$. Changing the NoF. **left:** NoF = 1, **right:** NoF = 10. (arrows indicate goldrod dumbbells)

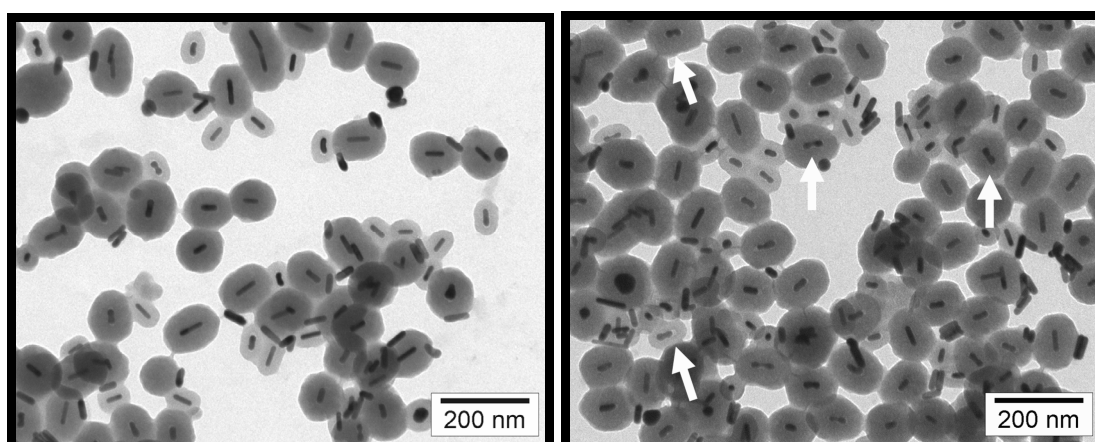


Fig. 4.6. Result of laser illumination $\lambda = 780 \text{ nm}$, NoF = 10, $OD = 1.24$. Changing the DT **left:** $DT = 8 \mu\text{s}$, **right:** $DT = 64 \mu\text{s}$. (arrows indicate goldrod dumbbells)

If all scans were correctly focused on the plane with particles these results could mean two things. First, that the deformation stopped because an AR was reached that was so small that the wavelengths used were not absorbed effectively enough to cause enough heating for further deformation. Such observations were made before by several groups. It also means that on the time scale between different pulses of intense laser light heat was not accumulating, as otherwise one would expect to still see effects of having more pulses hit the particles by an increase in dwell time or in number of scanned frames. The shortest repeat time scale is clearly that between pulses which is on the order of 10 ns, it is certainly possible that at that time scale most of the heat in the particles has already dissipated to the surrounding fluid.

There is however another reason possible. The full width half height of the intensity of a diffraction limited spot of the laser light is below a micrometer. This makes only scanning one plane very sensitive to small displacements of the sample and/or lens. For instance, it is certainly not inconceivable that the heating of the first pulse would lead to a shift of the carrying film on the TEM grid of several hundred nanometer.

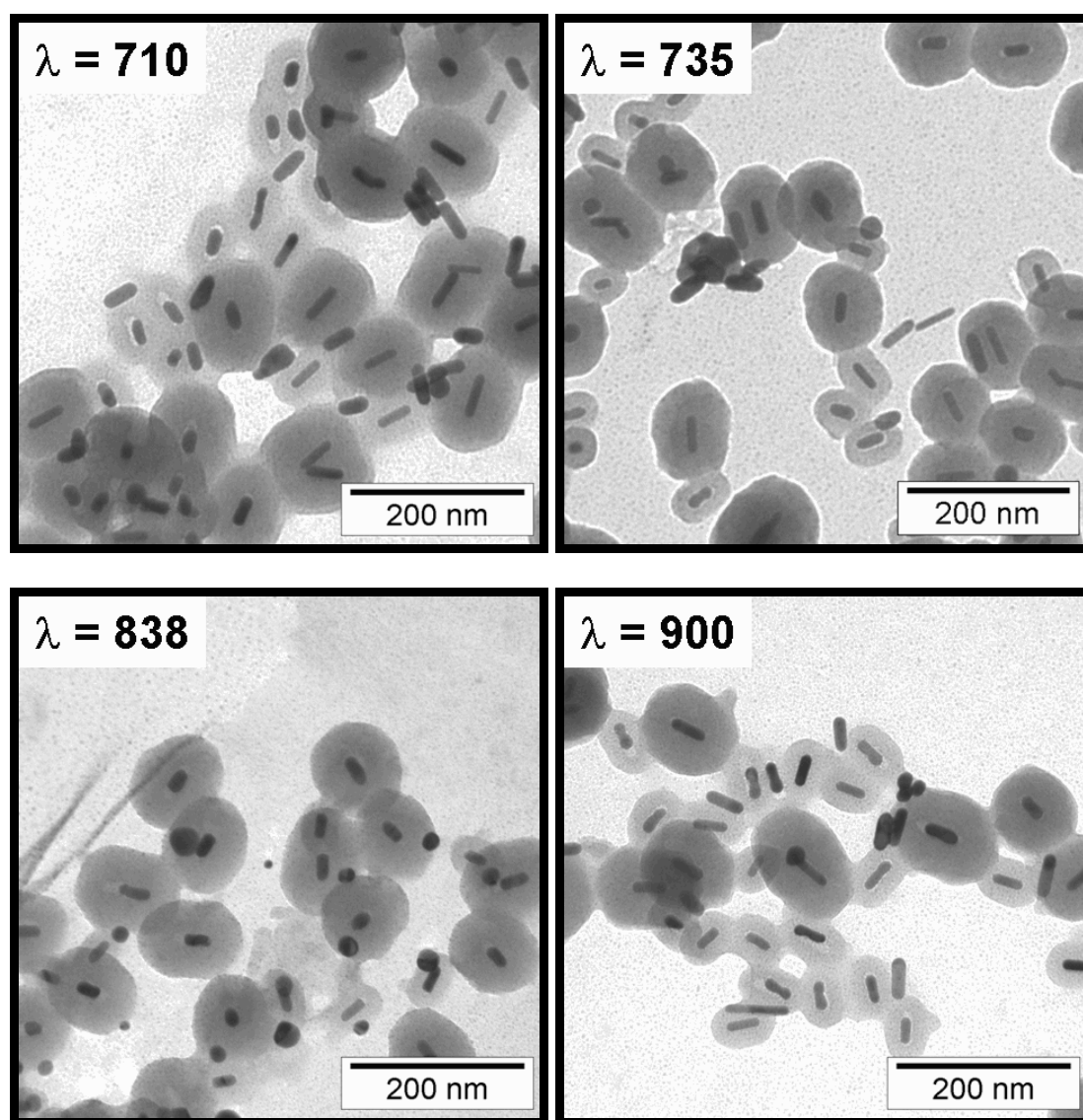


Fig. 4.7. Deformation of the three batches of gold rods: at various wavelengths. (Chameleon, $DT=64 \mu s$, $NoF=1$, $OD = 1.24$.) (arrows indicate goldrod dumbbells)

This would already drastically reduce the effect of subsequent pulses as the intensity falls with distance roughly exponentially. Therefore, a protocol in which a thin, oversampled, 3D box is scanned would be much less sensitive to these kind of artifacts. (It would make an estimate of how many photons were absorbed harder). In addition, it would also make the requirement for all particles within the $25 \mu\text{m}^2$ to be lying in the same plane within several hundred nm to be (much) less stringent.

When we changed the wavelength with the Chameleon, we expected to see a larger deformation of the AuNR at low wavelengths $\lambda = 710 \text{ nm}$ and 735 nm , while a higher deformation of AuNR@SiO₂ and AuNR@SiO₂ was expected at high wavelengths of $\lambda = 900 \text{ nm}$, because the absorption of the particles have their maxima at different wavelengths as is already shown in Figure 4.1.

This effect was not seen and certainly needs confirmation with the scanning protocol mentioned above, for which also the intensity within each pulse needs to be better checked as it is at odds with observations by others as well. Particles were affected at all wavelengths. This is best seen for the silica coated particles, since voids became visible where a gold rod used to be before deformation. In Figure 4.7, the results of the deformation of irradiation with 710, 735, 838 and 900 nm are shown, with OD = 1.24, DT = 64 and NoF = 1. It is remarkable however, that not all particles were affected evenly, even within the same field of view. As mentioned above, perhaps not all particles were exactly lying in focus as the surface they were lying on was certainly not optically flat. Furthermore, it is surprising that all particles irradiated with $\lambda = 838 \text{ nm}$ seem to be affected drastically, while the pulse intensity was lowest, compared to the other wavelengths.

The pulse energies we used in our experiment (1–25 pJ/pulse), are an order of magnitude smaller than those that are used in most other laser induced shape deformation experiments found in literature^{6, 15, 16}. For instance, Link and El Sayed used intensities of 0.5–20 $\mu\text{J}/\text{pulse}$ ¹⁶.

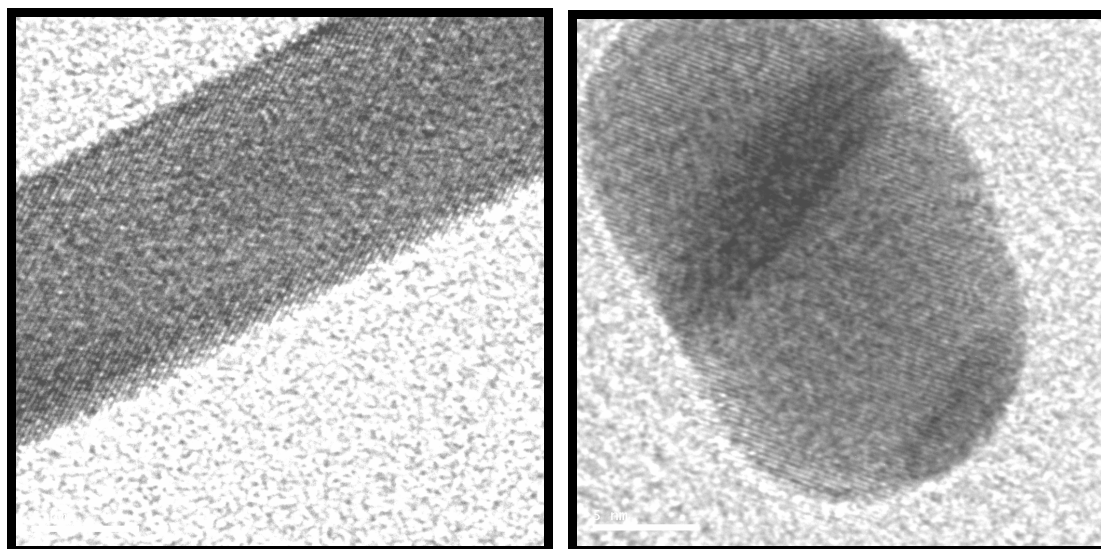


Fig. 4.8. HRTEM images of AuNR@SiO₂ before (left) and after (right) 780 nm laser illumination. A close look at the picture shows the crystal planes of the gold lattice. The lattice spacing of 2.35 Å corresponds to the distance between {111} planes¹⁷ (the view area is $22 \mu\text{m}^2$ in both pictures).

4.8. (left) The undeformed AuNR@SiO₂ shows a monocrystalline structure.

4.8. (right) The deformed AuNR@SiO₂ shows crystal defects caused by the ultrashort laser pulse.

An important difference between our set-up and theirs is, however, that we focus our beam through an objective on particles that are fixed, while in their experiments the laserbeam is focused much less to a spot of hundreds of μm .

This enabled us to deform a single group of individual particles. With a silica shell that is a few hundred nm thicker (see the previous chapter, Figure 3.5.) the specific deformation of a single gold rod will even be possible. Moreover, as was already said, because we perform our experiments at particles that were spread on a TEM grid, we were able to directly investigate the effects of radiation on the same particle before and after irradiation (see Figure 4.2.). If we assume a spotsize of our focused laser of 300 nm radius, we obtain fluences between 3.3-7.5 mJ/cm^2 which are of the same order as what was used in the experiments of Min Gu and coworkers^{10, 18}.

As discussed in the introduction El Sayed and coworkers⁴ suggested a mechanism for the shape deformation where a defect inside the crystal lattice of a gold rod, caused by the energy absorbed from the ultrashort laser pulse migrates outwards, resulting in some cases in the formation of ϕ -shaped particles. In none of our experiments such ϕ -shaped particles were observed however. Yet, we frequently found deformed AuNR@SiO₂ and AuNR@MPSiO₂ particles that contained gold rods with a dumbbell shape (Indicated by arrows in Figures 4.5, 4.6 and 4.7) and indeed, in the work Min Gu and coworkers^{10, 18} their deformed AuNR@SiO₂ look identical to ours and also do not display ϕ -shaped particles. It is not clear if this is due to the confinement effects of the silica shell as the ϕ -shaped intermediate structures were also not observed for the uncoated rods. What we did observe is loss of monocrystallinity as can be seen in Figure 4.8, suggesting that to the exact recrystallization path as described by El Sayed et al. is not followed. It is however not that strange that the details of this highly out of equilibrium process depend sensitively on many experimental conditions.

From our experiments it is hard to suggest a different mechanism as our observations do not show a crystalclear effect. From all the investigated parameter that are of influence, only the change in intensity (set by a change in OD) revealed a clear effect. At intensities lower than 2 pJ/pulse no deformation effect is seen, while at higher intensities the deformation increases. At an increasing DT a larger deformation is observed, but the effect is marginal (see Figure 4.6), suggesting that not much heat is accumulated at longer DT.

Hu and coworkers investigated the heat dissipation of gold nanoparticles and silica coated nanoparticles^{19, 20} and found a linear relation of heat dissipation in time with the surface area of a particle. Furthermore, they showed that AuNR and AuNR@SiO₂ have comparable heat relaxation time which is not more than hundreds of picoseconds. This is still much lower than our pulse repetition rate of 12.2 ns. This makes heat accumulation less likely in our experiments and does explain as mentioned above that there is not much effect of changing the DT and the NoF. This corresponds to the conclusion of Min Gu and coworkers that the use of a higher NA for focusing the beam to smaller focal spot sizes results in a lower rate of heat accumulation¹⁸

4.3.3. Heat induced shape deformation of gold rods

Figure 4.9.a and Figure 4.9.b show absorption spectra of AuNR@SiO₂ and AuNR@MPSiO₂ recorded after a concentrated drop was dried on a glass slide, put into an oven and heated for 30 minutes at increasing temperatures between 200 °C and 400 °C.

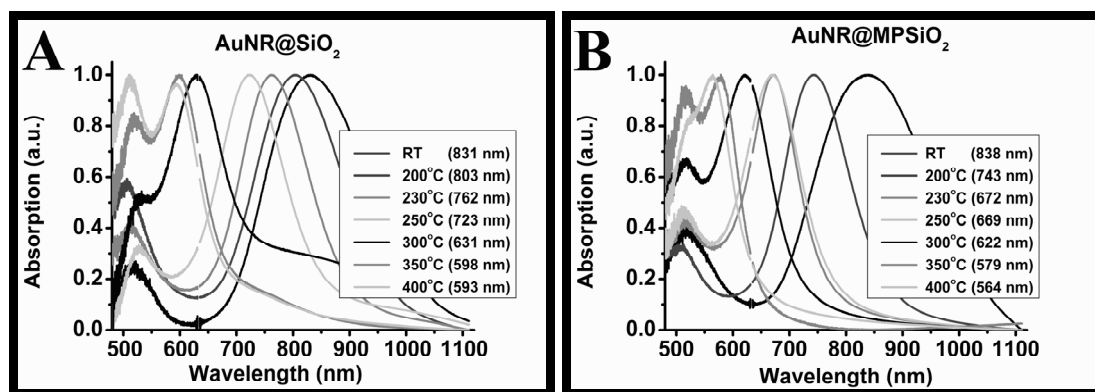


Fig. 4.9. Absorption spectra of silica coated gold rods after 30 min in the oven at elevated temperatures between 200 and 400 °C.

(a) Stöber silica coated gold rods (AuNR@SiO_2). (b) Mesoporous silica coated gold rods (AuNR@MPSiO_2).

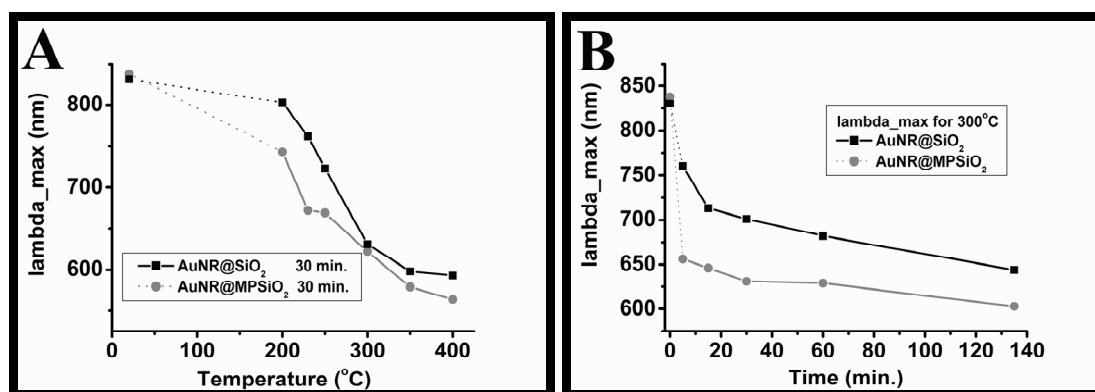


Fig. 4.10. Comparison between the maxima of the longitudinal plasmon absorption peaks as a function of (a) temperature and (b) time (at 300 °C) of Stöber silica (AuNR@SiO_2) and mesoporous silica coated gold rods (AuNR@MPSiO_2).

The maxima of the corresponding LSP absorption peaks are plotted in Figure 4.8.a. Here a blue shift of the maxima of the LSP absorption peaks in the absorption spectra as a function of the temperature is visible. In another experiment we looked at the effect of deformation in time. While the temperature was set at 300 °C and the heating time was a variable. In this case again a blue shift of the LSP absorption peaks was observed (as can be seen in Figure 4.10.b.).

After the absorption spectra were recorded we managed to redisperse the spot in a volume of about 100 μl and a drop of this dispersion was dried on a TEM grid. Figure 4.11 shows a TEM picture of the redispersed and dried AuNR@SiO_2 and AuNR@MPSiO_2 particles after 30 min heating at 300 °C, confirming a decrease of the AR. Comparing the deformation of AuNR@SiO_2 and AuNR@MPSiO_2 from Figure 4.10. it can be seen that the AuNR@MPSiO_2 particles deform faster than the AuNR@SiO_2 particles. It is known⁷ that CTAB stabilizes the {100} crystal facet of gold rods and thus if CTAB is burnt then surface melting can occur more easily. To further understand the melting/deformation behavior of our gold rods we performed heating experiments of the stabilizing polymers and surfactants present at the gold surface. Heating CTAB, PSS, PAH and PVP at temperatures of 200 °C – 400 °C in steps of 50 °C demonstrated that CTAB already decomposes at 200 °C followed by PVP at 250 °C, while PAH and PSS are stable up to 300 °C and 350 °C respectively.

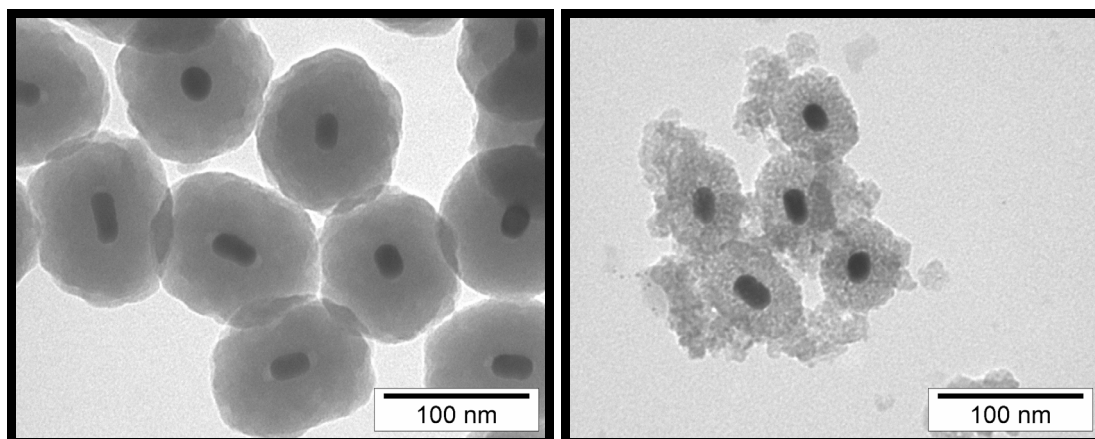


Fig. 4.11. (left) AuNR@SiO₂ with shortened aspect ratio (4.2 → 1.7) heated for 30 min at 300 °C. A void can be seen that is caused because the particle becomes shorter (and thicker). (right) AuNR@MPSiO₂ with shortened aspect ratio (4.1 → 1.8) heated for 30 min at 300 °C. The particles become brittle, some broken parts are visible after redispersion by sonication.

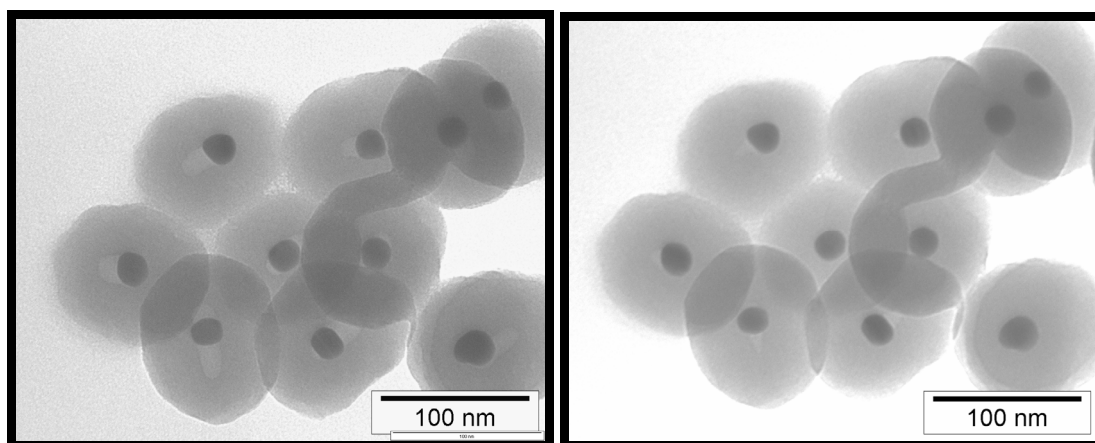


Fig. 4.12. Silica structure restructures by intense TEM beam heating. (left) Before intense TEM-beam illumination. (right) After 5-10 seconds illumination silica structure fills up the empty voids that were caused by melting of the gold rods.

Of course deviations may occur for the molecules as adsorbed compared to the pure substance. If we take the temperature of decomposition of the pure substances as a guideline, the first stabilizing agent on the silica surface (CTAB) already starts to decompose at 200 °C and thus already at this temperature surface atoms diffusion can be expected. AuNR@SiO₂ also is coated with PSS, PAH and PVP before silica is covering the nanorod. This may explain why surface mobility is more retarded for the AuNR@SiO₂ particles than for the AuNR@MPSiO₂ particles. An interesting question is whether or not the silica capping is able to hinder the reshaping of the gold particle by preventing the adaptation of a more round crystalline structure. With a simple calculation it can be shown that, taking the dimensions of AuNR@SiO₂, when 1 nm polymer surrounding the gold particle is burnt off this will result in an empty void of already 1/3rd of the volume of the gold rod. With a layer of 2 nm the void volume even becomes almost equal to the gold rod volume. Therefore, strong hindering of the rod shape transition by the silica shell is unlikely, as the thickness of only the PSS/PAH layer already exceeds 1 nm.²¹

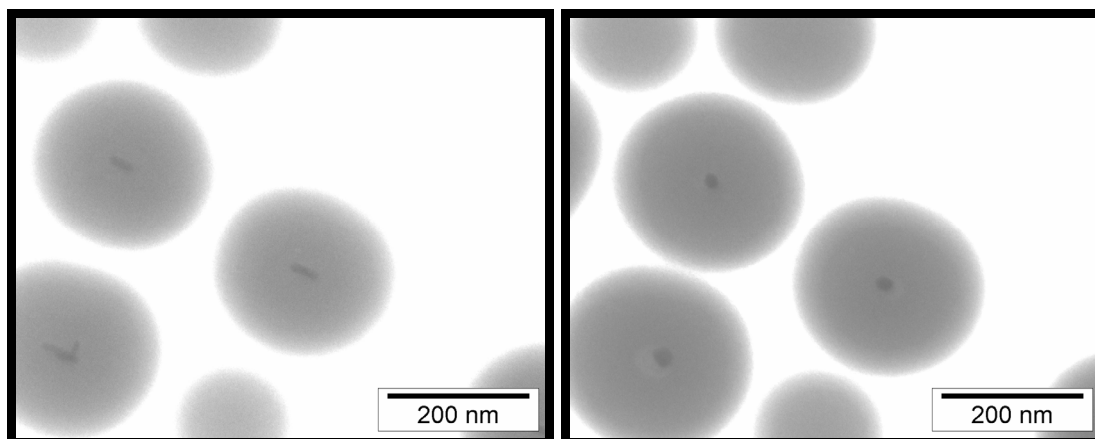


Fig. 4.13. Silica coated gold rods deformed at TEM by an intense 120 kV electron beam. (left) Undeformed gold rods in silica (only visibly, with effort, as a black rod). (right) Deformed into a sphere after tightly focusing the e-beam. (Because of the oversaturation of the detector, particles look smaller than they are)

Indeed we see, if a particle is heated to temperatures of 400 °C, the gold rod transform in an almost spherical particle, leaving a void, as can be seen with effort in Figure 4.12. The experiment where we kept the temperature at 300 °C and looked at the position of the LSP in time (see Figure 4.10.b) shows that the longer the particles are heated they continue to deform to a more spherical shape. At higher temperatures the kinetic energy of the mobile surface atoms is higher and thus the transformation goes faster. (see Figure 4.10.a).

As was reported before²², silica shrinks at elevated temperatures. For Stöber silica the temperature at which significant condensation takes place is around 950 °C²³. We found that if an intense electron beam of the TEM operating at 120 kV is focused at high magnification, the void that was found in the silica matrix disappears, as can be seen in Figure 4.12. This suggests that the local heating in a focused beamspace at TEM can reach temperatures where silica can significantly reorganize. If temperature would be the only factor, it is hard to explain that the gold would not reach similar temperatures and become more spherical during observation at the electron microscope. Surprisingly, only in one experiment where the beam was extremely focused to observe gold rods in a coat of ~ 150 nm silica, melting of the gold rod induced by the TEM beam was observed, as can be seen in Figure 4.13.

Because thermal contact of a sphere on a surface in vacuum is quite bad, the observation of melting of gold rods by heating of the electron beam is not surprising. It is more surprising that this effect has not been observed more frequently in our experiments.

4.4. Conclusions

We have shown to be able to deform gold rods and silica coated gold rods with femtosecond laser pulses into a more spherical shape and study the deformation of individual particles before and after irradiation. We achieved this by focusing the fs laser pulses to a diffraction limited spot in a set up designed for multiphoton microscopy. The same identical deformed particles could be found back with TEM after being illuminated by scanning the focussed spot over a small (25 μm^2) area. It is clear from these preliminary results that it will be even possible to select individual particles to be deformed if their spacing will exceed several hundred nanometer.

By selecting the wavelength of the longitudinal plasmon resonance of the gold rods we expected to see in our set-up a wavelength dependent deformation. This was not yet observed clearly. Possible reasons that need to be investigated and eliminated by use of a different illumination protocol are a strong sensitivity of the deformation to the correct positioning of the focussing plane. The effect of a larger dwell-time or an increase in the number of 2D frames scanned was small. This suggests that heat is dissipated before the next laserpulse arrives (12 ns) and that there is a wavelength dependence in the deformation. This observation is in agreement with those made by Hu¹⁹ et al. However, also these results should be checked by using an illumination protocol which scanned a thin 3D volume instead of a 2D plane to eliminate possible artefacts. Also a dependence of the deformation on the polarization of the light would be illuminating.

Our laser induced shape transformation seems to have a different mechanism than was proposed by Link and Sayed. We did not find any effect of confinement of the silica layer that would hinder the gold rod to deform towards a more spherical shape. Most likely this is because degradation of polymer and surfactant layers leaves enough space for the deforming gold particle. In accordance with earlier findings, a temperature induced shape transition already starts at temperatures above 200 °C most likely mobile atoms on the particle surface.

Acknowledgements

Dannis 't Hart and Menno Bergmeijer are thanked for their assistance in the experiments and useful discussions. Jonathan Palero is thanked for performing the laser irradiation experiments. Hans Gerritsen and Dave van den Heuvel are thanked for valuable discussions. We also appreciated the help of Hans Meeldijk with the HRTEM measurements.

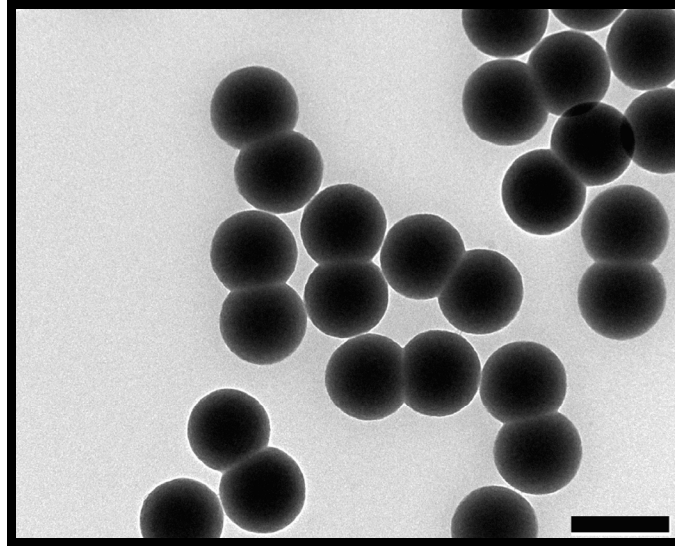
4.5. References

1. Link, S.; Burda, C.; Nikoobakht, B.; El-Sayed, M. A., *Laser-Induced Shape Changes of Colloidal Gold Nanorods Using Femtosecond and Nanosecond Laser Pulses*. *Journal of Physical Chemistry B* **2000**, 104, (26), 6152-6163.
2. Link, S.; Burda, C.; Nikoobakht, B.; El-Sayed, M. A., *How long does it take to melt a gold nanorod?: A femtosecond pump-probe absorption spectroscopic study*. *Chemical Physics Letters* **1999**, 315, (1-2), 12-18.
3. Chang, S. S.; Shih, C. W.; Chen, C. D.; Lai, W. C.; Wang, C. R. C., *The Shape Transition of Gold Nanorods*. *Langmuir* **1999**, 15, (3), 701-709.
4. Link, S.; Wang, Z. L.; El-Sayed, M. A., *How Does a Gold Nanorod Melt?* *Journal of Physical Chemistry B* **2000**, 104, (33), 7867-7870.
5. Dobrushin, R. L.; Kotecký, S.; Shlosman, R., *Translations of Mathematical Monographs: Wulff Construction: A Global Shape from Local Interaction* American Mathematical Society: Providence, Rhode Island, 1992; Vol. 104, p 1-204.
6. Petrova, H.; Juste, J. P.; Pastoriza-Santos, I.; Hartland, G. V.; Liz-Marzan, L. M.; Mulvaney, P., *On the temperature stability of gold nanorods: comparison between thermal and ultrafast laser-induced heating*. *Physical Chemistry Chemical Physics* **2006**, 8, (7), 814-821.
7. Wang, Z. L.; Gao, R. P.; Nikoobakht, B.; El-Sayed, M. A., *Surface Reconstruction of the Unstable {110} Surface in Gold Nanorods*. *Journal of Physical Chemistry B* **2000**, 104, (23), 5417-5420.
8. Khalavka, Y.; Ohm, C.; Sun, L.; Banhart, F.; Sonnichsen, C., *Enhanced Thermal Stability of Gold and Silver Nanorods by Thin Surface Layers*. *The Journal of Physical Chemistry C* **2007**, 111, (35), 12886-12889.
9. Pérez-Juste, J.; Rodríguez-González, B.; Mulvaney, P.; Liz-Marzán, L. M., *Optical Control and Patterning of Gold-Nanorod-Poly(vinyl alcohol) Nanocomposite Films*. *Advanced Functional Materials* **2005**, 15, (7), 1065-1071.
10. Chon, J. W. M.; Bullen, C.; Zijlstra, P.; Gu, M., *Spectral encoding on Gold Nanorods Doped in a Silica Sol-Gel Matrix and Its Application to High-Density Optical Data Storage*. *Advanced Functional Materials* **2007**, 17, (6), 875-880.
11. Moroz, A., *Photonic crystals of coated metallic spheres*. *Europhysics Letters* **2000**, 50, (4), 466-472.
12. van der Zande, B. M. I.; Koper, G. J. M.; Lekkerkerker, H. N. W., *Alignment of Rod-Shaped Gold Particles by Electric Fields*. *Journal of Physical Chemistry B* **1999**, 103, (28), 5754-5760.
13. van Blaaderen, A., *Colloids under External Control*. *MRS Bulletin* **2004**, 29, (2), 85-90.
14. Pérez-Juste, J.; Pastoriza-Santos, I.; Liz-Marzán, L. M.; Mulvaney, P., *Gold nanorods: Synthesis, characterization and applications*. *Coordination Chemistry Reviews* **2005**, 249, (17-18), 1870-1901.
15. Aguirre, C. M.; Moran, C. E.; Young, J. F.; Halas, N. J., *Laser-Induced Reshaping of Metallodielectric Nanoshells under Femtosecond and Nanosecond Plasmon Resonant Illumination*. *Journal of Chemical Physics B* **2004**, 108, (22), 7040-7045.

16. Link, S.; El-Sayed, M. A., Spectroscopic determination of the melting energy of a gold nanorod. *The Journal of Chemical Physics* **2001**, 114, (5), 2362-2368.
17. Huang, C.-J.; Chiu, P.-H.; Wang, Y.-H.; Chen, W.-R.; Meen, T.-H.; Yang, C.-F., *Preparation and characterization of gold nanodumbbells*. *Nanotechnology* **2006**, 17, (21), 5355-5362.
18. Zijlstra, P.; Chon, J. W. M.; Gu, M., *Effect of heat accumulation on the dynamic range of a gold nanorod doped polymer nanocomposite for optical laser writing and patterning*. *Optics Express* **2007**, 15, (19), 12151-12160.
19. Hu, M.; Hartland, G. V., *Heat Dissipation for Au Particles in Aqueous Solution: Relaxation Time versus Size*. *Journal of Physical Chemistry B* **2002**, 106, (28), 7029-7033.
20. Hu, M.; Wang, X.; Hartland, G. V.; Salgueiriño-Maceira, V.; Liz-Marzán, L. M., *Heat dissipation in gold-silica core-shell nanoparticles*. *Chemical Physics Letters* **2003**, 372, (5-6), 767-772.
21. Caruso, F.; Lichtenfeld, H.; Donath, E.; Mohwald, H., *Investigation of Electrostatic Interactions in Polyelectrolyte Multilayer Films: Binding of Anionic Fluorescent Probes to Layers Assembled onto Colloids*. *Macromolecules* **1999**, 32, (7), 2317-2328.
22. Slooff, L. H.; de Dood, M. J. A.; van Blaaderen, A.; Polman, A., *Effects of heat treatment and concentration on the luminescence properties of erbium-doped silica sol-gel films*. *Journal of Non-Crystalline Solids* **2001**, 296, (3), 158-164.
23. Míguez, H.; Meseguer, F.; López, C.; Blanco, Á.; Moya, J. S.; Requena, J.; Mifsud, A.; Fornés, V., *Control of the Photonic Crystal Properties of fcc-Packed Submicrometer SiO₂ Spheres by Sintering*. *Advanced Materials* **1998**, 10, (6), 480-483.

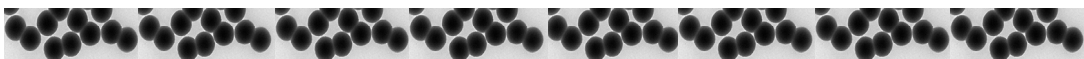
Chapter 5

The synthesis of colloidal silica dumbbells



Abstract

We describe the synthesis and characterization of stable suspensions of monodisperse fluorescently labeled silica dumbbell particles. Pure dispersions of silica dumbbells with center-to-center lengths from 174 nm to 2.3 μm were produced with a variety of aspect ratios. Individual particles in concentrated dispersions of these particles could be imaged with confocal microscopy. These particles can be used as a colloidal model system for addressing fundamental questions about crystal and glass formation of low aspect ratio anisotropic particles. They also have potential in photonic applications and electro-optical devices.



5.1. Introduction

Recent fundamental studies have shown that a combination of index matching and fluorescent labeling makes it possible to quantitatively study the structure and dynamics of concentrated colloidal dispersions of spheres on a single particle level with confocal microscopy¹⁻⁵. The extensive knowledge that is available to modify the surface of silica and latex particles allows the tuning of interactions from long-range repulsive^{6, 7}, to hard-sphere like^{1, 2, 8}, to even dipolar^{9, 10}. Thus far, almost all such fundamental quantitative real-space studies have been carried out only using colloidal spheres. However, a number of theoretical and experimental results show the wide variety of novel structure and dynamics for monodisperse anisotropic systems¹¹.

Experimental studies on anisotropic colloidal model systems have focussed mainly on high aspect ratio particles. Examples of Isotropic-Nematic phase behaviour have been observed with several different types of organic rods (FD-, TMV-viruses, Collagen, DNA,¹²⁻¹⁴) and inorganic materials (Vanadiumpentoxide (V_2O_5) β -ferric oxyhydroxide (β -FeOOH), boehmite (ALOOH))¹⁵⁻¹⁸. The first real-space observation of self-ordering behaviour of liquid crystals from rod-like colloidal particles on a single particle level has recently been reported by Maeda¹⁹, though the high refractive index of β -ferric oxyhydroxide will make it hard to extend these studies into three dimensions. In chapter 2 we have shown that fluorescently labelled high aspect ratio silica rods, suitable for single particle tracking via confocal microscopy and with a sufficiently high yield for phase behaviour studies, can be synthesized²⁰. Similarly, collective behaviour and quantitative confocal imaging were reported by Solomon et al²¹. These authors made fluorescently labelled ellipsoidal PMMA particles with high aspect ratios by stretching colloidal particles in a polymer matrix above the glass temperature²².

Theories and simulations of low aspect ratio hard core particles have predicted new phases, including a plastic crystal phase^{23, 24}, and novel colloidal glass behavior²⁵. These simulations also show that there is very little difference between the phase diagram of hard sphere dumbbells and that of hard spherocylinders of the same aspect ratio, suggesting that the exact shape may not be very important in this parameter region and that experimental results for low-aspect-ratio dumbbells may be representative for other particles such as spherocylinders²³. To experimentally test these theories, the synthesis of dispersions of anisotropic particles, properly labeled for confocal microscopy analysis, is essential. Such particles, with their optically anisotropic scattering properties and capacity to reorient in external fields, may also lead to new types of photonic materials²⁶⁻²⁸.

A few groups have reported methods to synthesize low aspect ratio anisotropic particles with relative standard deviations in size distribution below 20%. Recently, Manoharan et. al. have synthesized and separated small quantities of identically arranged particles in conglomerates of up to 13 spheres by aggregating colloids attached to the interface of liquid droplets in an emulsion²⁹. Yin et al. have been able to fuse spherical colloids on patterned substrates in small quantities³⁰. Liddel et al. have synthesized high refractive index zinc sulphide dumbbell particles with the goal of creating new photonic crystal structures³¹ though such systems are less interesting as model systems since index matching is not feasible. Snoeks et al. have used ion beam irradiation to produce ellipsoidal colloids³².

In this chapter we show how monodisperse anisotropic silica particles with aspect ratios below 2 and with fluorescently labeled cores can be synthesized. The particles

are designed to allow real space analysis of anisotropic model systems and may also serve as components of novel materials based on colloidal crystals, such as photonic crystals³³. The methods described in this paper are comparatively simple and can produce high yields of particles. Furthermore, the aspect ratio of these particles can be easily tuned.

5.2. Experimental

Anisotropic particles were formed by slightly destabilizing dispersions of spherical silica colloids to allow an initial stage of aggregation, i.e. dumbbell formation, to proceed. The process was terminated before significant amounts of aggregates composed of more particles had formed. The main method investigated in this article involved the use of shear-induced aggregation in ammonia/ethanol solutions (method 1) in which the silica particles were not completely stable. Following dumbbell formation, continuous growth of a silica layer in a seeded-growth step allowed the shape of the particle to be tuned, reducing the aspect ratio. We also present synthesis conditions and x-ray scattering results for pure dumbbell dispersions of much smaller particles synthesized from microemulsions for which the destabilizing mechanism is less well understood (method 2). For both methods, the dumbbells were separated from single spheres and larger aggregates via centrifugation techniques. The resulting dispersions contained pure dumbbells.

5.2.1. Chemicals Ammonia (29.7 w/w % of NH_3 in H_2O , Merck), fluoresceine isothiocyanate (FITC, Sigma), rhodamine B isothiocyanate (RITC, Aldrich), 3-aminopropyltriethoxy silane (APS, Fluka), were used as received. Ethanol (absolute, technical grade, Lamers & Pleuger) and tetraethoxysilane (TES, Fluka) were freshly distilled before use. For the microemulsion synthesis, cyclohexane (p.a. Merck), Igepal CO-520 (np5, Aldrich) were used as received. Sucrose (Sigma), for density gradient centrifugation, and dimethylsulfoxide (DMSO, Fluka), for index matching, were used as received. Molarities were calculated by assuming additivity of volumes of reagents/components.

5.2.2. Dumbbell synthesis

The spherical fluorescent silica core-shell particles used as precursors for dumbbells made using method 1 were made following a two-step process as described by van Blaaderen et al.^{34, 35}. The fluorescent core was synthesized by adding the reaction product of APS and FITC to a mixture of TES and ammonia in ethanol. 1.42 g APS (6.41 mmol) was coupled to 244 mg FITC (0.627 mmol) and stirred overnight in 10 ml absolute ethanol. This mixture was added together with 70 ml TES (0.31 mol) to a mixture of 175 ml ammonia and 1750 ml ethanol. The resulting cores radius was 200 nm with a polydispersity of 5%. These cores were grown further following a method described by Giesche³⁶. Separate TES/ethanol and ammonia/water/ethanol feeds under nitrogen atmosphere were added dropwise to a 0.6 M silica suspension in ethanol containing 8.0 M water and 0.6 M NH_3 until the desired particle size was achieved. The TES/ethanol feed contained 2.0 M TES in ethanol.

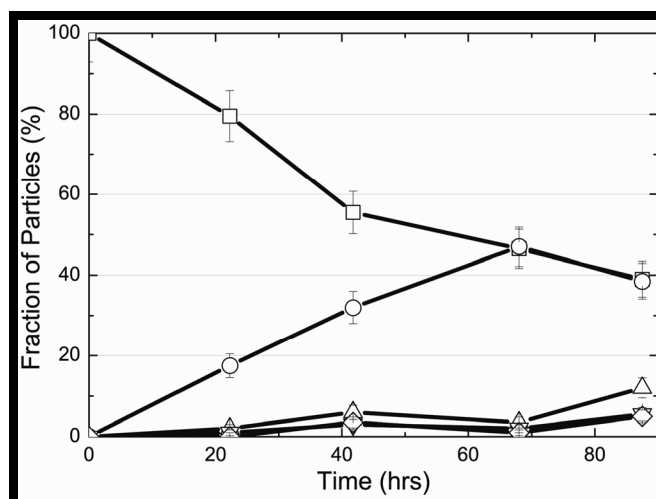


Fig. 5.1. The fraction of aggregates of different sizes as a function of time in a dispersion of 1.4 μm colloids in 120 ml/L ammonia and ethanol under shear (orthokinetic aggregation). Particles composed of 1, 2, 3, 4, and 5 or more spheres have the symbols square, circle, triangle, inverted triangle and diamond respectively. The number of dumbbells peaks at an anomalously high 45% after 70 hours, with few larger aggregates yet formed.

The ammonia/water/ethanol feed contained 1.2 M NH_3 and 16.0 M water in ethanol. This process resulted in spherical particles with FITC labeled silica cores and unlabeled silica shells. The particles were transferred via repeated slow centrifugation (<120 g) to 96% ethanol and could be stored indefinitely.

Method 1 involved destabilizing the particles through the addition of ammonia and then inducing aggregation through the application of shear (i.e., orthokinetic aggregation). Addition of ammonia increases both the surface charge of the colloids (at low ammonia concentrations) as well as the ion concentration. At high ammonia concentrations, the surface charge is no longer affected by the addition of ammonia thus the increase of ionic strength is the main effect which destabilizes the silica spheres.

A high yield of dumbbells was obtained under the following synthesis conditions. 1.4 μm diameter particles (1.5 v/v %) were dispersed in a mixture of 0.875 ml ammonia and 6.12 ml ethanol (ammonia 120 ml/L in ethanol). The dispersion was mixed in a cylindrical vial, 2 cm diameter, 5 cm length, which was rotated at 120 rpm horizontally on rollers with no stir bar (high but irreproducible dumbbell yields were also found using a stir bar rather than rollers.) Tests of lower ammonia concentrations (60ml/L) using otherwise the same conditions produced lower dumbbell yields.

The number of dumbbells produced as a function of time was tracked by taking small samples from the metastable dispersion at various times during the synthesis, diluting these samples by a factor of 20 in ethanol to stabilize the particles, and analyzing the stabilized sample under a fluorescence microscope. By observing the particles in the bulk of the diluted sample (up to 100 μm from the wall), and randomly choosing particles visually, the fraction of singles, dumbbells, triplets, and larger clusters could be measured as a function of time (Figure 5.1.). This process was also tested with an ammonia concentration of 60 ml/L however the resulting dumbbell formation rate was much slower and thus less ideal.

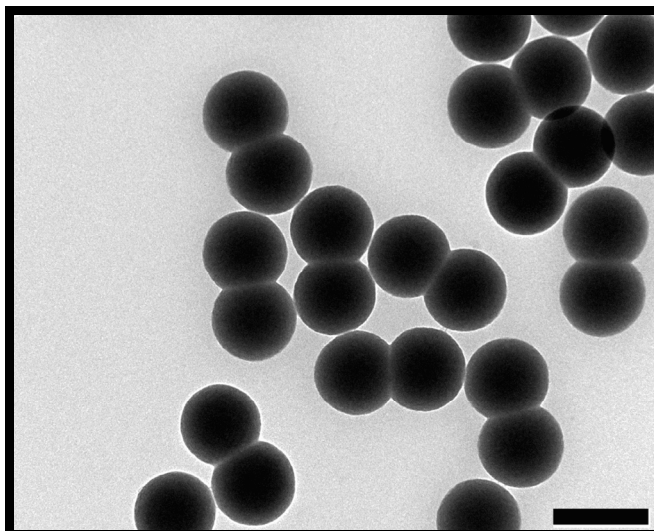


Fig. 5.2. TEM image of the silica dumbbells formed from seed particles grown in a microemulsion and aggregated by depletion effects (method 2). The polydispersities in diameter and length are both extremely low ($\sim 1.5\%$), suggesting that this is an excellent method for producing monodisperse nanoscale dumbbells. The scale bar represents 200 nm. Notice that overlapping particles (upper right) can be distinguished from dumbbell connections for particles of this size.

Much smaller silica dumbbells were also synthesized using a different method (method 2). First, small monodisperse spherical seed particles were synthesized in a water in oil microemulsion following the method of Osseo-Asare³⁷. 41 ml of Igepal CO520, a non-ionic surfactant, was mixed with 800 ml cyclohexane. 4.85 ml of ammonia was added and the mixture stirred for 30 minutes to form a micro-emulsion. Then 5.0 ml TES (22 mmol) was added under slow stirring and temperature control (20 °C) to form monodisperse silica particles (radius ~ 25 nm, polydispersity $\sim 3\%$).

The reaction was completed after a week at constant (20 °C) temperature. One third of these particles were grown to larger particles by first transferring the seed particles to a mixture of ethanol and ammonia. To this end, the cyclohexane was first removed by rotation evaporation and replaced with an equal amount of an ammonia in ethanol (100 ml/L) mixture. Then TES was added in batches to grow the particles to a radius of 86 nm. The added TES did not exceed 40 ml/L per batchwise addition, to avoid second nucleation. During this particle growth, dumbbells formed (Figure 5.2.). The destabilizing mechanism may be a depletion-induced attraction driven by micelles formed by the surfactant molecules. However, further study is necessary to confirm this hypothesis.

5.2.3. Lowering the size ratio

Once the dumbbells were formed, additional layers of SiO_2 were added to tune the dumbbell aspect ratio. To this end, a seeded growth method similar to that of Giesche³⁶ was again used in order to avoid secondary nucleation of spheres and new dumbbell formation. In some of the samples, the large dumbbell seeds were mixed with small (300nm diameter) silica spheres to prevent second nucleation (Samples 1A_1 and 1B). In samples with higher concentrations of dumbbell seeds (samples 1C_1 and 1C_2), no additional small spheres were added. All of the seed solutions contained initial concentrations of 30 ml/L ammonia.

Name of seeds (diameter) (nm)	Initial particle conc. (v/v%)		TES/EtOH feed		Remark	New L,D (nm)
	Dumbbell seeds	Additional (d = 300 nm)	TES conc. (v/v in EtOH)	Rate ((ml/hr)/duration)		
1A_1 (1400)	0.1 (60 ml)	0.1	0.05	1.7/42 hr	Small particles grown onto 10% of dumbbells	D = 1770 ±2% L = 1400 ±6%
1A_2 (1770)	0.1 (60 ml)	None	0.05	1.7/44 hr	2 nd Nucleation	D = 2300 ±2% L = 1400 ±6%
1B_1 (1400)	0.1 (60 ml)	0.1	0.01	1.7/35 hr		D = 1500 ±2% L = 1400 ±6%
1B_2 (1500)	0.1 (60 ml)	0.1	0.01	1.7/24 hr		D = 1610 ±2% L = 1380 ±2%
1B_3 (1610)	0.075 (60 ml)	None	TES and RITC added batchwise (see text)			D = 1630 ±2% L = 1370 ±3%
1C_1 (1400)	0.88 (20 ml)	None	0.05	1.17 (16hr)	2 nd Nucleation	D = 1690 ±2% L = 1430 ±3%
1C_2 (1690)	0.75 (20 ml)	None	0.25	1.15 (19.5hr)		D = 1810 ±2% L = 1440 ±3%

Table 5.1. Conditions for seeded growth. The starting dispersions consist of particles created via destabilization under shear flow (method 1), referred to as “dumbbell seeds”, mixed in some cases with additional 300 nm diameter spheres. Successive samples with the same letter (for example 1B_1, 1B_2, and 1B_3) use the previous sample as a seed dispersion. Starting ammonia concentrations for each sample was 30 ml/L. This concentration was held fixed for samples 1C_1 and 1C_2 by adding an additional ammonia/water/ethanol feed. The dumbbell particle dimensions given in the last column include an uncertainty that contains both the measurement uncertainty and the polydispersity. The measurement uncertainty of L was ~2%.

A feed of diluted TES in ethanol was added dropwise to the dispersions over different periods of time to create different aspect ratios. For samples 1C_1 and 1C_2 a second ammonia/water/ethanol feed was added dropwise through separate tubes to maintain a constant molar concentration of NH₃ and water during the synthesis³⁶. A complete list of synthesis conditions tested is given in Table 5.1.

One batch of dumbbells (sample 1B_3) was coated with an extra fluorescent layer to facilitate the tracking of particles with confocal microscopy. 2.6 mg of RITC (4.9 μmol) was mixed with 2.15 μl APS (9.2 μmol) in 0.5 ml 100% ethanol and stirred overnight to couple the RITC and APS. 19 μl of this mixture was added simultaneously with 125 μl TES batchwise to the dispersion. The same ammonia concentration (30ml/L) was used. This was repeated two times to create a 20 nm layer of rhodamine dyed silica. The polydispersity for different synthesis conditions was measured using scanning electron microscopy (SEM) for the larger particles and transmission electron microscopy (TEM) for the smallest particles.

5.2.4. Purification of Dumbbells

Synthesis conditions were chosen such that the dispersions produced after aggregation and seeded growth were a mixture of single spheres, dumbbells, and relatively small amounts of clusters of three or more particles. To separate small amounts of dumbbells from the dispersion two centrifugation techniques were used. Density gradient centrifugation^{29, 38} was used to create small yields of particles in one step.

The gradient was created with a two-cylinder gradient forming device (550 ml, Sigma-Aldrich). A Hettich Rotina 46S centrifuge with swing-out buckets was used at typical accelerations of 40 g to 160 g. Both sucrose-water and glycerol-water gradient mixtures were tested. The largest gradients used were 0.037 (g/ml)/cm. A wide centrifuge tube, with an inner diameter of 5.8 cm was used to maximize the yield. A thick (1/2 cm) band of colloids was loaded as an inverse gradient using the gradient forming device. The maximum inverse gradient loaded was $|\partial f / \partial z|_{\max} = 0.009 \text{ cm}^{-1}$, where f is the volume fraction of the colloids.

To achieve larger yields than with the density gradient method, repeated centrifugation in uniform solvents was also tested. Particles were centrifuged until dumbbells and larger aggregates had completely sedimented but a fraction of the spherical particles had not. The speed of dumbbell sedimentation was found to be up to 1.35 that of the spherical particles depending on the aspect ratio. The timing of the centrifugation was chosen such that roughly 15% of the single spheres could be removed with each step. This method requires more than 20 repeated separations to purify the dumbbells but has the potential to produce higher yields than density gradient centrifugation.

5.2.5. Small angle X-ray scattering

Low concentrations of the 174 nm diameter dumbbells created with method 1 were analyzed using Small Angle X-ray Scattering (SAXS) at the European Synchrotron Radiation Facility (ESRF) in Grenoble, France (ESRF, BM26 DUBBLE-beamline). X-rays of wavelength 1.24 Å were recorded at 8 m distance from the sample.

5.2.6. Confocal microscopy

Dense sediments of pure dumbbell samples were analyzed on a single particle level using confocal microscopy (Leica TCS SP2, 63x/N.A. 1.4 lens, 488 nm Ar/Kr excitation wavelength). Dispersions were prepared in an index of refraction matching solvent mixture (88% w/w DMSO/water) at 0.25 v/v % colloid concentration. In order to use the minimum amount of sample, narrow sedimentation vials were built by affixing a 3 cm length, 1 mm diameter hollow glass cylinder (the top of a Pasteur pipette) to a glass cover slip such that the cylinder stood vertically when the cover slip was horizontal. Silicone rubber (GE) was used to glue the cylinder to the cover slip. These sample holders were filled with the index matched dumbbell dispersion and mounted on an inverted scanning confocal microscope so that the colloids sedimented slowly onto the cover slip.

In this way, sediments of 100 to 200 μm thick were slowly formed and were analyzed. Particle tracking was achieved using IDL (RSI) and methods similar to those described by van Blaaderen et al.^{1,2} and Crocker and Grier³⁹.

5.2.7. Electric field

Exploring experiments to see how dumbbells behave in an electric field were also performed in the same setup as described in the previous section. This time the top of a Pasteur pipet was placed on an ITO coated glass cover slip, which was used as electrode. A conducting wire of 50 μm thickness was the opposite electrode. After a night of sedimentation in an electric field of ~ 100 V/mm the sediment was observed with a confocal microscope.

5.3. Results and Discussion

5.3.1. Synthesis results

Figure 5.3 shows SEM images of dumbbells in various stages of growth with aspect ratios of 1.0 (Figure 5.3.a), 0.80 (Figure 5.3.b), and 0.61 (Figure 5.3.c). Figure 5.3.d shows a superposition of the dumbbells (sample 1A) in the 3 stages of growth. As this image shows, a uniform layer of silica was grown with each step. The dumbbell size and aspect ratio are defined by the diameter of the component spheres, D , and the center-to-center distance between the spheres, L (Figure 5.2.b).

The polydispersity of dumbbells is characterized by the standard deviations from the mean for D and L , i.e. δD and δL . The dumbbells formed from the microemulsion (method 2) had a very low polydispersity in both L and D , with $\delta L / L \cong \delta D / D \cong 0.02$, particularly notable given the small size of the particles. This result suggests that dumbbell formation occurred suddenly, after which the dumbbells were coated. Polydispersities for the larger dumbbells (method 1) after different controlled growth conditions are given in Table 5.1.

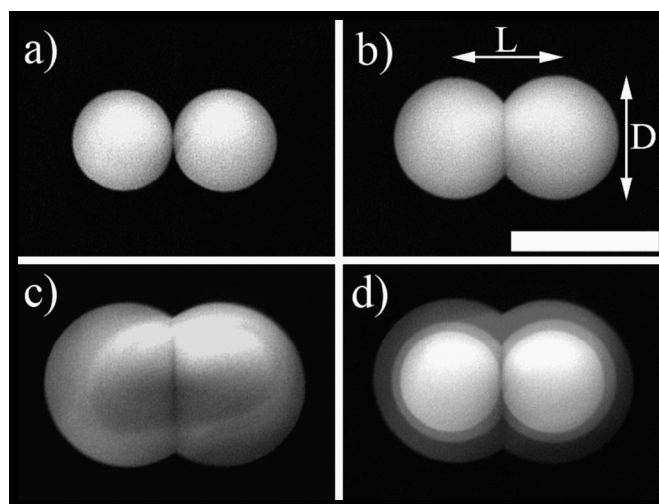


Fig. 5.3. SEM image of dumbbell growth by TES addition.

(a) $D=1.40$ μm , $L=1.40$ μm . (b) $D=1.74$ μm , $L=1.40$ μm (sample 1A_1) and (c) $D=2.30$ μm , $L=1.40$ μm (sample 1A_2).

The initial dumbbell shown in (a) was formed by destabilizing the dispersion in ammonia under application of shear (method 1). Subsequent stages in the growth of the same dispersion are shown in (b) and (c). The images (a-c) are superimposed in image (d) to illustrate the uniformity of the layers grown. Image (b) includes arrows that give the definition of L and D used in this paper. The scale bar in the lower right of image (b) is 2 μm which may be applied to all four images

During controlled growth the polydispersity remained roughly constant except in the case of sample 1A for which an increase in polydispersity in L occurred early in the seeded growth process

This may have occurred due to the somewhat higher TES feed rate (the product of the TES concentration and the TES/EtOH solution feed rate) for this sample, which may have increased the ion concentration and thus the likelihood that new dumbbells would form. It should be noted that the measurement uncertainty for L was on the order of 2% (due mainly to the uncertainty of finding the centers of each sphere), therefore the numbers given for polydispersity in L represent an upper bound. The low polydispersities in L throughout the growth for samples 1B and 1C is strong evidence that no new dumbbells were formed during the shell-growth steps for these samples.

Another factor affecting the synthesis of lower aspect ratio dumbbells was second nucleation and the growth of small spheres onto the surface of the dumbbells. For sample 1A_1 some of the added small spheres grew onto the surface of 10% of the dumbbells (see Table 5.1). For this reason, growth on this sample was continued with spheres removed (sample 1A_2) which led to second nucleation. This problem was eliminated in sample 1B, for which the concentration in the TES feed was substantially reduced. In sample 1C_1, for which no additional small particles were added and higher concentration of dumbbell seed particles were used, some second nucleation was observed. However in sample 1C_2 for which the concentration in the TES feed was reduced, no second nucleation was observed. Second nucleation was not necessarily a problem as the newly nucleated particles could be separated from the dispersion via centrifugation.

As seen in Figure 5.1., the peak dumbbell (number) concentration using method 1 was roughly 45% after about 70 hours, with about 5% variation from synthesis to synthesis and less than 5% statistical uncertainty. At this peak dumbbell fraction, the fraction of three and four particle clusters was still remarkably low (<5%). Simple models for diffusion and shear-induced aggregation predict a peak dumbbell fraction of less than 25%^{40, 41} and higher fractions of three and four particle clusters than those measured in our experiments. At a lower ammonia concentration (60ml/L) dumbbells formed more slowly, and three-particle clusters formed relatively faster. For example, after 140 hours, the dumbbell yield had peaked at roughly 25% with the number of three-particle clusters at roughly 10%.

We speculate the dumbbell yield may be determined by the thickness of the double layer and local hydrodynamic conditions specific to dumbbells. The dumbbell yield for method 2 was 20% also with a low fraction (~5%) of larger aggregates. It may be possible to further optimize the dumbbell yield of method 2.

5.3.2. Purification of dumbbells

We were able to purify large quantities of dumbbells through repeated centrifugation in a uniform solvent. Beginning with a 20% dumbbell mixture containing very few three-particle clusters (<0.5%), the dumbbell fraction was increased to 85% after centrifuging 17 times. During the centrifugation, several samples were taken and the fraction of dumbbells measured.

This process of gradual purification of the dumbbells through repeated centrifugation can be modeled theoretically. Assuming that a number fraction f_s of singles was removed at each step and that all of the dumbbells were retained in the sediment, a simple calculation gives the dumbbell fraction $F(n)$ after n centrifugation steps:

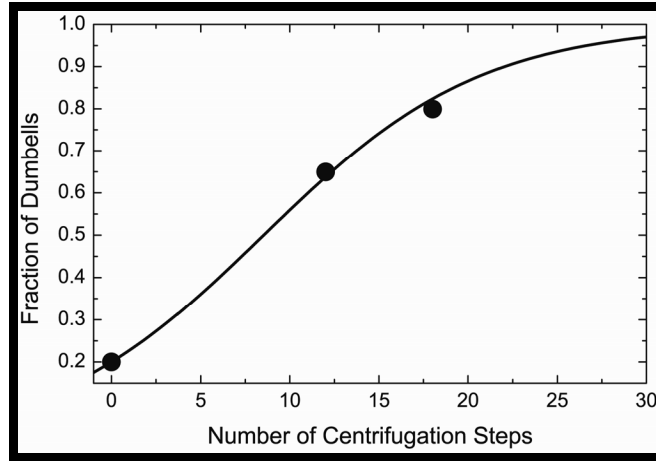


Fig. 5.4. The increasing fraction of dumbbells using repeated centrifugation (sample 1B_1). The circles are experimental values. Centrifugation speeds of 1000 RPM were used with volume fractions of ~0.5 %. The solid line is the theoretical fraction predicted by Eq. 5.1 with $f=0.15$, where f is the fraction of singles removed with each step.

$$F(n) = \frac{1}{1 + \left(\frac{1}{F(0)} - 1 \right) (1 - f_s)^n}. \quad (5.1)$$

This expression was fit to the data with f_s as the free parameter (Figure 5.4). Our result of $f_s=0.15$ is reasonable, considering that we removed less than the maximum number of singles to insure that no dumbbells were lost during each centrifugation step. In principle, this approach could provide large yields of pure dumbbells. Assuming the dumbbells sediment roughly 1.35 times as fast as single particles, the theoretical limit for f_s is 0.26.

Inserting this into equation 1 suggests a highly purified sample could be achieved (>99% dumbbells) with 20 centrifugation steps for $F(0)=0.2$ (although it would have taken 37 steps for $f_s=0.15$).

Smaller yields (~several milligrams of colloids) of pure (>99%) dumbbell dispersions were achieved in one step through density gradient centrifugation³⁸. This technique, while well established in a number of fields, has only recently been applied to large colloidal particles²⁹ thus we examine the optimal conditions in some detail here.

The theoretical limit for maximum loading of large, dense colloids, and thus optimum particle yield, can be calculated from simple considerations. In order for a liquid or complex fluid of non-uniform density to remain stable under a gravitational or centripetal force field, the fluid density must decrease with height³⁸, i.e.

$$\frac{\partial \rho(z)}{\partial z} \leq 0. \quad (5.2)$$

Here z is the height of the gradient, the origin of the z axis is at the top of the tube, and the direction of sedimentation (towards the bottom) is in the positive direction. If the fluid is a combination of colloids and a non-uniform solvent, we can express the density as

$$\rho = f_c \rho_c + (1 - f_c) \rho_s, \quad (5.3)$$

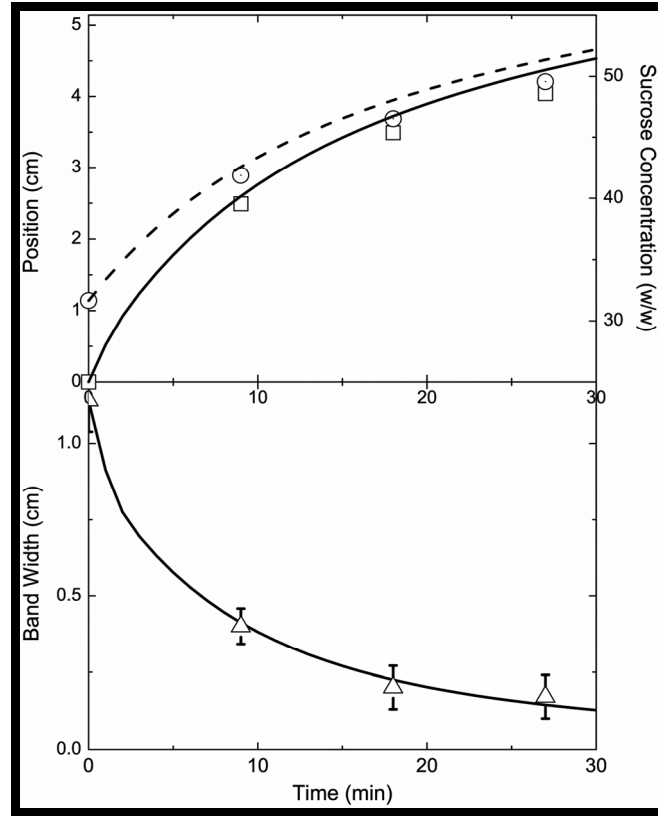


Fig. 5.5. Theoretical (lines) and experimental (symbols) values of the band position (top) and width (bottom) during centrifugation of $1.4 \mu\text{m}$ spheres (loading concentration gradient of 0.005 (g/ml)/cm) at 1000 RPM . The position is the radial position of the band in the centrifuge relative to its position at the beginning of centrifugation. The top and bottom of the band are marked by the squares and circles (experimental) and the solid and dashed lines (theoretical) respectively. The right hand side of the top plot gives the sucrose weight percentage in as a function of radius.

where ρ is the total density, ρ_c is the density of the colloid particles (i.e. $\rho_c \approx 1.9 \text{ g/ml}$ in the case of silica), $\rho_s = \rho_s(z)$ is the density of the non-uniform solvent, and $f_c = f_c(z)$ is the volume fraction of colloids. Assuming a linear gradient in density of the solvent, i.e. that $\rho_s(z) = ((\rho_1 - \rho_2)/\Delta z)z + \rho_2$, where ρ_1 is the solvent density at the top of the tube, ρ_2 is the solvent density at the bottom of the tube, and Δz the height of the gradient, the maximum gradient in the colloid fraction is found from equations (5.2) and (5.3):

$$-\frac{\partial f_c}{\partial z} \leq \frac{\rho_2 - \rho_1}{\Delta z} \frac{1}{\rho_c - \rho_1} \quad (5.4)$$

Here we have assumed $f_c \ll 1$ which is the case for the dense colloids used in this paper. The maximum gradient in the colloid concentration is achieved when $\rho_2 - \rho_1$ is maximized. The optimal yield for a given colloid density ρ_c occurs when $\rho_c = \rho_2$, in which case $|\partial f / \partial z|_{\text{max}} = 1 / \Delta z$. Using a sucrose solution with $\rho_2 = 1.34 \text{ g/ml}$ and $\rho_1 = 1.08 \text{ g/ml}$, and a tube height of $\Delta z = 7 \text{ cm}$ the maximum gradient is $|\partial f / \partial z|_{\text{max}} = 0.045 \text{ cm}^{-1}$.

To calculate the optimal time for centrifugation, the sedimentation depth as a function of time was calculated for the gradient solution. The rate of sedimentation $v(z)$ at any given height depends on the solvent viscosity $\eta(z)$, the solvent density $\rho(z)$,

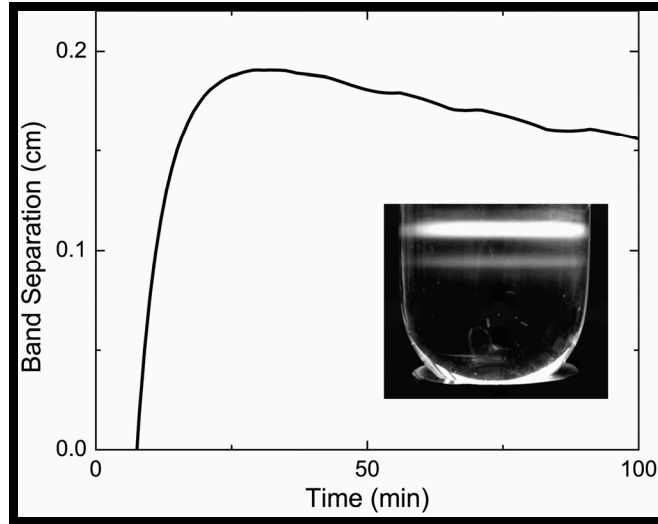


Fig. 5.6. Theoretical prediction of the band separation vs. time assuming a centrifuge speed of 1000 rpm and starting radius of 11 cm assuming that the dumbbells sediment 1.2 times as fast as the spheres. The theory predicts an optimum time to remove the bands. The inset shows a photograph of two bands formed after centrifugation for 20 min. at 1000 rpm using sample 1B_2. The top band is composed of single spheres, the bottom dumbbells. The photo shows that the bands are clearly separated and can thus be separately removed. The bottom band is nearly index matched with the sucrose solutions and is thus dimmer than the top band. There is also a very faint band of 3-particle aggregates which is not visible in this photo. The “ripples” in the theoretical curve are an artifact due to the limited resolution of the viscosity and density data for the sucrose solution.

the colloid effective radius, the centrifuge frequency, and ρ_c . Here we assume that the concentration of colloids is low enough that it is not a determining factor in $v(z)$. The total time to sediment from height z_i to z_f can be calculated numerically from the expression

$$t = \int_{z_i}^{z_f} \frac{1}{v(z)} dz \quad (5.5)$$

Using this expression, the position of the top and bottom of the colloid band as a function of time was calculated. This result was tested experimentally using 1.4 μm spheres in a sucrose solution with $\rho_2=1.30$ g/ml and $\rho_1=1.08$ g/ml, with the density $\eta(z)$ taken from standard tables for sucrose in water solutions⁴². As seen in Figure 5.5, the theoretically predicted depth as a function of time and the band thickness match the experiment with no adjustable parameters. An optimum centrifugation time was found by applying equation (5.4) to the case of bands of dumbbells and single particles. Equation (5.5) predicts a maximum in their separation; the ideal time for unloading the bands. As seen in Figure 5.6, this happens after 30 minutes of centrifugation at 1000 rpm with a starting position of 11 cm from

the center of the centrifuge. Here it was assumed that the dumbbells sediment 1.2 times as fast as the spheres, a result that will vary slightly depending on the dumbbell aspect ratio. At this time, the thickness of the band has decreased by a factor of ~ 10 due to the strongly non-linear increase of the viscosity with depth. This contraction increases the magnitude of the colloid concentration gradient $\partial f / \partial z$ in the band and must be taken into account when applying equation (5.3). Optimal results were obtained when using a centrifugation time slightly less than the theoretically optimal, for which the band thickness had decreased by roughly a factor of ~ 5 .

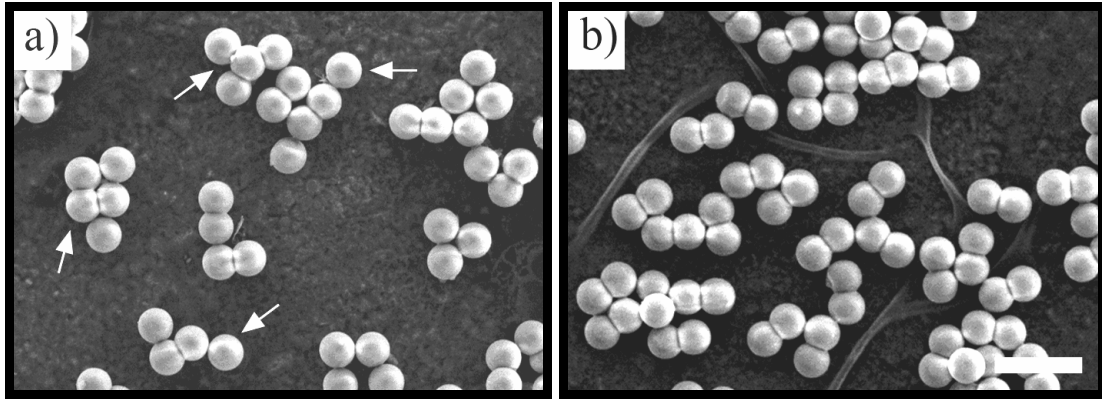


Figure 5.7. SEM image of sample 1A_1 before (a) and after (b) density gradient sedimentation. The arrows in (a) point to singles, a triple, and a quadruple particle. In the right figure only dumbbells remain. The scale bar in the lower right is 4 μm .

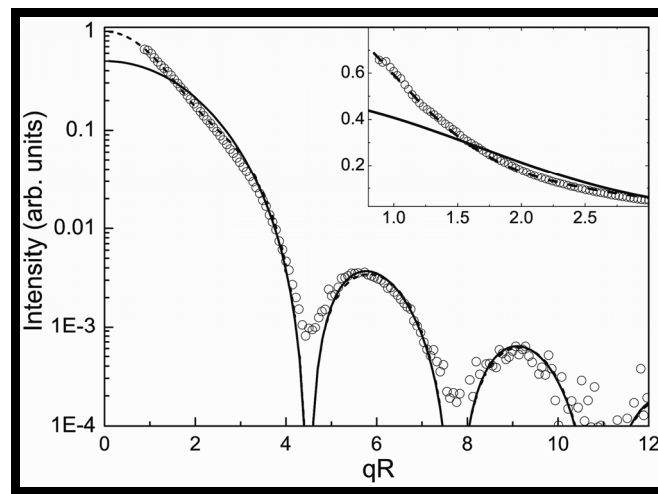


Fig. 5.8. Intensity of scattered x-rays vs. qR , where q is the wave number ($2\pi/\lambda$, where λ is the x-ray wavelength) and R is the radius of the spheres forming the dumbbell ($R=D/2$). The plot shows the measured data for a pure dumbbell sample with $D=174$ nm. The inset shows the same data on a linear scale over a narrower range of wave numbers. Also shown are the theoretical calculations for a dumbbell of aspect ratio 1 (dashed line), and for spheres of diameter 174 nm (solid line). As seen from the plot and the inset, the theory agrees well with the data. Also, it is clear that the main deviation of the dumbbell scattering from the prediction for spherical particles occurs at $qR < 4.5$, i.e. before the first minimum.

Using this centrifugation time, the maximum allowed loading of the colloids in the top band was $|\partial f / \partial z|_{\text{max}} = 0.045/5 = 0.009 \text{ cm}^{-1}$ producing a theoretical yield of 95 mg of dumbbells from a 40% dispersion (independent of particle size). Since this was more than sufficient for our measurements, we used somewhat lower colloid concentrations with net yields of ~ 15 mg. As seen in Figure 5.6, bands of single particles and dumbbells are clearly visible.

Figure 5.7. shows an SEM image of dumbbells before and after centrifugation. As seen in Figure 5.7.a, a number of singles, and a few triples and quadruples remained in the pre-centrifugation dispersion. After centrifugation the dispersion contains only dumbbells (Figure 5.7.b).

It can be difficult to distinguish between single spheres and dumbbells with scattering methods, except at small values of the scattered wave number. This was observed with X-ray scattering measurements of the small pure dumbbell samples

grown from the microemulsion (method 2) and can be explained theoretically. The theoretical form factor for scattering from a dumbbell with $L/D=1$, rotationally averaged, can be solved exactly using the Born approximation (single scattering).

$$F_{dumbbell} = F_{sphere} \cdot \left(1 + \frac{\sin(2qR)}{2qR} \right) \quad (5.6)$$

where q is the wave number and R is the radius of the spheres forming the dumbbell, and F_{sphere} is the form factor from a Mie sphere calculation^{43,44}. As seen in equation (5.6), $F_{dumbbell} \approx F_{sphere}$ for $qR \gg 1$. This makes small angle x-ray scattering a particularly useful approach for examining dumbbell particles since low values of q can be resolved. As seen in Figure 5.8, the dumbbell dispersion is well modeled by equation (5.6). The result for pure dumbbells clearly deviates from the predicted result for spherical particles⁴⁴ before the first scattering minimum ($qR=4.5$). The small discrepancies still visible may be related to the fact that the size ratio of these particles was not exactly 1 ($L/D=0.80$) and/or the presence of a small amount of higher aggregates.

5.3.3. Confocal microscopy results

Sediments of several samples of fluorescently labeled dumbbells were observed in the confocal microscope. The individual cores could be located and tracked using methods similar as described in references 1 and 2. At low concentrations, the location and orientation of individual dumbbells were easily found (Figure 5.9.a). At higher concentrations, this became difficult, since it was difficult to distinguish between two spheres that are part of the same dumbbell from two spheres that are in contact but belong to different dumbbells.

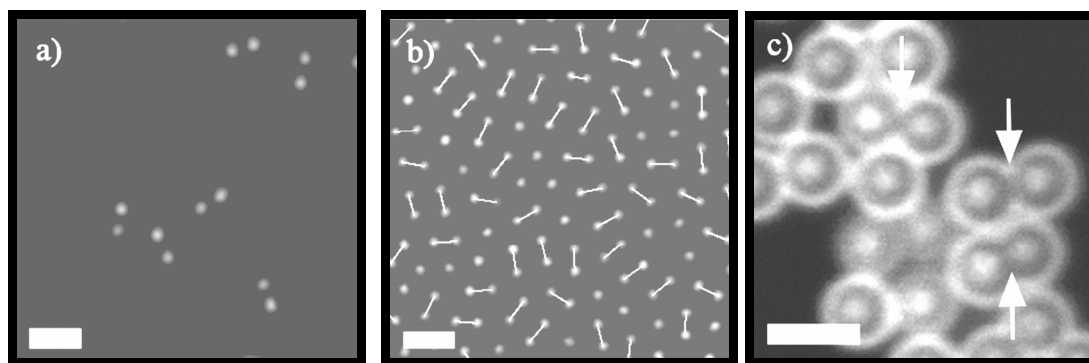


Fig. 5.9. Scanning laser confocal microscopy photos of FITC labeled dumbbells (sample 1C_2) at low (a) and high (b) concentrations, and of FITC core, RITC shell dumbbells, in a color picture the FITC core has a different color than the RITC shell. (c) a sample made under similar conditions to sample 1B_3). At low concentrations (a), the position and orientation of individual dumbbells can be easily resolved. At high concentrations (b), the position and orientation of individual dumbbells, as denoted by the solid white lines, were found by pairing up cores that were separated by less than D using image analysis software (IDL). Some of the dumbbells in (b) are tipped up with respect to the glass so that the coupled core cannot be seen. The arrows in (c) point out the lack of RITC at the center of dumbbells. This lack of signal distinguishes a dumbbell from two touching spheres. The scale bars are (a) $3 \mu\text{m}$ (b) $3 \mu\text{m}$ and (c) $2 \mu\text{m}$.

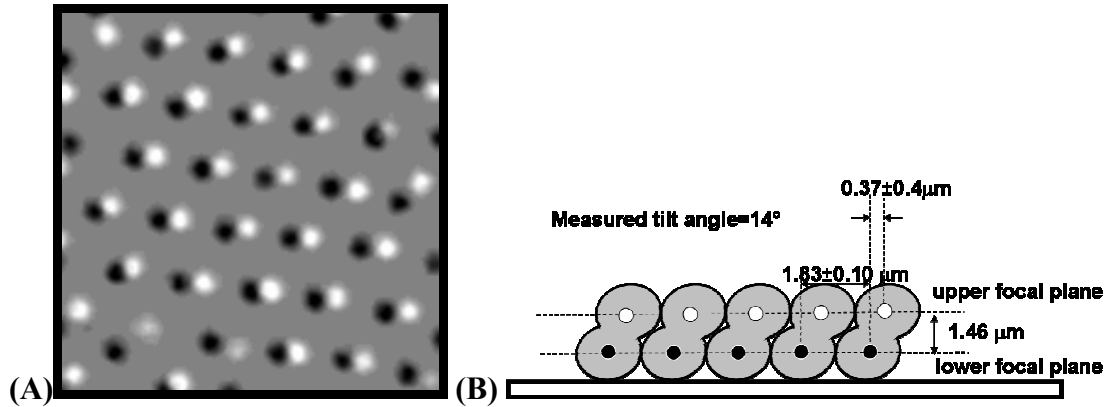


Fig. 5.10. (a) Image processed picture of 2 superimposed frames of a dumbbell sediment taken with confocal microscopy. The first layer (lower focal plane) is colored in black, the second (upper focal plane) is white. The dumbbell sediment shows a hexagonal arrangement, with the dumbbells not aligned vertically but slightly tilted with an angle of 14° . The picture measures 7.5 by $7.5 \mu\text{m}^2$
(b) Schematic representation of the dumbbell sediment (side view).

The simplest method of distinguishing these two cases is to measure the distance between the core centers of the two spheres. This distance is slightly less when the cores belong to the same dumbbell, depending on the dumbbell aspect ratio. Thus by finding all of the nearest neighbor distances, the tracking software can locate the dumbbells. To this end, a short IDL program was written to connect cores that belong to the same dumbbell (Figure 5.9.b). Once the cores belonging to the same dumbbell were determined, the position and orientation of all of the dumbbells in a three dimensional sediment could be determined.

If a dilute suspension of particles that were synthesized (1_C2) and purified sedimented with a concentration of roughly 0.1 vol.% in an index matching fluid of water and glycerol, they sedimented slowly because of the high viscosity of the water glycerol mixture. The bottom of the sedimentation tube is a glass cover slip and thus very smooth. This combination resulted in a locally ordered sediment of FITC dumbbells as can be seen in Figure 5.10.a. The particles at the bottom order in a hexagonal arrangement. Computer simulations confirm that dumbbells prefer this arrangement⁴⁵. Only the bottom layer was ordered the rest of the sediment was glassy.

The picture shows 2 superimposed confocal pictures of the first 2 focal planes with bright fluorescent cores in their view. Via image processing the fluorescent cores of the first layer are shown in white, while the cores of the second layer are shown in black. The particles seem to sediment in a hexagonal close packed layer. The difference in height between the 2 planes is $1.46 \mu\text{m}$. From this it was calculated that the dumbbell particles are not aligned straight up at the bottom but make a tilt angle of 21° . From a schematic draw, as depicted in Figure 5.10.b., it can be seen that the orientation of the long axis of the dumbbell is expected to vary with the aspect ratio of the rod.

Figure 5.11.a shows the particles of batch (1_C2) with the same concentration and dispersion, sedimented along the lines of an electric field of $\sim 100 \text{ V/m}$. The way the particles settle clearly deviates from that of sedimentation without electric field. In an electric field the dumbbells seem to order in a tetragonal crystal structure. The particles are aligned along the lines of the electric field. Therefore, in Figure 5.11.a.

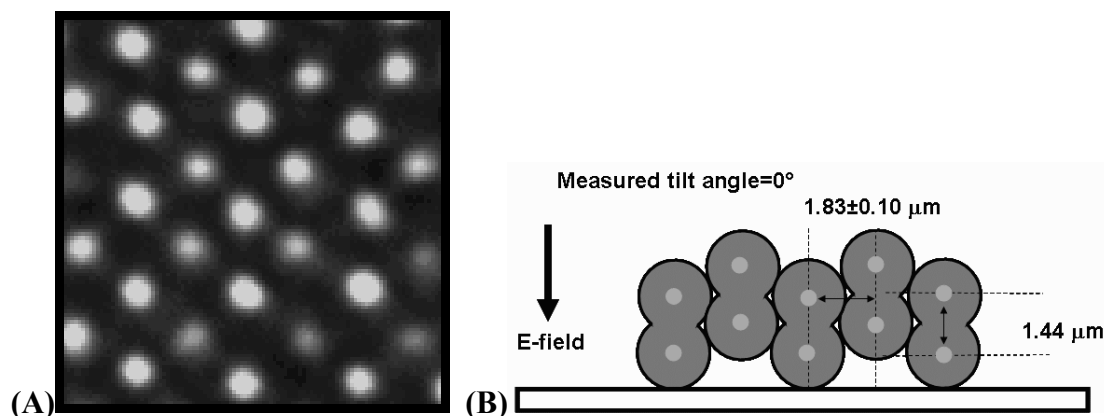


Fig. 5.11. (a) Confocal image of dumbbells sedimented in an electric field. (The field lines are equal to the gravitational field (perpendicular to the viewing area) The sediment shows a cubic crystal arrangement. The picture measures 6.4 by $6.4 \mu\text{m}^2$)
(b) Schematic representation of the dumbbell sediment (side view).

the cores of the particles that are in the centre of the focal plane can be seen in the same frame as the cores of the particles in the plane just above. Their centres appear smaller (and more grey) in the picture. The ordered structure the dumbbells form is clarified by a schematic representation of the sediment (see Figure 5.11.b.) where the side view is sketched.

As the aspect ratio of the dumbbells approaches one, using the core separation distance to distinguish dumbbells becomes more difficult. The RITC coated particles depicted in Figure 5.11.c offer a potential solution to this problem. In this case, two channels were measured with the confocal microscope. An FITC channel yielded the position of the dumbbell cores. The RITC channel located the shells of the particles. As pointed out by the arrows in Figure 5.11.c, the dumbbell particles have a reduced RITC signal between the cores compared with the signal between two touching cores.

In this way, two cores in the same dumbbells may be distinguished from cores in neighboring, touching dumbbells. Another possibility to distinguish which cores belong to which dumbbell particles may be to use the fact that the dynamics of the cores that are attached is strongly correlated.

5.4. Conclusions

We have shown that it is possible to create highly monodisperse dispersions of anisotropic particles with well-defined aspect ratios from 0 to 1. The cores of these particles can be labeled to allow for confocal and fluorescent microscopy measurements and quantitative structural analysis in three dimensions. The first preliminary results indicate that dumbbells locally can form crystalline structures. Future work includes the quantitative analysis of dense dispersions of these particles using confocal microscopy and light scattering techniques, characterization of crystalline and plastic crystalline phases, study of the effect of electric fields on dense dispersions of these particles, tuning the dumbbell interactions by changing the solvent properties, and modeling the effect of shear on the phase behavior. We are also investigating some of the anomalous aggregation phenomena encountered in this study.

Acknowledgements

We would like to thank Jacob Hoogenboom for synthesis of the FITC labeled core-shell spheres, Diana Maas for the microemulsion synthesis and Christina Graf for additional 300 nm silica particles, and Andrei Petukhov, Igor Dolbnya, Arnout Imhof and Job Thijssen, for helping us with x-ray scattering measurements at Grenoble, France (ESRF, BM26 DUBBLE-beamline) and the x-ray analysis.

The work presented here was done together with Patrick Johnson. This work was financially supported by the Foundation for the Fundamental Research of Matter (FOM), which is part of The Netherlands Organization for Scientific Research (NWO). Additional support for travel for one of the authors (Johnson) was provided by the Simmons College Fund for Research.

5.5. References

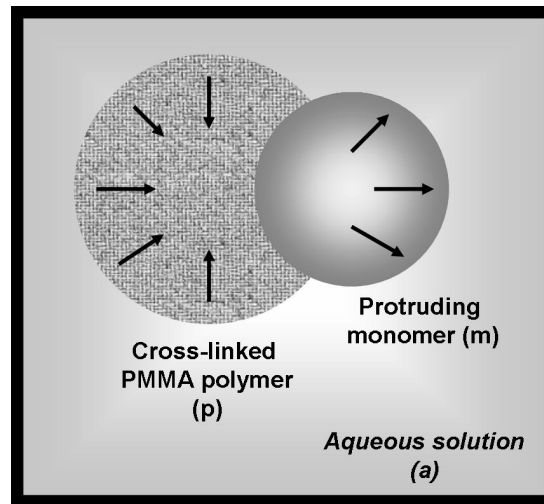
1. van Blaaderen, A.; Wiltzius, P., *Real-Space Structure of Colloidal Hard-Sphere Glasses*. *Science* **1995**, 270, (5239), 1177-1179.
2. van Blaaderen, A.; Ruel, R.; Wiltzius, P., *Template-directed colloidal crystallization*. *Nature* **1997**, 385, (6614), 321-324.
3. Kegel, W. K.; van Blaaderen, A., *Direct Observation of Dynamical Heterogeneities in Colloidal Hard-Sphere Suspensions*. *Science* **2000**, 287, (5451), 290-293.
4. Gasser, U.; Weeks, E. R.; Schofield, A.; Pusey, P. N.; Weitz, D. A., *Real-Space Imaging of Nucleation and Growth in Colloidal Crystallization*. *Science* **2001**, 292, (5515), 258-262.
5. Yethiraj, A.; van Blaaderen, A., *A colloidal model system with an interaction tunable from hard sphere to soft and dipolar*. *Nature* **2003**, 421, (6922), 513-517.
6. Hachisu, S.; Kobayashi, Y.; Kose, A., *Phase separation in monodisperse latexes*. *Journal of Colloid and Interface Science* **1973**, 42, (2), 342-348.
7. van Blaaderen, A., *From the de broglie to visible wavelengths: Manipulating electrons and photons with colloids*. *MRS Bulletin* **1998**, 23, (10), 39-43.
8. Pusey, P. N.; van Megen, W., *Phase behaviour of concentrated suspensions of nearly hard colloidal spheres*. *Nature* **1986**, 320, (6060), 340-342.
9. Dassanayake, U.; Fraden, S.; Blaaderen, A. v., *Structure of electrorheological fluids*. *Journal of Chemical Physics* **2000**, 112, (8), 3851-3858.
10. Martin, J. E.; Odinek, J.; Halsey, T. C.; Kamien, R., *Structure and dynamics of electrorheological fluids*. *Physical Review E* **1998**, 57, (1), 756.
11. Lekkerkerker, H. N. W.; Vroege, G. J., *Phase Transitions in Colloidal Dispersions*. In *Fundamental Problems in Statistical Mechanics VIII*. Elsevier Science: Amsterdam: 1994; p p. 207.
12. Stroobants, A.; Lekkerkerker, H. N. W.; Odijk, T., *Effect of electrostatic interaction on the liquid crystal phase transition in solutions of rodlike polyelectrolytes*. *Macromolecules* **1986**, 19, (8), 2232-2238.
13. Fraden, S.; Maret, G.; Caspar, D. L. D.; Meyer, R. B., *Isotropic-nematic phase transition and angular correlations in isotropic suspensions of tobacco mosaic virus*. *Physical Review Letters* **1989**, 63, (19), 2068.
14. Tracy, M. A.; Pecora, R., *Synthesis, characterization, and dynamics of a rod/sphere composite liquid*. *Macromolecules* **1992**, 25, (1), 337-349.
15. Maeda, H.; Maeda, Y., *Atomic Force Microscopy Studies for Investigating the Smectic Structures of Colloidal Crystals of β -FeOOH*. *Langmuir* **1996**, 12, (6), 1446-1452.
16. Pelletier, O.; Davidson, P.; Bourgaux, C.; Livage, J., *The effect of attractive interactions on the nematic order of V2O5 gels*. *Europhysics Letters* **1999**, 48, (1), 53-59.
17. Buining, P. A.; Philipse, A. P.; Lekkerkerker, H. N. W., *Phase Behavior of Aqueous Dispersions of Colloidal Boehmite Rods*. *Langmuir* **1994**, 10, (7), 2106-2114.
18. van Bruggen, M. P. B.; Dhont, J. K. G.; Lekkerkerker, H. N. W., *Morphology and Kinetics of the Isotropic-Nematic Phase Transition in Dispersions of Hard Rods*. *Macromolecules* **1999**, 32, (7), 2256-2264.

19. Maeda, H.; Maeda, Y., *Liquid Crystal Formation in Suspensions of Hard Rodlike Colloidal Particles: Direct Observation of Particle Arrangement and Self-Ordering Behavior*. Physical Review Letters **2003**, 90, (1), 018303.
20. van Kats, C. M.; Johnson, P. M.; van den Meerakker, J. E. A. M.; van Blaaderen, A., *Synthesis of Monodisperse High-Aspect-Ratio Colloidal Silicon and Silica Rods*. Langmuir **2004**, 20, (25), 11201-11207.
21. Mohraz, A.; Solomon, M. J., *Direct Visualization of Colloidal Rod Assembly by Confocal Microscopy*. Langmuir **2005**, 21, (12), 5298-5306.
22. Ho, C. C.; Keller, A.; Odell, J. A.; Ottewill, R. H., *Preparation of monodisperse ellipsoidal polystyrene particles*. Colloid & Polymer Science **1993**, 271, (5), 469-479.
23. Vega, C.; Monson, P. A., *Plastic crystal phases of hard dumbbells and hard spherocylinders*. Journal of Chemical Physics **1997**, 107, (7), 2696-2697.
24. Bolhuis, P.; Frenkel, D., *Tracing the phase boundaries of hard spherocylinders*. Journal of Chemical Physics **1997**, 106, (2), 666-687.
25. Letz, M.; Schilling, R.; Latz, A., *Ideal glass transitions for hard ellipsoids*. Physical Review E **2000**, 62, (4), 5173.
26. Yin, Y.; Xia, Y., *Self-Assembly of Monodispersed Spherical Colloids into Complex Aggregates with Well-Defined Sizes, Shapes, and Structures*. Advanced Materials **2001**, 13, (4), 267-271.
27. Velikov, K. P.; van Dillen, T.; Polman, A.; van Blaaderen, A., *Photonic crystals of shape-anisotropic colloidal particles*. Applied Physics Letters **2002**, 81, (5), 838-840.
28. Birner, A.; Wehrspohn, R. B.; Gösele, U. M.; Busch, K., *Silicon-Based Photonic Crystals*. Advanced Materials **2001**, 13, (6), 377-388.
29. Manoharan, V. N.; Elsesser, M. T.; Pine, D. J., *Dense Packing and Symmetry in Small Clusters of Microspheres*. Science **2003**, 301, (5632), 483-487.
30. Yin, Y.; Lu, Y.; Gates, B.; Xia, Y., *Template-Assisted Self-Assembly: A Practical Route to Complex Aggregates of Monodispersed Colloids with Well-Defined Sizes, Shapes, and Structures*. Journal of the American Chemical Society **2001**, 123, (36), 8718-8729.
31. Liddell, C. M.; Summers, C. J., *Monodispersed ZnS Dimers, Trimers, and Tetramers for Lower Symmetry Photonic Crystal Lattices*. Advanced Materials **2003**, 15, (20), 1715-1719.
32. Snoeks, E.; Blaaderen, A. v.; Dillen, T. v.; Kats, C. M. v.; Brongersma, M. L.; Polman, A., *Colloidal Ellipsoids with Continuously Variable Shape*. Advanced Materials **2000**, 12, (20), 1511-1514.
33. Vlasov, Y. A.; Xiang-Zheng, B.; Sturm, J. C.; Norris, D. J., *On-chip natural assembly of silicon photonic band gap crystals*. Nature **2001**, 414, (6861), 289.
34. van Blaaderen, A.; van Geest, J.; Vrij, A., *Monodisperse colloidal silica spheres from tetraalkoxysilanes: Particle formation and growth mechanism*. Journal of Colloid and Interface Science **1992**, 154, (2), 481-501.
35. Verhaegh, N. A. M.; Blaaderen, A. v., *Dispersions of Rhodamine-Labeled Silica Spheres: Synthesis, Characterization, and Fluorescence Confocal Scanning Laser Microscopy*. Langmuir **1994**, 10, (5), 1427-1438.
36. Giesche, H., *Synthesis of monodispersed silica powders II. Controlled growth reaction and continuous production process*. Journal of the European Ceramic Society **1994**, 14, (3), 205-214.
37. Osseo-Asare, K.; Arriagada, F. J., *Preparation of SiO₂ nanoparticles in a non-ionic reverse micellar system*. Colloids and Surfaces **1990**, 50, 321-339.

38. Hinton, R., *Density gradient centrifugation*. Elsevier: North-Holland 1976.
39. Crocker, J. C.; Grier, D. G., *Methods of Digital Video Microscopy for Colloidal Studies*. Journal of Colloid and Interface Science **1996**, 179, (1), 298-310.
40. Zeichner, G. R.; Schowalter, W. R., *Use of trajectory analysis to study stability of colloidal dispersions in flow fields*. AIChE Journal **1977**, 23, (3), 243-254.
41. Smoluchowski, M., Zeitschrift für Physikalische Chemie **1917**, 92, 129.
42. Birnie, D. D.; Rickwood, D., *Centrifugal Separations in Molecular and Cell Biology*. Butterworth: London, Boston: 1978.
43. Imhof, A., Private communication
44. Bohren, C. F.; Huffman, D. R., *Absorption and Light Scattering by Small Particles*. John Wiley and Sons: New York.: 1983.
45. Marechal, M., Unpublished results.

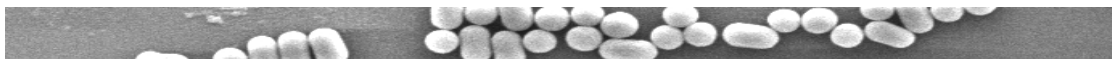
Chapter 6

The synthesis of anisotropic PMMA particles



Abstract

Until now no papers were published on the large scale production of anisotropic PMMA particles starting from spheres. Such systems are suitable for fundamental studies in real space because of the tunability of the potential, and the possibility to combine density and index matching. We tried to fill this gap by investigating if PMMA particles with protrusions could be made starting with cross-linked PMMA spheres followed by a swelling step with monomers and subsequent polymerisation similar to a method developed by Sheu¹ and further developed by others^{2,3} for polystyrene spheres. We did not succeed to make PMMA particles with protrusions, by swelling and polymerization, even after varying many parameters in the process used: initial diameter, polarity of the surface, polarity of the swelling monomers, crosslink density and others. However, we did come across an alternative way to make anisotropic particles of various regular shapes. We propose these particles were formed because the chosen monomer mixture in a second emulsion polymerisation growth step destabilizes the emulsion droplets. The growth monomer mixture we used had an increasing fraction (between 0 and 15 wt.%) of methacrylic acid mixed with methyl methacrylate. We found an increasing number of regular multimer formation at higher methacrylic acid fractions. The mechanism shows similarities with a recently published procedure by Pine et al. in which regular aggregates were formed by drying the oil out of an oil-in-water emulsion loaded with particles^{4,5}. Via density gradient centrifugation we showed that the various shapes and forms that resulted from our syntheses, could be collected and purified.



6.1. Introduction

In the introduction of this thesis and in the previous chapters it is explained why it is interesting to have well-defined colloidal model systems with an anisotropic shape for fundamental aspects in materials science and soft matter physics as well as a wide field of potential applications. This chapter describes the synthesis of polymer (PMMA) based anisotropic colloids starting from spherical particles and using these in a monomer swelling- and subsequent second polymerization step.

Under certain conditions explained in the next section the polymers formed in the second polymerization step can partially separate from the original monomer swollen polymer sphere forming a protrusion. Sheu et al.^{1,6} described such a seeded emulsion polymerization technique that resulted in polystyrene (PS) spherical with a spherical protrusion of PS. Their well-cited procedure was worked out for particles with characteristic size of several micrometers. They were not the first, however, to report on this kind of anisotropic monodisperse polymer particles^{7, 8} using this swell by monomers followed by a second polymerization procedure. Mock et al.³ recently importantly improved this method in order to obtain smaller anisotropic polystyrene particles in the sub micrometer size by producing more hydrophilic seed particles to facilitate the formation of anisotropic particles in the polymerization step after swelling. Their results are important because it allows the synthesis of anisotropic polymer particles more into the colloidal size range and thus more suitable for subsequent self organization procedures and model studies that rely on thermodynamic equilibrium.

Extensions of the methods of Sheu et al for several micron sized particles have also recently been developed². Other methods to produce anisotropic colloidal polymer particles are also described in the literature, but they have disadvantages, such as for instance a low yields^{5, 9}, and or were made up of composite materials of organic and inorganic materials¹⁰, which is less suitable for model studies which often rely on index matching. Until now anisotropic dumbbell-like (also called “snowman”¹¹) particles were made mainly from polystyrene. Polystyrene has the disadvantage of a high refractive index as not many procedures have been developed to make these particles with suitable stabilising molecules for less polar solvents.

To be able to study the physics and dynamics of dumbbell particles in real space with a confocal microscope, we tried to extend the dumbbell synthesis to PMMA. It has already been shown that with this material index *and* density matching combined with a fluorescent core can be realized. In addition, potentials tunable from hard-sphere like to very long-ranged has been shown as well^{12, 13}. The anisotropy in shape can furthermore be combined with external fields, such as shear or electric fields that can align the particles. In the following we will first give a theoretical description of the process by which Sheu and others realized monodisperse anisotropic polystyrene particles. Next we will describe how we tried to adapt this procedure to PMMA and how an alternate procedure ended up giving an interesting route to achieve monodisperse anisotropic particles instead.

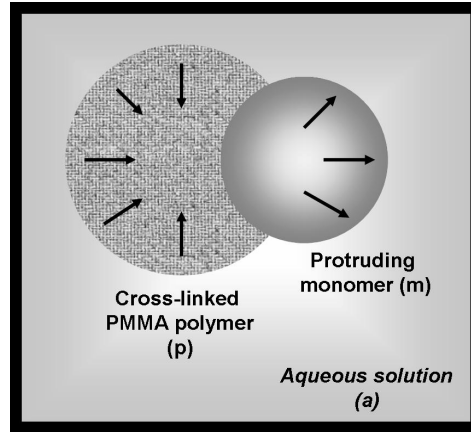


Fig 6.1. Schematic representation of a protrusion after swelling and 2nd polymerization.

6.2. Theory

For an interpretation of the formation of protrusions on latex particles made by swelling latex spheres that were first made by emulsion polymerization and a subsequent polymerization step, the thermodynamics of the swelling of the cross-linked initial spheres has been well studied and described by Sheu et al.^{6,1} A thermodynamic model of the swelling of the particles was arrived at as the result of an analysis of the free energy of the system, describing the tendency of particles to contract or expand during the swelling and polymerization process. If we take a system of (cross-linked) polymer particles mixed with monomers in an aqueous mixture, the chemical potential of monomers in the particle's phase ($\Delta G_{m,p}$) is equal to the chemical potential of monomers in the aqueous phase ($\Delta G_{m,a}$) if they can exchange freely and fast enough to stay in equilibrium. A schematic representation for such a system is given in Figure 6.1. For monomers with a low solubility in water the chemical potential of monomers in the aqueous phase can be ignored and then the chemical potential of the monomers in the particle phase can be approximated by the sum of three terms that contribute to the free energies of bringing monomer inside the seed particles:

$$\Delta G_{m,p} = \Delta G_m + \Delta G_{el} + \Delta G_t \quad (6.1)$$

Where ΔG_m is the mixing of monomer and polymer, ΔG_{el} is the elastic free energy of the cross-linked polymer network and ΔG_t is the interfacial tension between the particle and the water. Now equation (6.1.) can be rewritten by substitution of the Flory- Huggins expression for ΔG_m , the Flory- Rhener equation for $\Delta G_{m,p}$ and the Morton equation for ΔG_t . This gives

$$\Delta G_{m,p} = RT[\ln(1 - v_p) + v_p + \chi_{mp} v_p^2] + RTN V_m (v_p^{1/3} - 0.5 v_p) + 2V_m \gamma / a \quad (6.2)$$

Here, R is the ideal gas constant, T is the absolute temperature, v_p is the volume fraction of polymer in the swollen seed particle, χ_{mp} is the monomer-polymer interaction parameter, N is the effective number of chains in the network per unit volume (which is proportional to the cross-link density), V_m is the monomer molar volume, γ is the interfacial tension between the particle and water, and a is the radius of the swollen seed particle. The first term in expression (6.1) and (6.2) gives a

negative contribution to the chemical potential of the monomer in the particles and therefore promotes seed particle swelling, while the other two terms encourage seed particle contraction^{6 3}. Furthermore, the forming of a protrusion in a swollen and polymerizing system will depend strongly on the interfacial tensions between the polymer and the aqueous phase, $\gamma_{p,a}$, the particle and the monomer, $\gamma_{p,m}$ and the monomer and the aqueous phase, $\gamma_{m,a}$. Analogous to Young's equation¹⁴ for the force balance of a flat surface with on top of it a liquid droplet in equilibrium with its vapor, we can now write an expression for the surface tension of the polymer and the aqueous phase:

$$\gamma_{p,a} = \gamma_{p,m} + \gamma_{m,a} \cos \theta \quad (6.3)$$

Here, θ is the contact angle between the monomer and the seed particle. So as the contact angle becomes larger, the protrusion of the polymerized product will be more pronounced. From eq (6.3) it can be seen that the protrusion will become more distinct, as the difference between the surface tensions of the polymer and the aqueous phase ($\gamma_{p,a}$) and that of the polymer and the swelling monomer ($\gamma_{p,m}$) decreases. Therefore a proper choice of the added monomer during the swelling process and or a change in polymer composition of the particles' surface can improve the formations of protrusions.

6.3. Experimental

Materials:

Prior to use the monomers methacrylic acid (MA, Fluka) and methyl methacrylate (MM, Fluka) were run through an inhibitor remover column (Sigma), to remove the inhibitor hydroquinone methyl ether (MEHQ) and hydroquinone respectively. The inhibitor of styrene (Fluka), 4-t-butyl catechol, was removed by washing it with a 0.1 M sodium hydroxide solution. Azobisisobutyronitril (ADIB, Janssen Chimica) was recrystallized in acetone before use. Ethylene glycerol dimethacrylate (EGDMA, Sigma-Aldrich) was used as cross-linking agent, 1-dodecanethiol (DDM, Fluka), potassium persulfate (KPS, $K_2S_2O_8$, Aldrich), glycerol (Sigma) were all used as received.

6.3.1. Synthesis of PMMA spheres

The PMMA seed particles were prepared via a surfactant free emulsion polymerization of the monomers, the method of Paquet et. al.¹⁵ was followed. A 250 mL round bottom flask equipped with a Teflon-coated stirring bar and a reflux cooler was filled with 90 mL of deionized water and 0.24 g of potassiumpersulphate (KPS). The flask was put in a thermostatted oil bath at 80.0 °C and kept at that temperature for 30 minutes to allow for radical formation of the KPS. A separate vial was filled with 10.0 g (10% v/v) of monomer (consisting of mixtures of methylmethacrylate (MM) and methacrylic acid (MA), with respectively 0, 5, 10 and 15 wt.% MA), 0.1 g (1%) cross-linking agent (ethyleneglyceroldimethacrylate (EGDMA)) and 47.4 μ L of 1-dodecanethiol (DDM). The content of the vial with the monomer mixture was added to the round bottom flask under vigorous stirring. The polymerization was allowed to proceed for 120 to 150 minutes.

6.3.2. Seeded growth of PMMA spheres

For the seeded growth of PMMA spheres the method of Kalinina et. al.¹⁶ was followed. The synthesis was scaled on the amount of seeds. For a typical seeded growth, a 250 mL round bottom flask equipped with a Teflon-coated stirring bar and a reflux condenser was used. 60 ml (2.5 v/v %) of a diluted and cleaned seed dispersion was added to the round bottom flask along with 0.01 g of azobisisobutyronitrile (ADIB). The flask was put in a thermostatted oil bath at 80.0 °C and kept at that temperature for 30 minutes. Then a 24.44 g MM/MA mixture, 0.1123 g EGDMA, 71.1 µL DDM and 0.1805 g ADIB were added dropwise with approximately 1 drop every 3 seconds whilst stirring rapidly over a period of 30 minutes. The reaction was allowed to proceed for 2 hours in total before the reaction was stopped.

6.3.3. Swelling and polymerization

In the attempts to let the particles swell before polymerization we swelled our particles in the same way as the polystyrene particles were swollen following the method described by Mock et al.³ For the swelling experiment the particles from the seeds (see section 6.3.1.) or the result from the seeded growth (see section 6.3.2.) were used. The batches that were used were cleaned from some large coagulates by filtration. Then 0.5 ml of particle suspension was diluted 20 times by adding 9.5 ml deionized water. So the start concentration for swelling the seeds was ± 0.5 v/v % while for the seeded grown particles it was ± 1.5 v/v %. Varying amounts and mixtures of the additional monomers were added as swelling agent. Typically the ratio of swelling agent to particles volume was 1:1, as higher swelling concentrations resulted in higher amounts of secondary nucleated particles. The vials were magnetically stirred for 16 hours. The swelling agents were chosen such that they had increasing polarity; swelling experiments with styrene, MM and MA (and mixtures of these methacrylates) were performed.

After swelling the reaction mixture was polymerized as follows: 6.7 mg ADIB dissolved in 0.333 mL of swelling monomer was introduced into the vials which were thermostatted at 80.0 °C in an oil bath and allowed to polymerize for 2 hours. Besides varying the swelling agent, the influence of inhibitor concentration, temperature, monomer mixture and monomer concentration were investigated.

6.3.4. Density Gradient Centrifugation

To separate synthesized particles with different weight we used a density gradient centrifugation¹⁷ as described in the previous chapter.

Two separate water/glycerol mixtures were prepared. One with 70% w/w glycerol (high density) and one with 20% w/w glycerol (low density). A centrifugation tube with an inner diameter of 5.8 cm was filled with the gradient mixture. The sample was loaded on top of the gradient by adding 4 mL of 0.1% v/v dispersion on top of the gradient.

The centrifuge tube was subsequently centrifuged for 45 minutes at 2500 RPM on a Hettich Rotina 46S centrifuge with swing-out buckets (radius 15 cm). The bands in the centrifuge tube were collected by inserting a Pasteur pipet with an upwardly curved end into the centrifuge tube just below the band of interest. Via a syringe connected to the pipette the band was collected and centrifuged, before studying with the electron microscope with TEM. TEM grids were prepared by evaporation of a centrifuged sample collected from a band of the density gradient solution.

6.4. Results and Discussion

6.4.1. Seeds of PMMA

Seed particles with a MA and MM mixture were made with the method described in section 6.2.1. The content of MA in the seeds was varied from 0, 5, 10 to 15 wt.% of MA. The idea behind varying the composition of the PMMA is to promote the formation of protrusions by changing the surface tension of the particles for the swelling experiments, as is explained in the theoretical section (6.2.) of this chapter.

However, all syntheses yielded spherical particles varying in size from 410, 375 and 440 respectively. The synthesis of particles with 15% MA aggregated during syntheses. Higher contents of MA gave the same negative result. Although coagulum was observed in syntheses with a lower content of MA as well, after removal of the coagulum stable dispersions with polydispersities between 5 and 10% were obtained. The dispersions crystallized after sedimentation, an indication of their monodispersity and unaggregated state. The appearance of a coagulum in the synthesis has been observed by others as well^{3, 16} and surprisingly did not affect the result of the bulk particles. A typical result of the seeds is shown in Figure 6.2.a

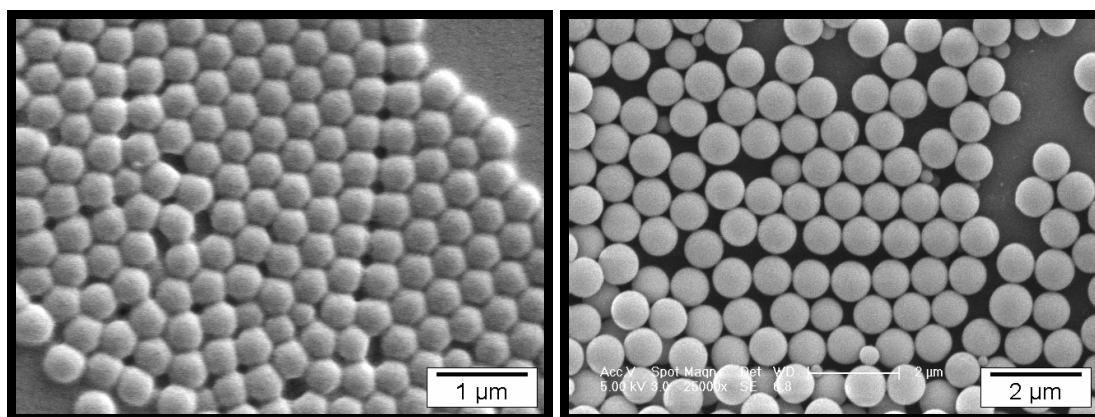


Fig 6.2. (a, left) Monodisperse PMMA seeds with a diameter of 410 nm (pure MM) **(b, right)** The result after swelling and polymerizing with polystyrene (spheres with a diameter of 830 nm diameter, with a very small fraction of secondary nucleated particles).

Other syntheses in which the physical properties of the particles were changed were tried: A higher cross-link density of the seeds, through addition of 2 and 5% of EGDMA. A trial to grow a layer of Acrylic Acid³ (AA), instead of a mixture of only MM and MA change the surface tension of the particles and the aqueous phase, $\gamma_{p,a}$ to facilitate protrusions. All these attempts resulted in unstable suspensions. No further experiments were possible with these batches.

6.4.2. Seeded growth of PMMA

From equation (6.2) it can be seen that the formation of protrusions should be facilitated if the third term is lowered. To this end we increased the particle radius (a) by seeded growth.

Synthesis	Seed particle composition (wt%) (MM/MA)	Seed particle size (ϕ , nm)	Added monomer(s) (MM/MA)	Final size (ϕ , nm)	Dumbbells (%)	n-mers (%)
A	100/0	410	100/0	670	0	0
B	100/0	400	100/0	970	0	0
C	100/0	410	0/100	410	0	0
D	100/0	970	0/100	1070	0	0
E	95/5	375	95/5	620	3	2
F	95/5	375	0/100	385	0	0
G	90/10	440	100/0	650	17	17
H	90/10	440	95/5	690	16	16
I	90/10	440	90/10	580	16	16
J	90/10	440	85/15	710	24	33
K	85/15	X	-	-	-	-
L	80/20	X	-	-	-	-

Table 6.1. Overview of seeded PMMA growth syntheses.

To vary the surface composition of the PMMA particles and to start with larger spheres seeded growth was achieved on the particles described in section 6.3.2. An overview of the PMMA seeded growth syntheses is given in Table 6.1. The seeded growth of PMMA particles was performed with different monomer feeds varying in MM/MA constitution. Again, in all syntheses a coagulum was formed, as was seen in the seed syntheses, but could be easily removed without affecting the non coagulated particles. Furthermore, it is obvious from these results that the growth of MM seeds with MM (A and B) resulted in significant growth in agreement with the findings of Kumacheva¹⁶, while the growth of MM with pure MA (C, D and F) showed no or minimal growth of the particles. Surprisingly, if a mixture of MM and MA was used in the seeded growth a large number of dumbbells were observed in the final result. If the seeds contained 10 % MA and the feed contained 15 % MA the number of dumbbells found in the synthesis result even increased to almost 25 %, but also many multimer particles were found. A variety of multimer particles obtained from synthesis I is shown in Figure. 6.3. The observed failures in seeded growth with pure MA (C, D and F) indicate that outcome of the emulsion polymerization changes with an increase in the amount of MA, and thus an increase of the polarity of the reaction mixture.

MA is a more polar monomer than MM and therefore MA mixes with water, while MM is only slightly soluble in water¹⁸. Therefore, the formation of a stable emulsion with a growth of pure MA is less likely. This could explain why the seeded growth with MA failed. It may also explain that a seeded growth with an increasing content of MA resulted in a higher instability of the particles. Possibly, if the emulsion is less stable a variation of emulsion droplet sizes can be formed. This would explain why two, three or more particles (n-mers) end up in a colloidal cluster.

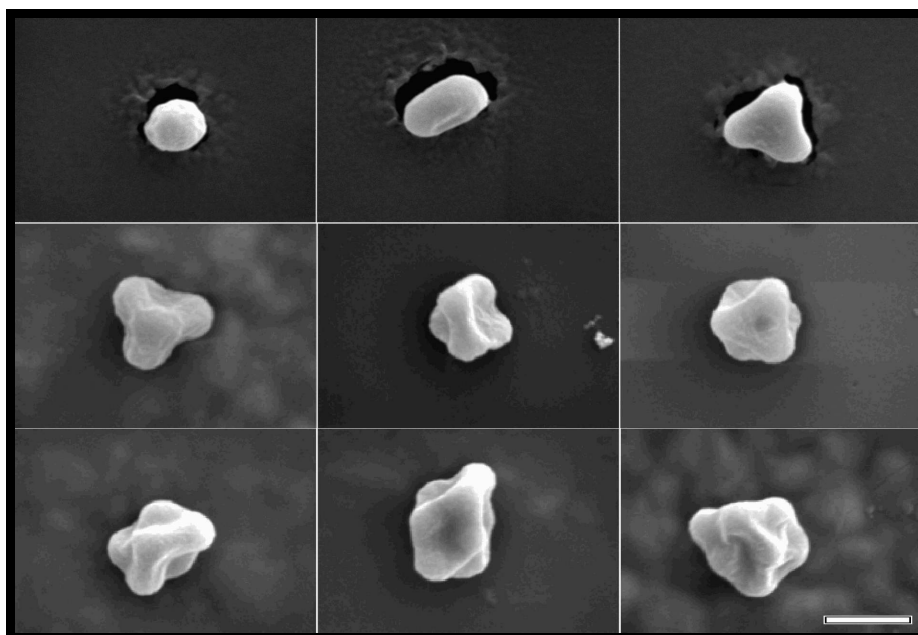


Fig. 6.3. Variation of shapes of n -mers of clustered particles after a second growth step. (scalebar represents 1 μm)

In Figure. 6.3. it is seen that the multiplet particles that were formed look regular. This further supports the idea of growth of the seed particles in a large monomer emulsion droplet where they were still free to move before they clustered and polymerized as one particle. Polymer particles with similar symmetric form, after drying in large emulsion droplets were also seen by Manoharan et al.^{4, 5}, although the mechanism for the final form of multimers is slightly different, it seems that also in our case the second moment of the mass distribution is minimized after the second polymerization step. Recent results from Kraft¹⁹ with protruded polystyrene spheres also resulted in the formation of symmetric multimer particles. There it was postulated that the symmetrical n -mers they found resulted from collisions of n particles, which had protrusions that were not yet polymerized. After the particle formed a protrusion, the monomer from the protrusion could collide with other protruded particles forming symmetric clusters of n -mers, before the final polymerization occurred. It remains unclear whether such a mechanism could be applicable to our PMMA particles as well. Perhaps tomography in combination with TEM could resolve the structures better.

6.4.3. Swelling and polymerization

The 3 different seeds with 0, 5 and 10 % MA (410, 375 and 440 nm respectively) and most results from the seeded growth listed in Table 6.1 were swollen and polymerized with MM and MA in a way that was comparable to the method of Sheu¹ and Mock³.

The parameters that were varied during the swell and growth procedures were: The constitution of the swelling agent, the ratio between MM and MA as well as swelling with styrene. Also the polymerizing temperature and initiator concentration were varied. In short: in not one of the experiments we found protrusions of polymer bulging out of the seed particle, contrary to what was found by Sheu and Mock for polystyrene seed particles.

Swelling of PMMA particles from pure MM swollen with MM resulted in particle growth and showed a second nucleation. The secondary nucleation was much more profound when the amount of monomer for swelling was larger than the volume of the particles, therefore most swell experiments were performed with an amount of swelling monomer equal to the amount of polymer in the seeds. It should be mentioned that, although we followed the same procedure as Mock³ and Sheu¹ and coworkers, they do not mention a formation of secondary nucleated particles.

As seen in the seeded growth, also swelling with pure MA and polymerization afterwards yielded no growth or polymerization of the particles. However, swelling of PMMA with styrene did yield a clear growth of the particles, but still without formation of protrusions. It has already been shown that the swelling of styrene particles with MM clearly gives protrusions². In our case, the reverse, protrusions of PS from swelling in PMMA was not seen, while PMMA particles with a different crosslinking agent (3-(trimethoxysilyl)propylmethacrylate, TPM) can result in particles with protrusions²⁰.

The reason for not observing a protrusion in any of our experiment remains unclear. Although we tried to adapt the work of Sheu and Mock, some deviations are obvious. First of all we used a different monomer to form protrusions (MM and MA instead of styrene). Secondly, our particles were smaller than Sheu et al, although comparable in size with the ones Mock and coworkers used. Apparently, the use of PMMA particles with methacrylates as swelling monomers influences the balance of the chemical potential of the monomers in the particle in such a way that it discourages the formation of protrusions.

Yet, we need to be careful to apply the theory of Sheu et al.⁶ for forming protrusions in the way as described in the theoretical section as it only holds for swelling monomers that do not mix well with water, while MA is known to be miscible with water, MM is only slightly and styrene is insoluble in water¹⁸. The solubility may make it unfavorable for the monomers to swell the particles and form a protrusion.

6.4.4. Density gradient centrifugation

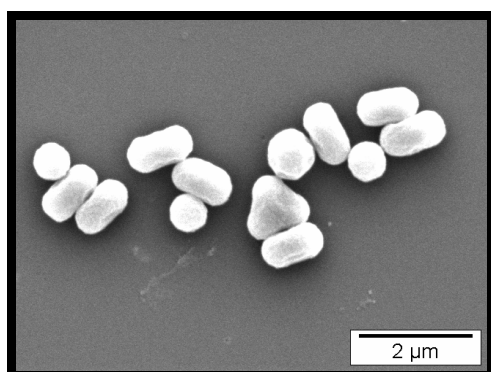


Fig 6.4. A mixture of dumbbell and triplet (and multimers not seen in this picture) formed after seeded growth of 10% MA PMMA particles grown with a 10% MA mixture. (Result of synthesis I from table 6.1)

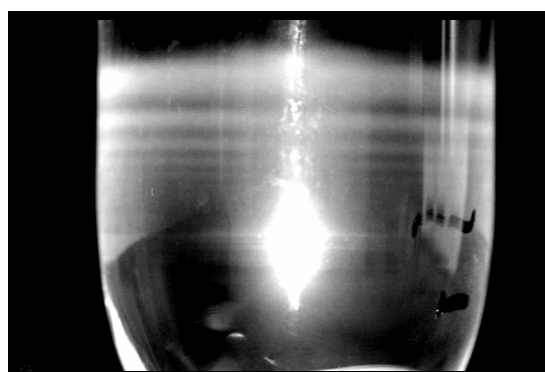


Fig 6.5. Separated bands formed after density gradient centrifugation of seeded grown PMMA particles (synthesis I) in water glycerol density gradient. EM pictures of the separated 2nd and 3rd band are shown in Fig. 6.6.

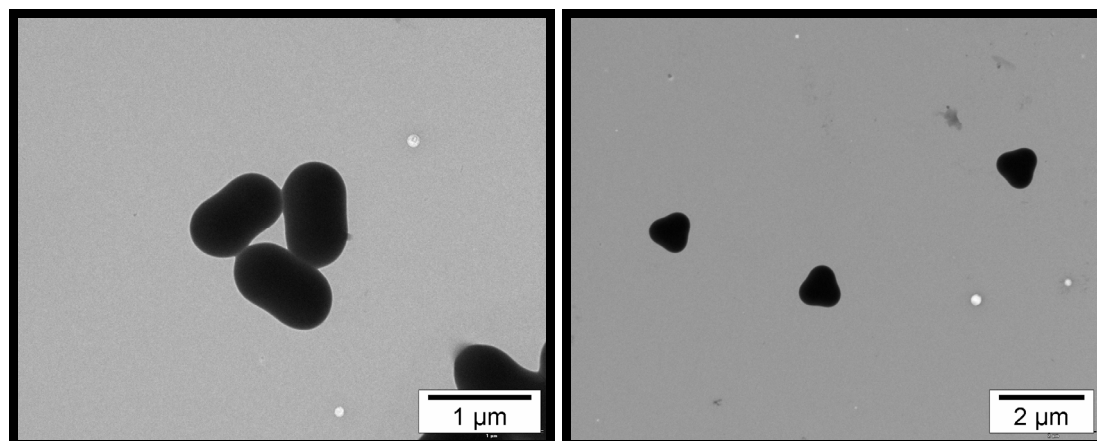


Fig 6.6. (a, left) A dumbbell rich PMMA batch collected after density gradient centrifugation. (b, right) A triplet rich PMMA batch collected after density gradient centrifugation.

Table 6.1. shows that the growth of PMMA particles with a weight fraction of 10 % MA, with a feed containing a mixture of MA and MM, resulted in multiplet formation. The higher the MA contents in the feed the higher the multiplet formation.

Figure 6.4. shows the result of synthesis I. Because of the high fraction of dumbbells a density gradient centrifugation was performed to separate them. This resulted in the formation of many bands indicating that a large variety of cluster sizes was formed (see also Figure. 6.3.)^{4, 17}. Before centrifugation a mix of particle sizes was observed as shown in Figure. 6.4. After density gradient centrifugation the first 3 bands of the separated PMMA particles were most distinct and were separated a few millimeters from each other and therefore could be collected (see Figure 6.6). Batches of 90 % pure dumbbells and triplets were obtained this way. The result is shown in Figure 6.6.a for the 2nd dumbbell band and in Figure 6.6.b for the 3rd triplet band. Unfortunately the bands of the higher n-mers were too thin and not enough separated to collect pure batches. Nevertheless those formed multimers are promising building blocks to study their phase behaviour with confocal microscopy.

In near future effort will be put into transferring the particles from water into index and density matching solvents.

6.5. Conclusions

The physical chemistry of swelling and polymerizing of particles of PMMA is different than that for polystyrene. We did not succeed in making PMMA particles with protrusions from cross-linked PMMA by swelling and subsequent polymerisation. Nevertheless we showed it is possible to grow a mixture of regular n-mer aggregates with increasing numbers of PMMA particles that can be purified into separate batches of dumbbells, triplets etc via density gradient centrifugation. This enables us to study the interactions of a new class of PMMA polymer particles and gives an opening in the field of studying the formation of complex assemblies that might find applications as photonic materials.

Acknowledgements

Wessel Vlug is gratefully acknowledged for performing most of the experiments. Daniela Kraft is thanked for fruitful discussions.

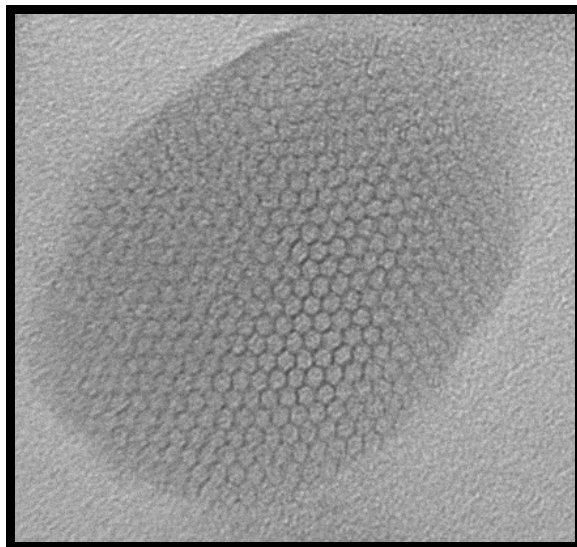
6.6. References

1. Sheu, H. R.; El-Aasser, M. S.; Vanderhoff, J. W., *Uniform nonspherical latex particles as model interpenetrating polymer networks*. Journal of Polymer Science Part A: Polymer Chemistry **1990**, 28, (3), 653-667.
2. Kim, J. W.; Larsen, R. J.; Weitz, D. A., *Synthesis of Nonspherical Colloidal Particles with Anisotropic Properties*. Journal of the American Chemical Society **2006**, 128, (44), 14374-14377.
3. Mock, E. B.; DeBruyn, H.; Hawkett, B. S.; Gilbert, R. G.; Zukoski, C. F., *Synthesis of Anisotropic Nanoparticles by Seeded Emulsion Polymerization*. Langmuir **2006**, 22, (9), 4037-4043.
4. Yi, G.-R.; Manoharan, V. N.; Michel, E.; Elsesser, M. T.; Yang, S. M.; Pine, D. J., *Colloidal Clusters of Silica or Polymer Microspheres*. Advanced Materials **2004**, 16, (14), 1204-1208.
5. Manoharan, V. N.; Elsesser, M. T.; Pine, D. J., *Dense Packing and Symmetry in Small Clusters of Microspheres*. Science **2003**, 301, (5632), 483-487.
6. Sheu, H. R.; El-Aasser, M. S.; Vanderhoff, J. W., *Phase separation in polystyrene latex interpenetrating polymer networks*. Journal of Polymer Science Part A: Polymer Chemistry **1990**, 28, (3), 629-651.
7. Ugelstad, J.; Mørk, P. C.; Kaggerud, K. H.; Ellingsen, T.; Berge, A., *Swelling of oligomer-polymer particles. New methods of preparation*. Advances in Colloid and Interface Science **1980**, 13, (1-2), 101-140.
8. Skjeltorp, A. T.; Ugelstad, J.; Ellingsen, T., *Preparation of nonspherical, monodisperse polymer particles and their self-organization*. Journal of Colloid and Interface Science **1986**, 113, (2), 577-582.
9. Mohraz, A.; Solomon, M. J., *Direct Visualization of Colloidal Rod Assembly by Confocal Microscopy*. Langmuir **2005**, 21, (12), 5298-5306.
10. Reculosa, S.; Poncet-Legrand, C.; Perro, A.; Duguet, E.; Bourgeat-Lami, E.; Mingotaud, C.; Ravaine, S., *Hybrid Dissymmetrical Colloidal Particles*. Chemistry of Materials **2005**, 17, (13), 3338-3344.
11. Perro, A.; Reculosa, S.; Bourgeat-Lami, E.; Duguet, E.; Ravaine, S., *Synthesis of hybrid colloidal particles: From snowman-like to raspberry-like morphologies*. Colloids and Surfaces A: Physicochemical and Engineering Aspects **2006**, 284-285, 78-83.
12. Royall, C. P.; Leunissen, M. E.; van Blaaderen, A., *A new colloidal model system to study long-range interactions quantitatively in real space*. Journal of Physics: Condensed Matter **2003**, 15, (48), S3581-S3596.
13. Yethiraj, A.; van Blaaderen, A., *A colloidal model system with an interaction tunable from hard sphere to soft and dipolar*. Nature **2003**, 421, (6922), 513-517.
14. Adam, N. K., *Use of the Term "Young's Equation" for Contact Angles*. Nature **1957**, 180, (4590), 809-810.
15. Paquet, C.; Allard, M.; Gledel, G.; Kumacheva, E., *Guest-Host Colloid Crystals: Experimental Study and Simulations*. Journal of Chemical Physics B **2006**, 110, (4), 1605-1613.
16. Kalinina, O.; Kumacheva, E., *A "Core-Shell" Approach to Producing 3D Polymer Nanocomposites*. Macromolecules **1999**, 32, (12), 4122-4129.
17. Johnson, P. M.; van Kats, C. M.; van Blaaderen, A., *Synthesis of Colloidal Silica Dumbbells*. Langmuir **2005**, 21, (24), 11510-11517.

18. Weast, R. C., *Handbook of Chemistry and Physics, 50th edition*. CRC Press: 1969-1970.
19. Kraft, D., *Unpublished results, private communication*. In van 't Hoff Laboratory for Physical & Colloid Chemistry, Utrecht University, **2008**.
20. Nagao, D.; van Kats, C.M.; Hayasaka, K.; Imhof, A.; Konno, M.; van Blaaderen, A., *Synthesis of Anisotropic Hollow, Silica Particles Containing Movable Spheres (in preparation)* **2008**.

Chapter 7

Controlling the porosity of colloidal silica from macroporous to ultramicroporous



Abstract

Materials with micro-, meso- and/or macropores find a wide range of applications in materials chemistry. In this chapter some examples are given of syntheses of colloidal particles where the formation of porous silica structures plays a key role. We show that the pore size of materials made from colloidal silica can be controlled from macroporous to ultramicroporous via a variety of synthesis routes. The synthesis techniques of these methods are not complex and easy to reproduce.



7.1. Introduction

Porous materials are classified by their size. According to IUPAC notation¹, microporous materials have pore diameters of less than 2 nm and macroporous materials have pore diameters of larger than 50 nm; the mesoporous category has pore sizes in between. Dubinin recommended subdividing micropores into ultramicropores (diameter of $< 7 \text{ \AA}$) and supermicropores (diameter between 7 \AA and 20 \AA)². The argument for this subdivision is that these categories have specific properties, such as size selective separation of molecules in the case of ultramicropores.

In materials chemistry the control of pore size is of interest for catalysis, chromatography, filtering, molecular sieves, filler materials with low dielectric constants, and hosts for optically active compounds³. The technological importance of colloidal materials with tailored structural and surface properties also is undebated, because of their wide applicability in modern materials science. Porous (and hollow) colloidal particles can be used in the area of (bio)sensors, separation, catalysis, diagnostics and to encapsulate chemicals (for instance for the controlled release of drugs)⁴. Many examples of porous silica materials can be found in the literature. We will focus on porous materials containing silica, and porous colloidal particles made of silica in this chapter by giving examples that were taken out of synthetic work performed by ourselves. From the results presented it is clear that a general synthetic procedure in which many kinds of particles can be covered by a layer of silica and made to become hollow by using a dissolution or chemical route. Moreover, although not all experiments were performed with this idea in mind, it is also clear that such a hollow silica shell can be filled with a liquid and subsequently closed by (almost) closing the pores with silica. This provides for a very general scheme to prepare functional particles with additionally great control over shape as well.

7.2. From macroporous to ultramicroporous colloidal silica

We demonstrate that a combination of what is found in literature enables us to have full control of the sizes of pores that materials based on colloidal silica can have. From micrometer to (even beyond) nanometer control. We will illustrate the control of pore sizes with materials made by ourselves. A detailed description of the synthesis methods of these examples is given in the appendix.

7.2.1. Micrometer control, macroporous structures

Mechanically pores can be drilled into solid materials to construct substrates with macropores. The first papers that reported full photonic bandgaps in the microwave wavelength regime comprised methods of materials that were constructed via literally drilling holes into materials⁵. Via self organization of particles into a crystal and removing the particles subsequently many groups have constructed photonic materials of various materials^{6, 7}. These materials find applications in photonic applications. Other examples of applications where the pore size is important for manufacturing functional materials are size selective membranes⁸. Free standing membranes with regular micrometer size holes, have been prepared with help of Langmuir Blodgett technique by depositing a floating layer of hydrophobic TPM-coated particles⁹ surface active

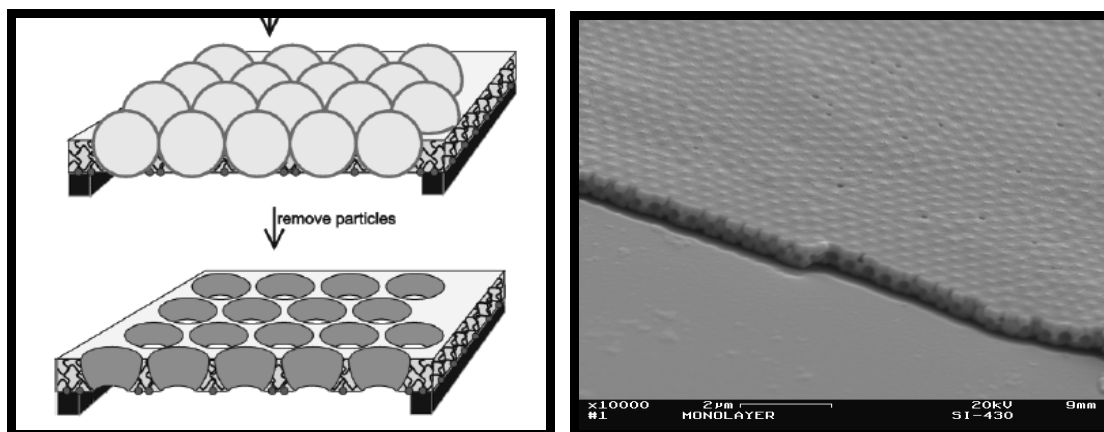


Fig 7.1. (a, left) Schematic picture of a free standing film before and after removal of the silica particles.¹⁰ (b, right) SEM picture of a free standing film with TPM coated silica particles not yet removed.

polymers, cross-linking the polymer, and then removing the colloids to generate thin membranes with uniform holes¹⁰.

This technique is applicable for various size ranges of colloids. This way the pore size of the membranes can be finetuned. Fig. 7.1.a. shows a schematic picture of the idea to form a membrane, Fig.7.1.b. shows the experimental result before removal of the colloids.

7.2.2. Nanometer control, mesoporous colloidal silica

The use of zeolites as porous materials in catalysis and water purification is well known and has a long history¹¹. Since the discovery of ordered synthetic mesoporous materials¹², a series of novel ordered mesoporous materials have been successfully synthesized by the use of hydrocarbon surfactants^{13, 14}. With these methods pore size control in the range from 5 to 30 nm became available¹⁵. Mesoporous particles are also frequently used in biomedical applications; Lin et al showed it was possible to extend the syntheses of mesoporous particles by functionalizing them with a fluorescent (FITC) marker, so they can serve as cell markers¹⁶. While incorporating the mesopores with Gadolinium (Gd) makes them suitable as new MRI contrasting agent¹⁶.

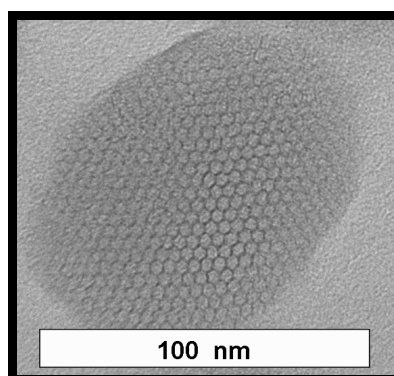


Fig 7.2. Example of a fluorescent mesoporous silica particle with hexagonal pore structure with a pore size of 4 nm, synthesized according to Lin et al¹⁶.

ⁱ Figure 7.1.(left) is reproduced with permission from Langmuir, 18 (6), 2363 -2367, 2002

In Fig. 7.2. an example is shown of a mesoporous silica particle made according to the method of Lin et al¹⁶. Furthermore it is proposed that mesoporous materials can act as a convenient reservoir for drugs and biomolecules.

7.2.3. Ångström precision, microporous colloidal silica.

Silica is a material that is abundant in many varieties. In nature it is commonly found as sand or quartz, besides it is a principal component of most types of glass and substances such as concrete¹⁷. Although in colloidal synthesis, the most commonly studied route to produce silica as a model system is the Stöber synthesis, there are various different ways to make silica. These techniques all result in silica with different densities. For instance quartz, which is crystalline SiO₂, has a high density of 2.65 g/ml¹⁸, whereas natural opals consisting of amorphous SiO₂ have a density of 2.20 g/ml. Silica synthesized from the Stöber method generally has a density close to 2.0 g/ml, while commercial silica (Ludox) has a higher density of 2.20 g/ml¹⁹. The reason for these differences in density is caused by differences in particle morphologies. Synthetic silica most commonly is made from tetraethoxysilane, therefore before siloxane bonds are formed the ethoxy groups need to be hydrolyzed followed by a condensation reaction of the silanol groups. The number of siloxane bonds varies in the different synthesis techniques, this causes differences in their densities¹⁹. If other chemicals than tetraethoxysilane are incorporated into the silica the number of siloxane bonds will decrease due to sterical hinder of the incorporating molecule. It is therefore expected that for instance silica incorporated with a fluorescent dye²⁰ or silica that is grown in presence of Polyvinylpyrrolidone (PVP)²¹ has a lower density than normal Stöber silica. And indeed it can be shown with TEM that the internal structure of a core-shell particles made with a fluorescent FITC core and a silica shell according to van Blaaderen et al.²⁰ has a more porous structure in the core than in the outer shell, as can be seen in fig. 7.3.

Fig. 7.3. illustrates a sliced fluorescent silica particle, resulting in a disc where the inner structure of the silica core becomes visible with transmission electron microscopy. The internal structure of an FITC-silica core silica shell is made visible by a microtome technique as described by Labrosse and Burneau²². The inner core containing FITC incorporated in silica,

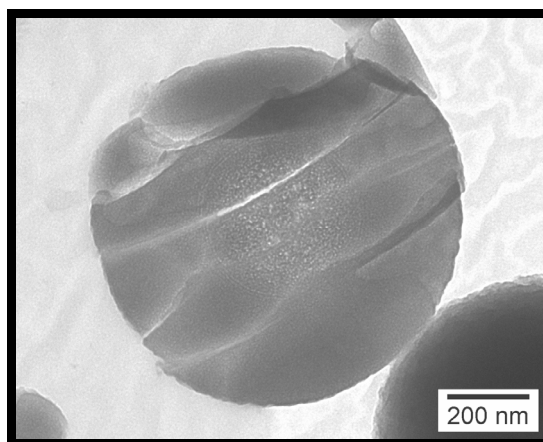


Fig 7.3. TEM picture from a microtomed fluorescent silica particle. The internal structure of silica with dye clearly is more porous than the outer part without the dye.

clearly shows a more open structure than the Stöber silica shell. The sample was made by drying a sediment of FITC-silica particles, filling it with an epoxy resin that is polymerized to obtain a solid structure that can be cut. Thin slices are cut with a microtome (diamond knife) (see Fig. 7.3.).

In their study, Labrosse and Burneau used silica without a dye. Apart from TEM measurements the pore size of silica can also indirectly be measured by BET-absorption techniques and IR spectrometry²². This way they determined the pore size of silica to be between 3 Å and 9 Å. It should be mentioned that the result of BET absorption measurements are strongly affected by the nature of the inert gas used²³. Moreover, it is well known¹⁹ that more than 10% w of water leaves the silica particles if heated at temperatures that do not yet condense the silica (e.g. ~ 100 °C). Therefore, Walcarius et al. developed a method to determine the pore size of silica particles by letting the silanol groups inside the pores of silica react with bases of increasing size²⁴. Thus allowing the pores to act as molecular sieves. They found that Stöber grown silica has an average pore size of 3 Å. A nice example of size selectivity of a silica shell was given by Matijevic²⁵. Matijevic showed that hydrogen molecules are able to reduce the inner core of silica coated hematite spindles and that the water resulting from the reaction could escape as well, obtaining silica coated iron spindles. Those particles were not oxidized after the hydrogen was diffused into the particles at elevated temperatures. The pores were too small to allow oxygen to diffuse in.

7.3. Controlling the pore size of colloidal silica.

7.3.1. Hollow colloidal particles

As can be seen from Fig 7.3. incorporation of other molecules than TES during the Stöber synthesis can increase the internal pore size of silica. This opens the possibility to create a new route for the synthesis of hollow silica particles. It has already been shown, for instance by Sacanna and co-workers²⁶, that a layer of silica containing Polyvinylpyrrolidone, (PVP-assisted silica coating according to the method of Graf and coworkers²¹) is porous. Sacanna showed that hydrogen chloride is able to diffuse through a layer of silica of ~30 nm thickness to dissolve the inner hematite core, which clearly could also pass the pores.

This concept of coating particles with a penetrable silica layer can be applied by a large range of colloids varying in size and shape. It is known that silica can be coated onto a large variety of materials²¹. This way new classes of hollow silica particles can be made. A few examples of anisotropic particles that were synthesized through different ways, where the core is dissolved through penetration of a liquid that dissolves the core (a) and through evaporation of the core by burning the core in an oven at 500 °C (b), are shown in Fig 7.4. In Fig. 7.4.a it can be seen that if the silica coated onto the particle is very thin (less than 10 nm) the structure becomes flexible, whereas silica normally is more brittle. The collapsing of the silica is comparable with hollow particles made of silica and dimethyldiethoxysilane (DMDES)²⁷.

Fig. 7.5.a. shows that the inner core of polystyrene (PS) particles coated with a layer of 30 - 35 nm silica can be penetrated by tetrahydrofuran (THF), while some (dark) particles are impenetrable for the THF. In that case the PS core stays intact.

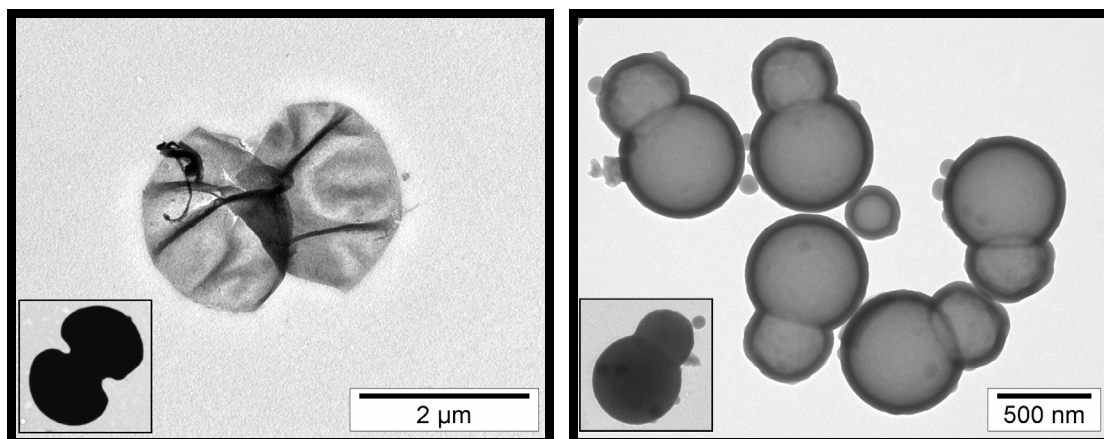


Fig 7.4. (a, left) A silica shell left after dissolution of the hematite dumbbell that was inside (the insert shows an example of the original hematite dumbbell, before dissolution of the core) **(b, right)** The Shell left after a snowman type Polystyrene/PMMA colloid was burnt out, demonstrating a general method to make anisotropic hollow silica particles. (The insert shows an example of the original silica coated Polystyrene dumbbell, before burning the core)

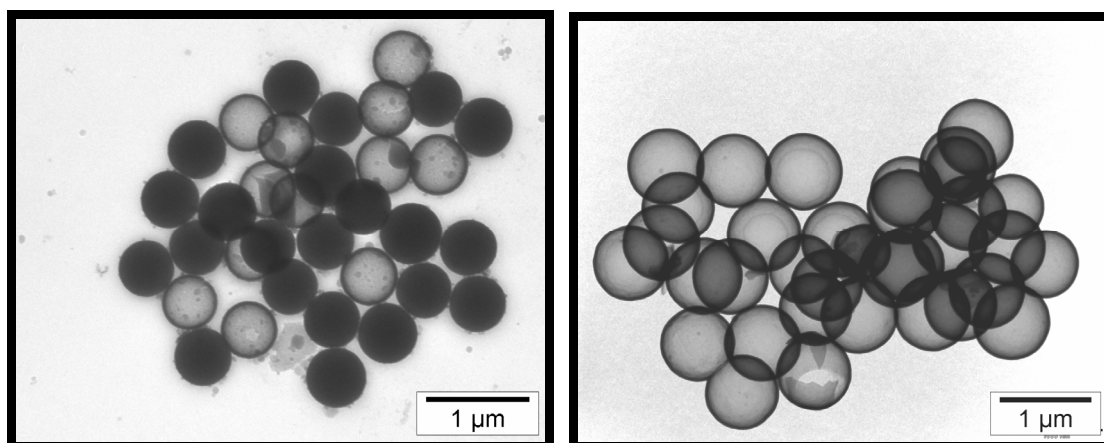


Fig 7.5. (a, left) Silica coated polystyrene (PS) particles penetrated by Tetrahydrofuran (THF). Some silica shells are impenetrable for the THF (black), while at others the PS is dissolved by the THF leaving an empty silica shell. **(b, right)** Silica shells are left after all PS that was inside was burnt out in an oven at 500 °C.

This implies that the pores of the silica are on the order of the size of the THF molecule. Fig 7.4.b. as well as Fig 7.4.b. show that burning into an oven at 500 °C results in hollow silica particles. In these cases all PS is burnt out, resulting in hollow silica particles. Furthermore, we have demonstrated that the silica coated gold rods described in chapter 3 and 4 are penetrable for aqua regia, therefore, the gold core of these particles can also be dissolved. Fig. 7.6.a shows that dissolving the gold core through mesoporous coated silica is easier than through the Stöber grown silica on gold cores (Fig 7.6.b.). Visual inspection of the dissolving process learned that dissolving the core of gold from the mesoporous silica coated gold goes within seconds. The pores are mesopores and therefore aqua regia reaches the gold cores easily. On the other hand a few minutes of dispersing the Stöber silica coated gold rods is not enough to completely dissolve the gold core: The silica has pore in the size range of the nitric acid and hydrochloric acid molecules.

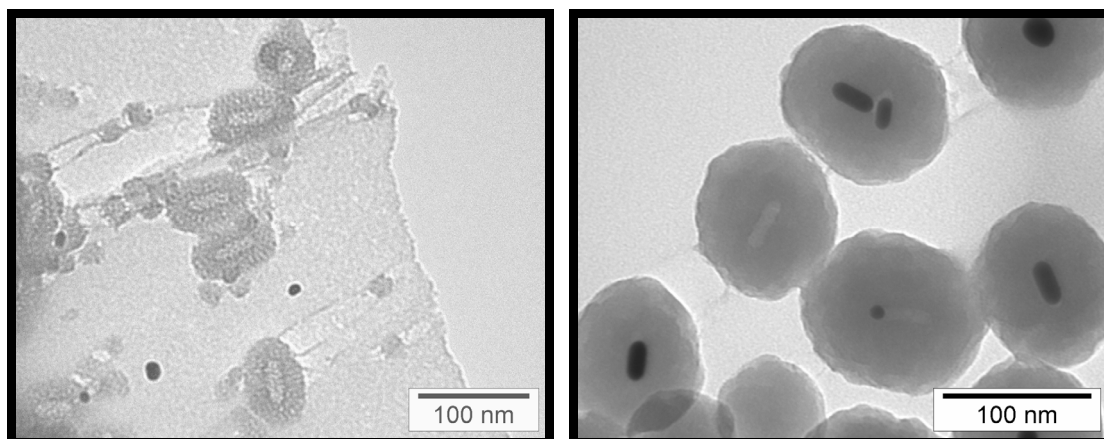


Fig. 7.6. (a, left) The gold core of mesoporous silica coated gold rods completely disappears within seconds after dispersing the rods into aqua regia, while **(b, right)** in case of Stöber grown silica onto the gold rods the core is only partly dissolved.

The microporous structure of PVP incorporated silica is still open enough to let aqua regia diffuse in slowly. The structure of the hollow mesoporous silica particle is very brittle and therefore a lot of decomposed silica material is seen on a TEM grid, the carrying film also does not survive in the acidic supernatant as can be seen in Fig. 7.6.a.

7.3.2. Closing the pores of colloidal silica: Ultramicroporous silica

The method of dissolving liquids through the pores of silica to the inner part of silica coated particles can be used to make core shell particles that contain a liquid with a closed impenetrable shell. By closing off the pores sufficiently fast particles with many different properties could be made. Moreover, an ultramicroporous silica layer on the outside might also select specific molecules to enter the core, but exclude larger ones. Therefore, silica coating with the standard Stöber method will not be suitable anymore. Sintering silica is a known method to get a smooth silica surface with ultramicropores or a completely closed off shell, the disadvantage of sintering is that it only happens at elevated temperature and therefore might at the same time damage the inner core of for instance fluorescent material. In 1996 Buining, Liz-Marzan and Philipse published a method of a simple preparation of smooth silica spheres²⁸. They quickly diluted a sodiumsilicate solution with ethanol, which initiated silica particles to nucleate. The idea is that the solubility of silica is so low in ethanol solutions, that supersaturation of sodiumsilicate is quickly reached, causing a nucleation of silica particles. If seed particles are already present the newly formed silica nucleates on the particles already present in the suspension. Since the particles are very smooth, the general idea is that the microporosity of the particles is very low. The microporosity of hollow dye filled particles coated with a dense silica layer produced by the quick and easy silica deposition described above was indirectly checked by first enabling dye to permeate into the particles in an aqueous environment. Then adding a small amount of a diluted (0.2 wt.%) sodium silicate solution, followed by a quick ethanol dilution. A washed sample of such a dispersion showed that the dye was still observable under confocal microscopy, showing that the dye had not diffused out of the particle in the wash steps as is shown in Fig. 7.7. This implies that the pores where initially the dye diffused in are now closed for the molecules with the size of the dye.

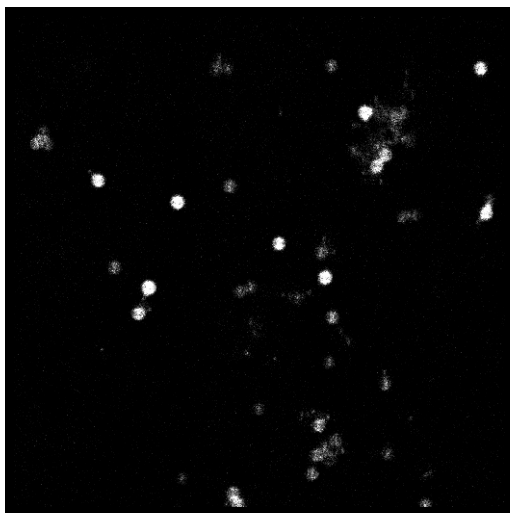


Fig. 7.7.

Confocal microscopy picture of Rhodamine filled hollow silica particles capped with an impenetrable silica layer. The dye is caught inside the hollow silica and cannot diffuse out anymore. (The picture measures $37.5 \mu\text{m}^2$.)

It is likely that this same more dense layer of silica can be grown from a Stöber reaction mixture if high concentrations of water are used that are subsequently quenched with ethanol.

Lu and coworkers²⁹ proved that indeed a silica layer can be synthesized that is so dense that it becomes impenetrable for small ions like chloride. To prove that the pore of the dye really has decreased to smaller than the 3 Å described by Walcarius and coworkers²⁴ a study was performed where protons were allowed to diffuse into the pores of FITC dyed silica. With pore sizes as large as 3 Å protons can easily diffuse in and out the pores of an FITC particle. Since the emission of FITC is pH dependent³⁰, it can be checked whether or not FITC silica has pores where ions can diffuse in and out or not internally changing the pH. A lower pH results in a lower extinction of FITC. Checking the emission spectra of their particles they confirmed that upon addition of hydrogen chloride to a suspension of FITC colloids the internal pH of the particles lowered. With a method comparable to the method of Buining they synthesized a dense silica layer around their particles by heating a solution containing sodium silicate. Then they showed these particles became impenetrable for hydrogenchloride and thus their fluorescence became pH insensitive. The microporous silica is turned into ultramicroporous silica.

Acknowledgements

Several of the examples shown in this chapter were done in collaboration with others: Hui Xu and Werner Goedel (University of Ulm, Germany) are thanked for the cooperation in the preparation of the free standing porous membranes. Chris Schneijdenberg and Hans Meeldijk are thanked for their help in preparing samples with the microtome. Daisuke Nagao (Tohoku University, Japan) is thanked for the synthesis of the snowman colloids. Menno Bergmeijer and Dannis 't Hart are thanked for their help with synthesis of the gold core silica shell particles. Maria D'Acunzi (MPIP, Mainz) is thanked for useful discussions and for providing the Polystyrene particles of Fig. 4.5.b.

Appendix: Synthesis methods

Hydrophobic TPM coated particles (Fig 7.1):

Fluorescent TPM coated silica particles were made by a combination of the methods of van Blaaderen²⁰, and Philipse⁹. For the synthesis of fluorescent silica particles typically 1.4202 g APS and 0.2440 g FITC is added to 10.0 ml Ethanol (100%). 175 ml ammonia (29 wt%) is mixed with 1750 ml distilled ethanol and 70 ml distilled TES is added at once together with the APS-FITC solution. Fluorescent particles with a diameter of roughly 400 nm were made. An extra layer of silica was made by addition of 2 ml extra TES after 16 hrs. From this batch a 250 ml 1.6%v/v solution of fluorescent particles in ethanol containing 20 ml ammonia (29 wt%) were grown with 2.0 ml TPM. Ammonia was removed by distilling the particles and adding absolute ethanol. The particles measured 440 nm in diameter with a polydispersity of 4% after TPM coating.

Mesoporous fluorescent silica (Fig 7.2):

Fluorescent Mesoporous silica particles (MPFS) were made according to the method described by Lin and coworkers¹⁶.

First FITC dye was coupled to aminopropyl triethoxysilane (APS). 1.0 mg FITC and 78.2 μ l APTES were dissolved in 4.0 ml ethanol (100% absolute) and kept stirring for 4 hrs. Meanwhile a solution of 0.58 g cetyltrimethylammoniumbromide (CTAB), was dissolved into 300 ml water, 4.83 ml ammonia (29 wt%) was added and stirred at 47 °C in an oil bath. Then 5.0 ml 0.2 M TES in ethanol was added. After 2.5 hrs another 5.0 ml 0.2 M TES in ethanol was added together with 2.22 ml of the FITC-APS mixture. After 16 hrs the reaction was stopped and the suspension was washed by repeated centrifugation and redispersed into pure ethanol.

Fluorescent FITC core- silica shell particles (Fig 7.3.):

For a typical synthesis of FITC core silica shell particles we refer to section 5.2.2.

Hematite dumbbells coated with silica (Fig 7.4.a):

Hematite dumbbells were made by the method described by Sugimoto³¹. To 50 ml of well-stirred 2.0 M iron(III)chloride solution, in a 200 ml Pyrex bottle, 45 ml of 6.0 M NaOH were slowly added during about 5 min followed by the addition of 5 ml water containing 0.43 g sodiumsulfate (2M) and the agitation was continued for an additional 10 min. The tightly stoppered bottle was placed in a laboratory oven preheated at 100 °C and was aged for 8 days. 25 ml of a washed and diluted suspension, containing 325 mg hematite dumbbells were washed with 60 ml PVP solution containing 4 g PVP (MW 10 kg/mol). After 3 hrs stirring 13 ml of this suspension was centrifuged and resuspended into 0.66 ml water and 9.24 ml Ethanol was added. Followed by addition of 0.1 ml 1% v/v TMAH suspension (Tetramethylammoniumhydroxide). The reaction was stirred and 30 μ l TES was added. This caused a silica coating of the dumbbell particles.

The hematite particles were dissolved by dispersion of the particles into concentrated hydrochloric acid. After several wash steps a TEM grid was dipped into a diluted dispersion and the result of the TEM picture is given in Fig. 7.4.a.

Snowman hollow silica particles (Fig 7. 4.b):

Hollow silica snowman were made by an unpublished method of Daisuke Nagao³². Deionized water (78.7 g) was bubbled with nitrogen for 30 minutes, then 96 μl (4 mM) 3-methacryloxypropyltrimethoxysilane (TPM) was added. After an hour 5.29 ml Methyl Methacrylate ([MM] 0.5 M) was added. The inhibitor of MM was removed by putting the liquid through an inhibitor removal column. After 30 min stirring the temperature was heated to 65 °C and 108 mg potassium persulfate (KPS, 4 mM) in 10 ml water was added. After 10 minutes 21 mg sodiumstyrenesulfonate (5 ml of 1 mM NaSS) was added and the reaction was allowed to stir for 2 hrs at elevated temperature. This way monodisperse crosslinked PMMA particles were made.

The protrusion of polystyrene on PMMA was obtained as follows: 5 ml of the as synthesized PMMA particles were dispersed in 83.9 ml deionized water. The solution was purged with nitrogen for 30 minutes followed by addition of 2.3 ml styrene (0.2 M) (inhibitor was removed, by washing with 0.1 M sodium hydroxide solution). After 2 hrs waiting the reaction mixture was heated to 65 °C and 81 mg KPS was added (3 mM solution). After 4 hrs protrusions of PS onto PMMA particles were formed.

To coat the particles with silica 0.8 ml of Polyallylhydrochloride solution (1 g/L containing 0.05 M sodiumchloride) was added to 2 ml of the PMMA-PS protruded particles (1.2 wt%). After 2 times centrifugation the particles were redispersed into 7 ml water containing 49 mg PVP (PVP MW 360 kg/mol). Another 2 times centrifugation was followed to remove excess of PVP. Finally it was redispersed into 10 ml ethanol. 0.8 ml ammonia (29 wt%) was added followed by addition of 100 μl TES. A part of this sample was dried, followed by a heat treatment for 2 hrs in an oven at 500 °C. The resulting particles are shown in fig 7.4.b.

Hollow silica particles after dissolving or burning of polystyrene (Fig. 7.5)

The synthesis of polystyrene was performed according to a method of Zou and coworkers³³. The inhibitor of styrene was removed by washing with an 1 M NaOH solution. For the synthesis of particles with a diameter of ~520 nm the procedure was as follows. 165 ml water was purged with nitrogen before 17.5 g styrene (10 %v/v) and 0.35 g divinylbenzene were added. The solution was vigorously stirred for 30 min. The a solution of 0.040 g potassiumpersulfate (0.22 wt %) in 10.0 ml water was added under vigorous stirring. After reaction overnight in a 80 C heated oil bad PS spheres had formed. The dispersion was dialyzed to get rid of unreacted reaction products.

For the coating of the particles we followed the same procedure as the coating of the snowman particles described above. Then the particles were dispersed into tetrahydrofuran (THF) , dried and redispersed in ethanol. A drop was put on a TEM grid and observed at the electronmicroscope, resulting in Fig. 7.5.a.

The polystyrene particles in Fig 7.5.b. measure 830 nm in diameter and were provided by Maria D'Acunzi (MPIP, Mainz). The silica coating procedure was equal to the snowman and smaller PS particles. The picture is taken after a heat treatment of the silica coated particles for 2 hrs in an oven at 500 °C.

7.4. References

1. Rouquerol, J.; Avnir, D.; Fairbridge, C. W.; Everett, D. H.; Haynes, J. M.; Pernicone, N.; Ramsay, J. D. F.; Sing, K. S. W.; Unger, K. K., *Recommendations for the characterization of porous solids (Technical Report)*. Pure and Applied Chemistry **1994**, 66, (8), 1739-1758.
2. Romm, F., *Microporous media: synthesis, properties, and modeling*. Dekker: New York, 2004.
3. Ozin, G. A., *Nanochemistry: Synthesis in diminishing dimensions*. Advanced Materials **1992**, 4, (10), 612-649.
4. Caruso, F., *Nanoengineering of Particle Surfaces*. Advanced Materials **2001**, 13, (1), 11-22
5. Yablonovitch, E.; Gmitter, T. J.; Leung, K. M., *Photonic band structure: The face-centered-cubic case employing nonspherical atoms*. Physical Review Letters **1991**, 67, (17), 2295.
6. Wijnhoven, J. E. G. J.; Vos, W. L., *Preparation of Photonic Crystals Made of Air Spheres in Titania*. Science **1998**, 281, (5378), 802-804.
7. Link, J. R.; Sailor, M. J., *Smart dust: Self-assembling, self-orienting photonic crystals of porous Si*. Proceedings of the National Academy of Sciences **2003**, 100, (19), 10607-10610.
8. Ayrál, A.; Julbe, A.; Roualdes, S.; Rouessac, V.; Durand, J.; Sala, B., *Silica Membranes- Basic principles*. Periodica Polytechnica Chemical Engineering **2006**, 50, (1), 67-79.
9. Philipse, A. P.; Vrij, A., *Preparation and properties of nonaqueous model dispersions of chemically modified, charged silica spheres*. Journal of Colloid and Interface Science **1989**, 128, (1), 121-136.
10. Xu, H.; Goedel, W. A., *Polymer-Silica Hybrid Monolayers as Precursors for Ultrathin Free-Standing Porous Membranes*. Langmuir **2002**, 18, (6), 2363-2367.
11. Mumpton, F. A., *La roca magica: Uses of natural zeolites in agriculture and industry*. Proceedings of the National Academy of Sciences **1999**, 96, (7), 3463-3470.
12. Kresge, C. T.; Leonowicz, M. E.; Roth, W. J.; Vartuli, J. C.; Beck, J. S., *Ordered mesoporous molecular sieves synthesized by a liquid-crystal template mechanism*. Nature **1992**, 359, (6397), 710-712.
13. Xiao, F.-S., *Ordered mesoporous silica-based materials templated from fluorocarbon-hydrocarbon surfactant mixtures and semi-fluorinated surfactants*. Current Opinion in Colloid & Interface Science **2005**, 10, (3-4), 94-101.
14. Schumacher, K.; Grün, M.; Unger, K. K., *Novel synthesis of spherical MCM-48*. Microporous and Mesoporous Materials **1999**, 27, (2-3), 201-206.
15. Zhao, D.; Feng, J.; Huo, Q.; Melosh, N.; Fredrickson, G. H.; Chmelka, B. F.; Stucky, G. D., *Triblock Copolymer Syntheses of Mesoporous Silica with Periodic 50 to 300 Angstrom Pores*. Science **1998**, 279, (5350), 548-552.
16. Lin, Y. S.; Tsai, C. P.; Huang, H. Y.; Kuo, C. T.; Hung, Y.; Huang, D. M.; Chen, Y. C.; Mou, C. Y., *Well-Ordered Mesoporous Silica Nanoparticles as Cell Markers*. Chemistry of Materials **2005**, 17, (18), 4570-4573.
17. Wikipedia Silica 2008: <http://en.wikipedia.org/wiki/Silica>.
18. Weast, R. C., *Handbook of Chemistry and Physics, 50th edition*. CRC Press: 1969-1970.

19. van Blaaderen, A.; Kentgens, A. P. M., *Particle morphology and chemical microstructure of colloidal silica spheres made from alkoxysilanes*. Journal of Non-Crystalline Solids **1992**, 149, (3), 161-178.
20. Van Blaaderen, A.; Vrij, A., *Synthesis and characterization of colloidal dispersions of fluorescent, monodisperse silica spheres*. Langmuir **1992**, 8, (12), 2921-2931.
21. Graf, C.; Vossen, D. L. J.; Imhof, A.; vanBlaaderen, A., *A General Method To Coat Colloidal Particles with Silica*. Langmuir **2003**, 19, (17), 6693-6700.
22. Labrosse, A.; Burneau, A., *Characterization of porosity of ammonia catalysed alkoxysilane silica*. Journal of Non-Crystalline Solids **1997**, 221, (2-3), 107-124.
23. Giesche, H., *Synthesis of monodispersed silica powders II. Controlled growth reaction and continuous production process*. Journal of the European Ceramic Society **1994**, 14, (3), 205-214.
24. Walcarius, A.; Despas, C.; Bessière, J., *Molecular sieving with amorphous monodisperse silica beads*. Microporous and Mesoporous Materials **1998**, 23, (5-6), 309-313.
25. Ohmori, M.; Matijevic, E., *Preparation and Properties of Uniform Coated Inorganic Colloidal Particles: 8. Silica on Iron*. Journal of Colloid and Interface Science **1993**, 160, (2), 288-292.
26. Sacanna, S.; Rossi, L.; Kuipers, B. W. M.; Philipse, A. P., *Fluorescent Monodisperse Silica Ellipsoids for Optical Rotational Diffusion Studies*. Langmuir **2006**, 22, (4), 1822-1827.
27. Zoldesi, C. I.; Imhof, A., *Synthesis of Monodisperse Colloidal Spheres, Capsules, and Microballoons by Emulsion Templating*. Advanced Materials **2005**, 17, (7), 924-928.
28. Buining, P. A.; Liz-Marzán, L. M.; Philipse, A. P., *A Simple Preparation of Small, Smooth Silica Spheres in a Seed Alcosol for Stöber Synthesis*. Journal of Colloid and Interface Science **1996**, 179, (1), 318-321.
29. Lu, Z.; Xu, J.; Han, Y.; Song, Z.; Li, J.; Yang, W., *Robust fluorescein-doped silica nanoparticles via dense-liquid treatment*. Colloids and Surfaces A: Physicochemical and Engineering Aspects **2007**, 303, (3), 207-210.
30. Lanz, E.; Gregor, M.; Slavík, J.; Kotyk, A., *Use of FITC as a Fluorescent Probe for Intracellular pH Measurement*. Journal of Fluorescence **1997**, 7, (4), 317-319.
31. Sugimoto, T.; Khan, M. M.; Muramatsu, A., *Preparation of monodisperse peanut-type [alpha]-Fe₂O₃ particles from condensed ferric hydroxide gel*. Colloids and Surfaces A: Physicochemical and Engineering Aspects **1993**, 70, (2), 167-169.
32. Nagao, D.; van Kats, C.M.; Hayasaka, K.; Imhof, A.; Konno, M.; van Blaaderen, A., *Synthesis of Anisotropic Hollow, Silica Particles Containing Movable Spheres (in preparation)* **2008**
33. Zou, D.; Derlich, V.; Gandhi, K.; Park, M.; Sun, L.; Kriz, D.; Lee, Y. D.; Kim, G.; Aklonis, J. J.; Salovey, R., *Model filled polymers. I. Synthesis of crosslinked monodisperse polystyrene beads*. Journal of Polymer Science Part A: Polymer Chemistry **1990**, 28, (7), 1909-1921.

Summary

The driving forces for fundamental research in colloid science are the ability to manage the material properties of colloids and to unravel the forces that play a role between colloids to be able to control and understand the chemical, biological and physical processes where colloids play an important role. Therefore we are searching for colloidal materials with specific physical properties to better understand the world surrounding us.

Until recently research in colloid science was mainly focused on spherical (isotropic) particles. Monodisperse spherical colloids serve as a model system as they exhibit similar phase behaviour as molecular and atomic systems. Nevertheless, in many cases the spherical shape is not sufficient to reach the desired research goals. Recently the (generally) more complex synthesis methods of anisotropic model colloids has strongly developed. A broad area of model colloids has now become available. This thesis should be regarded as a contribution to this research area. Anisotropic colloids can be used as a building block for complex structures and are expected not only to lead to the construction of full photonic band gap materials. They will also serve as new, more realistic, models systems for their molecular analogues. Therefore the term ‘molecular colloids’ is sometimes used to qualify these anisotropic colloidal particles.

In nature colloidal crystals can be found in opals. Silicondioxide (silica) is a widely applied inorganic material in colloid science, because it can be easily chemically modified. Therefore, the forces between particles can well be controlled. Other widespread used colloidal material is latex (polystyrene and polymethylmethacrylate (PMMA)). These are also the main materials from which we constructed the anisotropic particles described in this thesis. Moreover, (in chapter 3) we describe a synthesis method of gold rods, because they have such a characteristic interaction with light. In the chapter 1, the introduction of this thesis, we give an overview of the main synthesis techniques for anisotropic colloidal systems. Some of these techniques were used in the synthesis of the systems described in the next chapters.

In Chapter 2 we describe the method of etching silicon wafers to construct monodisperse silicon rods. Pre-patterned p-type silicon wafers were electrochemically etched in electrolyte solutions containing hydrogen fluoride. By modulating the current density while etching, deep cylindrical pores were formed. Overlap of the pores resulted in silicon rods with controllable modulated diameters. The resulting rods were transformed in monodisperse silicon rods of 5.5 μm length and 300 nm width by sonication. They subsequently were oxidized and labeled (coated) with a fluorescent silica layer. The first explorative phase behaviour of these silica rods was studied. The particles showed a nematic ordering in charge stabilized suspensions. Refractive index matching of these particles will enable the study of concentrated dispersions quantitatively on a single particle level with confocal microscopy.

Chapter 3 describes the synthesis of colloidal gold rods and the (mesoporous) silica coating of gold rods. Chapter 4 describes the physical and optical properties of these particles when thermal energy is added. This is compared to the case where the particles are irradiated with femtosecond laserpulses of variable wavelengths. In Chapter 3 we show that we have full control of the aspect ratio of the synthesized gold rods, thus we also have full control over the frequency where the longitudinal surface plasmon absorption peak of our system is at maximum. We also show that we can grow a silica layer on the gold rods with controllable thickness. Amorphous as well as mesoporous silica can be grown on the gold rods. When a thick silica layer is grown

on the gold rods the particles become (almost) spherical. Therefore, those particles can form a 3D colloidal crystal where the gold core of the particles can have any desirable orientation. In future this can be used to control the alignment of the gold rods a 3D crystal in an electric field. The silica coated gold rods are a promising step forward towards the achievement of optical switches.

In chapter 4 we show to have a very local control of changing the aspect ratio of gold rods by irradiation with femtosecond laserpulses. We show that irradiation of femtosecond laserpulses with a repetition rate of 82 MHz have a threshold of ~ 2 picojoules to deform the particles. Furthermore, we show that by heating particles to temperatures between 200 °C and 400 °C the particles also show a transformation, resulting in particles with a decreased aspect ratio. This is a much lower temperature than the melting temperature of bulk gold. Atoms at the surface of gold rods have more kinetic energy and more freedom to move at elevated temperature and thus the lowered shape transformation of the particles is explained by surface melting.

In chapter 5 and 6 we show how, starting from spherical particles, dimers (dumbbells), trimers and multimers can be formed by controlled aggregation. Chapter 5 describes the synthesis of colloidal silica dumbbells, while chapter 6 illustrates the synthesis of PMMA (polymethylmethacrylate) dumbbells, trimers and multimers (n-mers). The mix of n-mer particles were separated through a density gradient centrifugation resulting in separated, dumbbell, triplet and multimers batches. The silica dumbbells described in chapter 5 contain a fluorescent dye which makes them suitable for confocal studies. First explorative research of pure silica dumbbell sediments in and outside an electric fields, made clear that it is possible to make 3D crystals from the synthesized dumbbells. The PMMA dumbbells made in chapter 6 were made by a different mechanism than originally was aimed at. Attempts of making PMMA dumbbells through the formation of protrusions of cross-linked PMMA particles that were swelled with methacrylic acid and methylmethacrylate mixtures all failed. The proposed arguments for these failures are the increased hydrophilicity of the monomers and improved miscibility with water, which disfavours the formation of protrusions.

Chapter 7 finally shows an overview of syntheses where the pores of (mainly) silica particles is decreased. Therefore most given examples show anisotropy in constitution rather than anisotropy in shape. We show that the pores of the given particles could be decreased from macroporous to (ultra)microporous. Finally we show that it is even possible to completely close the pores of silica with a dense silica layer, making them impenetrable for small molecules as well. Through a full control of pore size particles can selectively be filled with materials (for instance a drug) and be controllably closed. This opens a route for synthesis of particles that can be used as molecular filters or in biomedical applications such as smart drug delivery.

Samenvatting voor een breder publiek

Scheikunde is de kunst van het scheiden. Als een stof wordt gesplitst tot zijn elementaire basiseenheid komt men uit op moleculen en atomen. De meesten zullen zich dit nog herinneren van hun eerste chemielessen, waarin het begrip “schei-kunde” wordt uitgelegd. Wanneer men bijvoorbeeld een zandkorrel (*siliciumdioxide*, ook wel *silica genoemd*) neemt en die zo ver mogelijk probeert fijn te malen, dan zullen de resterende deeltjes veel groter zijn dan atomen en of moleculen. De deeltjes zullen een afmeting krijgen van enkele micrometers (dat is grofweg 1/100 maal de dikte van papier). Bovendien hebben deze deeltjes een grillige, niet ronde (*anisotrope*) vorm. Als de deeltjes nog iets kleiner worden gemaakt, in de grootte orde van een nanometer (1 miljoenste van een millimeter) tot micrometers, dan spreekt men van colloïden. Dit is een (eenvoudige) manier om een colloïdaal systeem te maken.

Om een goed modelsysteem te verkrijgen is het echter belangrijk dat de deeltjes gelijke vorm en (enigszins) gelijke afmeting hebben, zodat de onderlinge krachten die tussen de deeltjes heersen goed in kaart gebracht kunnen worden. Het anisotrope colloïdsysteem dat we op de hierboven beschreven manier maakten, is niet uniform en vertoont een grote variatie in afmeting, het is daardoor niet geschikt als colloïdaal modelsysteem. Het onderzoek aan bolvormige (*isotrope*) colloïden, in veel gevallen energetisch de meest gunstige verschijningsvorm van de deeltjes, is in de laatste decennia reeds ver gevorderd en breed onderzocht. Omdat het maken (*synthetiseren*) van niet bolvormige modelsystemen (*anisotrope model colloïden*) vaak een complexere bereidingsmethode heeft, is dit onderzoeksterrein veel minder ver ontgonnen. Dit proefschrift moet worden gezien als een bijdrage aan de verdere verkenning van dit onderzoeksveld.

Zonder het onszelf te beseffen komen we bijna dagelijks in contact met colloïden en colloïdsystemen, hieronder geïllustreerd door 2 willekeurig gekozen voorbeelden. Bij het smeren van een boterham met boter, smeert men eigenlijk waterbolletjes van (sub)colloïdale afmeting op het brood die geëmulgeerd zijn in vet, water en vet mengen normaal niet, maar door de waterbolletjes te stabiliseren (*emulgeren*) ontmengen vet en water niet in boter. Als men niest, sproeit men waterdruppeltjes van colloïdale afmeting in de lucht, die zo klein zijn dat ze door de lucht kunnen worden “gedragen” (*aerosol*). Op deze manier, door de lucht gedragen, genesteld op minuscule waterdruppels, kunnen virussen zich verspreiden. De voorbeelden van colloïden om ons heen zijn te talrijk en te divers om ze allemaal hier te bespreken. Net als moleculen en atomen kunnen colloïden meerdere samenstellingen hebben. Moleculen kunnen in verschillende verschijningsvormen (*fasen*) voorkomen. Zo kunnen moleculen en atomen vaste stoffen, vloeistoffen of gassen vormen, we noemen dit fasengedrag. Ook colloïden kunnen dit fasengedrag vertonen, dit is een reden waarom colloïdsystemen goed model kunnen staan voor atomaire systemen. Omdat de afmeting van de colloïden veel groter is vertonen de colloïdsystemen ook andere fysische eigenschappen die zeer interessant zijn om te bestuderen.

De drijvende krachten achter het fundamentele onderzoek aan colloïden zijn het beheersen van materiaaleigenschappen en het in kaart brengen van de onderlinge krachten die tussen colloïden spelen. Op die manier kunnen we chemische, fysische en biologische processen, waarin colloïden een rol spelen, beter beheersen en begrijpen. Daarom zijn we op zoek naar materialen met specifieke fysische eigenschappen om technologische vooruitgang te kunnen boeken en de wereld om ons heen een stukje beter te kunnen begrijpen.

Colloïdale systemen hebben een bijzondere interactie met licht. De afmeting van colloïdale deeltjes is namelijk in dezelfde orde grootte als de golflengte van het licht. In een geconcentreerd aerosol, (bijvoorbeeld mist) zal licht verstrooien in alle richtingen waardoor een ondoorzichtige witte wolk gezien zal worden. In een colloïdaal kristal, waarin alle deeltjes regelmatig geordend zijn, kan het licht zodanig interacteren dat sommige golflengtes kunnen reflecteren op het kristal, men zal dan, afhankelijk van de hoek waarop men het kristal bekijkt, kleuren gereflecteerd krijgen.

In de natuur komt een colloïdaal kristal voor in de vorm van een opaal (siliciumdioxide). Siliciumdioxide, ofwel silica, is een veelgebruikt anorganisch materiaal in de colloïdchemie, omdat het oppervlak goed chemisch te modificeren is, waardoor de onderlinge krachten van colloïden goed te beheersen zijn. Andere materialen, die veelvuldig gebruikt worden zijn polystyreen (“*een plastic polymeer*”) en polymethylmethacrylaat (PMMA, o.a. het basismateriaal voor perspex). Ook in dit proefschrift zijn dit de voornaamste materialen waarvan de anisotrope model colloïden die worden beschreven gemaakt zijn. Daarnaast wordt ook (in hoofdstuk 3) de synthese van goudstaafjes beschreven, die zoals hieronder besproken, een karakteristieke interactie met licht hebben. In de introductie van dit proefschrift worden diverse methodes beschreven om colloïden te maken die kunnen dienen als anisotroop model systeem. Enkele van deze synthese technieken zijn toegepast om de in de overige hoofdstukken beschreven colloïdsystemen te vervaardigen.

In Hoofdstuk 2 wordt een methode beschreven hoe gelijkvormige (*monodisperse*) silicium en silica staafjes gemaakt kunnen worden door een plakje silicium te etsen. Dit werk is deels uitgevoerd in het natuurkundig laboratorium (NatLab) van Philips. Via een lithografische etsmethode is een regelmatig patroon van putjes op een plaat silicium vorgeëtst. Door een stroom te laten lopen door deze siliciumplaat werden poriën geëtst die elkaar zodanig overlappen dat er lange staafjes werden gecreëerd, met een regelmatig alternerende dikte. De afmeting van deze siliciumstaafjes kon zeer exact worden gereguleerd door de stroomsterkte te variëren, waardoor een zeer monodispers systeem overbleef nadat de staafjes van de siliciumplaat werden afgetrild. Door de staafjes te oxideren werden silica staafjes verkregen die uitstekend kunnen dienen als modelsysteem. De staafjes zijn gemaakt van halfgeleider materiaal, zijn eenvoudig chemisch te modificeren en hebben controleerbare afmeting. Dit maakt ze uitermate geschikt voor een breed scala aan toepassingen, o.a. voor gebruik in micro-electronica. Om deze reden is deze bereidingsmethode gepatenteerd (“*Dispersies van staafvormige nanodeeltjes gemaakt van halfgeleider materiaal*”). Door de silica staafjes vervolgens ook te voorzien van een fluorescerend laagje werd het systeem eveneens geschikt gemaakt voor confocale microscopie. Een onderzoekstechniek waarbij de driedimensionale structuur van (colloïdale) systemen kan worden onderzocht, wat het materiaal nog geschikter maakt om te gebruiken als modelsysteem.

Hoofdstuk 3 beschrijft de bereidingsmethode van staafvormige colloïden van goud al dan niet bedekt met een (poreuze) silica coating. Hoofdstuk 4 beschrijft de optische en fysische eigenschappen van deze deeltjes wanneer er energie wordt toegevoegd in de vorm van warmte of wanneer wordt bestraald met laserpulsen van verschillende golflengte en energie. Door de lengte breedte verhouding (*aspect ratio*) van goud staafjes te veranderen, volgens de methode die in hoofdstuk 3 beschreven wordt, verandert de kleur (*golflengte*) die wordt geabsorbeerd. In hoofdstuk 3 laten we zien dat we controle hebben over de golflengte die de goudstaafjes absorberen. Bovendien wordt een methode beschreven waarbij we de staafjes met silica kunnen aangroeiën met een controleerbare schildikte. Met een dikke silicalaag om het goudstaafje heen

groeit het deeltje weer naar een bolvorm toe. Dit heeft als voordeel dat de deeltjes zich goed kunnen ordenen in een regelmatig kristalrooster, waarbij de goudstaafjes in de bollen zich nog wel kunnen oriënteren in alle richtingen. De toekomstplannen met deze deeltjes zijn erop gericht om de goudstaafjes uit te lijnen via een opgelegd elektrisch veld. Door het al dan niet uitlijnen van de deeltjes kunnen we de absorptie van bepaalde golflengtes aan of uit schakelen, waarbij we een schakeling met licht (*optische schakeling*) kunnen creëren. In hoofdstuk 4 tonen we aan dat we op zeer lokaal niveau controle hebben op het veranderen van de aspect ratio van de goudstaafjes, door energie in de vorm van laserpulsen toe te dienen. De deeltjes worden korter door het beschieten met zeer korte (*~femtoseconde*) laserpulsen, boven een bepaalde intensiteit (*2 picojoule*). Ook door de deeltjes te verhitten tussen 200 °C en 400 °C vervormen de deeltjes. Dit zijn temperaturen die veel lager liggen dan de smelt temperatuur van goudstaven die in de kluis van een bank liggen opgeborgen. Dat komt door de veel kleinere afmeting van de colloïdale goudstaafjes, waar atomen op het oppervlak zich makkelijker kunnen verplaatsen, waardoor het deeltje een andere (meer bolvormige) vorm aan kan gaan nemen. De combinatie van het controleren van de golflengte die de goudstaafjes absorberen, het ordenen in een kristalrooster, en het zeer lokaal veranderen van de dimensies (en daarmee de absorptiegolflengte) van een kleine groep of wellicht individuele deeltjes, opent de weg voor nieuwe toepassingen, zoals optische schakelingen en optische data opslag.

In hoofdstuk 5 en 6 laten we zien hoe we, uitgaand van bolvormig deeltjes, via gecontroleerde samenklontering van deeltjes (*clustering of aggregatie*), dimeer (*dumbbells*), trimeer en multimeer deeltjes kunnen maken. Hoofdstuk 5 handelt over dumbbells die gemaakt zijn van silica, terwijl de deeltjes die in hoofdstuk 6 staan beschreven van PMMA gemaakt zijn. De gecontroleerde aggregatie levert een mix van deeltjes op, die via een slimme scheidingsmethode (*sedimentatie in een dichtheidsgradiënt*) gezuiverd kunnen worden in oplossingen met vrijwel uitsluitend dumbbells, tripletten en of multimeren. Door sedimentatie in een klein capillair op een vlakke bodem, met en zonder elektrisch veld, laten we zien dat dumbbells zich ordenen. De ordening in een elektrisch veld strekt zich uit over meerdere lagen waardoor een klein colloïdaal kristal van dumbbells ontstaat. Mogelijk kunnen met dumbbells, tripletten of multimeren als bouwstenen kristallen gemaakt worden die licht in geen enkele richting kunnen voortplanten een zogenaamd fotonisch kristal. De zoektocht naar fotonische kristallen is van fundamenteel belang om de voortplanting van licht volledig te kunnen begrijpen en daarmee uiteindelijk licht te kunnen sturen. Uiteindelijk kan men ook hierbij denken aan een toepassing als optische schakeling, waarbij analoog aan electronengeleiding bij halfgeleiders, toegepast in transistoren nu lichtpulsen (*fotonen*) geleiding plaatsvindt.

Tenslotte wordt in hoofdstuk 7 een overzicht gegeven van colloïd syntheses, waarbij de poriën van de vervaardigde materialen steeds kleiner kunnen worden gemaakt. Van macroporeus, waarbij de poriegrootte in de orde van een micrometer is, via mesoporeus tot (ultra)microporeus, met poriën kleiner dan 1 nanometer. Deze deeltjes kunnen wederom in een zeer breed spectrum aan onderzoeksgebieden worden toegepast. Deeltjes met macroporiën kunnen worden gebruikt als dragermateriaal voor katalysatoren, deeltjes met mesoporiën kunnen worden gebruikt voor biomedische toepassingen, zoals de opslag en (gecontroleerde) afdracht van biomoleculen (en of medicijnen). Uiteindelijk kunnen deeltjes met (ultra)microporiën voor dezelfde doeleinden worden toegepast, maar eveneens werken als moleculair filter. Tenslotte als afsluiter, tonen we aan dat het mogelijk is de deeltjes volledig af te kunnen sluiten, zodat ze voor vrijwel alle moleculen ondoordringbaar zijn geworden.

Dankwoord

”Wetenschap is nooit af”; het motto van de Universiteit Utrecht. Ook het verhaallijnen uit dit boek zullen een vervolg krijgen, maar over een paar pagina’s is dit boek wel aan zijn einde. Aan het einde van *mijn* verhaal, wil ik graag nog mensen bedanken die op diverse wijzen hebben bijgedragen aan de totstandkoming van dit proefschrift. Dat zijn er velen, want al moet je het promotiewerk zèlf doen, je doet het niet alléén...! Om niemand te vergeten, wil ik op deze plek allereerst iedereen die ik vergeten ben te noemen ook hartelijk danken voor hun bijdragen.

Alfons, mijn promotor, wil ik als eerste bedanken. We hebben samen de Soft Condensed Matter groep groot zien groeien. In de begintijd heb ik me tijdens jouw afwezigheid vaak gekscherend “waarnemend professor” genoemd. Dat kan, omdat professor geen beschermde titel is. De laatste tijd durfde ik dat niet meer, omdat het meer dan duizendpootschap wat jij laat zien, inmiddels zulke grote verantwoordelijkheden met zich meedraagt, dat voor jouw functie een zelfbenoemde plaatsvervanger bij lange na niet meer volstaat. Het zou mooi zijn, als er in plaats van een “waarnemend professor”, een assistent professor bij zou kunnen komen. Het is dan ook jammer dat jouw deur, die altijd openstond, de laatste tijd vaker (tijd)noodgedwongen dicht is. Ik hoop voor jou en voor alle collega’s dat er binnenkort meer tijd komt om weer vaker een open deur te kunnen instappen (en desnoods in te kunnen trappen, want dat hoor je met open deuren te doen :-).

Arnout, mijn co-promotor wil ik danken voor zijn rust. Jouw input in het bespreken van de hoofdstukken hebben ook mijn gemoedsrust goed gedaan. Je straalde vertrouwen uit dat het toch nog wel goed zou komen met mijn proefschrift, op momenten dat ik richting wanhoop dreigde te gaan.

Patrick Johnson ben ik grote dank verschuldigd. Jij hebt in onze samenwerking, zowel hoofdstuk 2, maar vooral ook hoofdstuk 5 naar een hoger niveau weten te tillen. Ik heb met veel plezier met je samengewerkt en heb heel veel van je geleerd. Jouw systematiek, inventiviteit en daadkracht hebben een grotere inspirerende uitwerking op mij gehad, dan je zelf zult vermoeden.

Dannis, jouw clean desk/fumehood methode conflicteerde af en toe met mijn ‘werkstijl’, dat neemt niet weg dat ik fijn met je heb samengewerkt. Al met al hebben we mooie dingen bereikt samen, bedankt daarvoor!

Ik heb ook het genoeg gehad studenten te mogen begeleiden. Menno Bergmeijer dank ik voor het engelengeduld in alle pogingen mooie goudstaafjes te maken, dat vereist een groot doorzettingsvermogen. Wessel, jou bijdrage aan hoofdstuk 6 is gigantisch. Bovendien is vermeldenswaardig dat je experimenteren niet tot het lab hebt beperkt. Ik heb zeker ook al je experimenten uit je oven thuis gewaardeerd, daar is het je wel gelukt prachtige (en lekkere!) protrusions te bakken.

Ik wil de mensen op het “Natlab” van Philips danken voor het in staat stellen ook buiten de universitaire omgeving te kunnen experimenteren en voor de fijne werksfeer aldaar. In het bijzonder wil ik Jan van den Meerakker danken voor de coaching en Anton Kemmeren voor zijn hulpvaardigheid in alles. Dit leerzame uitstapje zou niet hebben plaatsgevonden zonder John Kelly, hem wil ik ook danken voor zijn adviezen en de getoonde interesse in het bereiken van mijn doel.

Jonathan Palero heeft ons fantastisch geholpen met onze ‘laserquest’ experimenten, dankjewel. Ook Hans Gerritsen en Dave van den Heuvel hebben geïnteresseerd meegekeken en geholpen in de discussies, terwijl met Dmitry Turchinovic verkennende experimenten zijn uitgevoerd. Dave, als jarenlange kamergenoot dank ik je voor het gezelschap, eveneens ben ik je dankbaar dat je in onze kamer vaak je

koptelefoon hebt gebruikt, want, bijvoorbeeld, *The Carpenters* is echt niet meer van deze tijd, al heb je gelukkig ook muziek die af en toe wel even luid en unplugged mag (*RHCP*). ☺

Dit proefschrift staat vol met mooie electronenmicroscopie plaatjes, maar er zijn er nog minstens duizend gemaakt die het proefschrift niet hebben gehaald. Hans Meeldijk en Chris Schneijdenberg hebben mij vele malen uit de brand geholpen bij de EM als bijvoorbeeld “*de electronenbundel weer eens in Bunnik stond*”. Ook Pim van Maurik, John Geus en Henk Pluijgers wil ik danken voor de hulpvaardigheid door de jaren heen.

Een leuke werksfeer vereist collega's die voor je klaar staan en voor je open staan. María Delgado Florès, het sociale hart van de groep, verdient hiervoor een eervolle vermelding, het klopt niet als jij er niet bent. Als je zolang bij de groep werkt is er echter een veeel langere lijst collega's en ex-collega's die het werken bij SCM&B leuk hebben gemaakt.

Dank aan mijn ex-SCM collega's: Job 'reciprocal space' Thijssen, nooit te beroerd om “even” wat uit te leggen, Didi 'RAS' Derks, Carmen 'hickup' Zoldesi, Dirk 'duizendpoot' Vossen, Jacob '400.000.000' Hoogenboom, Krassimir '10L-shaker' Velikov, Mirjam 'Kips' Leunissen, maar ook Christina (Krissi), Christina G., Anand, Antti-Pekka, Astrid, Joan, Andrea, Slava, Yu Ling, Catherina, Andy C., Zuocheng, Alexander, Paddy, Matthias, Eduardo, Alejandro, Chantal, Hans, Gerard (Gerrit), Johan.

Natuurlijk ook dank aan mijn huidige SCM collega's: Esther, Peter, Dannis, Johan, Stephane, Jacob, Allesandro, Teun, Laura, Frank, Rao, Anke, Ahmet, Marjolein, Matthieu, Michiel, Jamal, Peter, Gülsen, Thea, Maria, maar ook de konijntjes op het Princetonplein en de muizen op Peter's kamer.

Ook bij 'de burens' heb ik leuke en zinnige contacten, al gaat het te ver iedereen te noemen, een enkeling wil ik met naam noemen omdat ik mijn roots niet kan (en wil) verloochenen. Dominique, (“mijn colloïden moeder”), Haran (“mijn synthese vader”), Diane, Judith, Nathalie en Chantal. Albert, Henk, Willem, Bonny, Emile, Ben, Andrei, Daniela, Maurice, Dirk, Roel, en ook ALLE andere (ex-)collega's van het van 't Hoff Laboratorium; DANK voor de vele jaren vruchtbare samenwerking. Eveneens dank aan alle collega's van Biofysica en alle andere bewoners van het Ornsteinlaboratorium en het Debye Instituut (voor nanomaterialen onderzoek)

Dan zijn er nog mensen waarmee ik heb gewerkt, waarvan bij niet iedereen deze samenwerking een plek heeft gekregen in het proefschrift, omdat het in mijn dubbelfunctie als research assistent minder raakvlakken had met het werk beschreven in dit boekje. Echter van elke samenwerking doe je weer nuttige kennis op, daarom ook speciale dank aan groepen waar mee is samengewerkt in Utrecht of in het buitenland.

Special Thanks to :

Werner Goedel, Hui Xu, (University of Ulm, Germany), Andy Hollingsworth, (NYU, New York), The Solomon Group; Mike Solomon, Mike Kogan, Claire Dibble and Laura Shereda, (Ann Arbor, University of Michigan). Maria D' Ancuzi, Ewa Ilska, Doris Volmer, (MPIP, Mainz, Germany). Volker Bormuth, (Technical University Dresden, Germany), Holger Reiber, (University of Mainz, Germany), Yves Hennequin, UvA, Amsterdam.

Er zijn nog meer mensen, binnen en buiten de universiteit, die mij geholpen hebben over de eindstreep te komen. Mentale steun is namelijk minstens zo belangrijk. Daarom ook dank aan de Fylakra redactie en de VGM'ers. Naast *de fysica* is ook *het fysieke* onontbeerlijk geweest voor mij. Daarom was het altijd fijn dat ik bij

volleybalvereniging Switch even mijn hoofd leeg kon knallen. Ik hoop dat promoveren dit jaar ook met ons H3 team gaat lukken. Wat een dijk van een cluppie is dat toch, waar zelfs de zwakste nog goed is. Ik heb me er altijd als een kom in een guppie gevoeld. Mijn hoofd leegschoffelen kon ik met de Julianagroen-groep. En mijn hoofd leegwaaien met de zeilers van “de Krijger”. De mooiste club vrienden is de NSC-gang, een vriendengroep, waar niet mijn hoofd, maar mijn hart vol van is. Al meer dan de helft van mijn leven krijg ik er energie van; ik hoop dat dat nooit verloren gaat. Leerzaam, nuttig, maar vooral ook gezellig waren de CPPT sessies met Annemiek en Esther.

Voor de steun, niet alleen in de laatste 3 kwartier van mijn promotieperiode wil ik graag Sjors en Igor, mijn paranimfen, danken. Onvoorwaardelijke steun en liefde ontvang ik ook van mijn (schoon)familie. Het woordje dank is eigenlijk te klein om mijn dankbaarheid voor jullie hier te uiten.

Tenslotte, Lucienne, Femke, *Bram*, *voor altijd in mijn hart* en Koen de laatste zin van dit dankwoord is voor jullie:

*Now droem ik van ów in mien ermen
Van hoe ik ów taege meej aan druk
Ów wil ik veur altied verwerpen
Veur altied, met 'n bitje geluk*

(Uit: Liefde, Rowwen Heze)

Curriculum Vitae



Carlos Maria van Kats werd geboren op 21 maart 1969 te Jaguariuna (Brazilië). Na het behalen van het VWO diploma (1987, Niels Stensen College, Utrecht), studeerde hij Scheikunde, met als afstudeerrichting Fysisch Organische Chemie (1987-1993, Universiteit Utrecht (UU)). Na deze studie begon zijn carrière in de colloïdchemie op het van het Hoff laboratorium voor Fysische en Colloïd Chemie als onderzoeks assistent (1994-1995, UU). Na hierop aansluitend een jaar als onderzoekstechnicus gewerkt te hebben bij de groep Spectroscopie van Gecondenseerde Materie (1995-1996, Universiteit van Amsterdam (UvA)), keerde hij terug naar de Universiteit Utrecht om te gaan werken bij de Utrechtse Colloïd Synthese Faciliteit. Eerst als onderzoeksassistent (1996-1997), daarna als manager (1997-1999).

Vervolgens ging hij aan de slag in de nieuwe groep Soft Condensed Matter van Prof. van Blaaderen, waar hij tot op heden als onderzoeksmedewerker werkt (1999-heden, Debye Institute for Nanomaterials Research, UU). Diverse gasten uit binnen- en buitenland, alsmede directe collega's zijn in deze periode begeleid om de vaardigheden van colloïd synthese over te dragen. Ook werd het buitenland bezocht voor korte onderzoeksstages; In de groep Organic and Macromolecular Chemistry van Prof. Goedel (2001, Universität Ulm, Duitsland) en in de groep Chemical Engineering van Prof. Solomon (2005, University of Michigan, Ann Arbor, USA).

Het promotiewerk, dat werd verricht naast het reguliere werk, staat beschreven in dit boek. In deze onderzoeksperiode resulteerde een deeltijds detachering bij Philips Natlab (2002-2003) tot het patent: *Dispersion of nanowires of semiconducting material*.

Het onderzoek beschreven in dit boek is op diverse wetenschappelijke bijeenkomsten in binnen- en buitenland gepresenteerd (o.a. *Particles 2004* Orlando, USA, *6th Liquid Matter Conference*, 2005 Utrecht, *Jülich Soft Matter Days*, Rolduc, Kerkrade, FOM bijeenkomsten: *Gecondenseerde Materie*, *Statistische Fysica*, *Physics*, Veldhoven en Lunteren, NWO-CW bijeenkomsten: *Vloeistoffen en Grensvlakken*, Lunteren).

List of Publications

Publications related to the work in this thesis:

van Kats, C. M.; Johnson, P. M.; van den Meerakker, J. E. A. M.; van Blaaderen, A.,
Synthesis of Monodisperse High-Aspect-Ratio Colloidal Silicon and Silica Rods.
Langmuir **2004**, 20, (25), 11201-11207. (Chapter 2)

Johnson, P. M.; van Kats, C. M.; van Blaaderen, A.,
Synthesis of Colloidal Silica Dumbbells.
Langmuir **2005**, 21, (24), 11510-11517. (Chapter 5)

Nagao, D.; van Kats, C.M.; Hayasaka, K.; Imhof, A.; Konno, M.; van Blaaderen, A.,
Synthesis of Anisotropic Hollow, Silica Particles Containing Movable Spheres.
(in preparation) **2008** (Chapter 7)

Zhang, L.; D'Acunzi, M.; Kappl, M.; Auernhammer, G.K.; Vollmer, D.; van Kats,
C.M.; van Blaaderen, A.,
Hollow silica spheres; Synthesis and mechanical properties
(in preparation) **2008** (Chapter 7)

Patent:

Dispersion of nanowires of semiconducting material
C. M. van Kats, A. van Blaaderen, and J. E. A. M. van den Meerakker,
EP 02079837.7 (filed November 18, 2002).

Other Publications:

Bormuth, V.; Jannasch, A.; Ander, M.; van Kats, C. M.; van Blaaderen, A.; Howard,
J.; Schäffer, E.
Optical trapping of coated microspheres. Optics Express **2008** *(accepted for
publication)*.

van Dillen, T.; Polman, A.; van Kats, C. M.; van Blaaderen, A.
Ion beam-induced anisotropic plastic deformation at 300 keV.
Applied Physics Letters **2003**, 83, (21), 4315-4317.

de Dood, M. J. A.; Berkhout, B.; van Kats, C. M.; Polman, A.; van Blaaderen, A.
Acid-Based Synthesis of Monodisperse Rare-Earth-Doped Colloidal SiO₂ Spheres.
Chemistry of Materials **2002**, 14, (7), 2849-2853.

Raming, T. P.; Winnubst, A. J. A.; van Kats, C. M.; Philipse, A. P.
The Synthesis and Magnetic Properties of Nanosized Hematite (α -Fe₂O₃) Particles.
Journal of Colloid and Interface Science **2002**, 249, (2), 346-350.

Snoeks, E.; van Blaaderen, A.; van Dillen, T.; van Kats, C. M.; Velikov, K.;
Brongersma, M. L.; Polman, A.
Colloidal assemblies modified by ion irradiation.

Nuclear Instruments and Methods in Physics Research Section B: Beam Interactions with Materials and Atoms **2001**, 178, (1-4), 62-68.

van Dillen, T.; Snoeks, E.; Fukarek, W.; van Kats, C. M.; Velikov, K. P.; van Blaaderen, A.; Polman, A.

Anisotropic deformation of colloidal particles under MeV ion irradiation.

Nuclear Instruments and Methods in Physics Research Section B: Beam Interactions with Materials and Atoms **2001**, 175-177, 350-356.

Snoeks, E.; van Blaaderen, A.; van Dillen, T.; van Kats, C. M.; Brongersma, M. L.; Polman, A.

Colloidal Ellipsoids with Continuously Variable Shape.

Advanced Materials **2000**, 12, (20), 1511-1514.

Lettinga, M. P.; van Kats, C. M.; Philipse, A. P.

Rotational Diffusion of Tracer Spheres in Packings and Dispersions of Colloidal Spheres Studied with Time-Resolved Phosphorescence Anisotropy.

Langmuir **2000**, 16, (15), 6166-6172.

Lettinga, M. P.; van Zandvoort, M. A. M. J.; van Kats, C. M.; Philipse, A. P.

Phosphorescent Colloidal Silica Spheres as Tracers for Rotational Diffusion Studies.

Langmuir **2000**, 16, (15), 6156-6165.

Megens, M.; van Kats, C. M.; Bosecke, P.; Vos, W. L.

Synchrotron Small-Angle X-ray Scattering of Colloids and Photonic Colloidal Crystals. Journal of Applied Crystallography **1997**, 30, (5 Part 2), 637-641.

Megens, M.; van Kats, C. M.; Bosecke, P.; Vos, W. L.

In Situ Characterization of Colloidal Spheres by Synchrotron Small-Angle X-ray Scattering.

Langmuir **1997**, 13, (23), 6120-6129.

Vos, W. L.; Megens, M.; van Kats, C. M.; Bosecke, P.

X-ray Diffraction of Photonic Colloidal Single Crystals.

Langmuir **1997**, 13, (23), 6004-6008.

Vos, W. L.; Megens, M.; van Kats, C. M.; Bosecke, P.

Transmission and diffraction by photonic colloidal crystals.

Journal of Physics: Condensed Matter **1996**, 8, (47), 9503-9507.

de Wolf, F. A.; Demel, R. A.; Bets, D.; van Kats, C.; de Kruijff, B.

Characterization of the interaction of doxorubicin with (poly)phosphoinositides in model systems Evidence for specific interaction with phosphatidylinositol-monophosphate and -diphosphate.

FEBS Letters **1991**, 288, (1-2), 237-240.

